

TIME DOMAIN ANALYSIS OF THREE DIMENSIONAL SOIL-STRUCTURE INTERACTION PROBLEMS

by

RAVU VENUGOPALA RAO

CE
1995
D
RAO
TIM



DEPARTMENT OF CIVIL ENGINEERING

INDIAN INSTITUTE OF TECHNOLOGY KANPUR

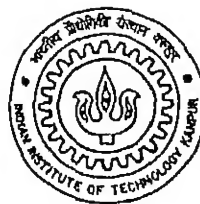
NOVEMBER, 1995

TIME DOMAIN ANALYSIS OF THREE DIMENSIONAL SOIL-STRUCTURE INTERACTION PROBLEMS

*A Thesis Submitted
in Partial Fulfilment of the Requirements
for the Degree of*

DOCTOR OF PHILOSOPHY

by
RAVU VENUGOPALA RAO



to the
DEPARTMENT OF CIVIL ENGINEERING
INDIAN INSTITUTE OF TECHNOLOGY KANPUR

November, 1995

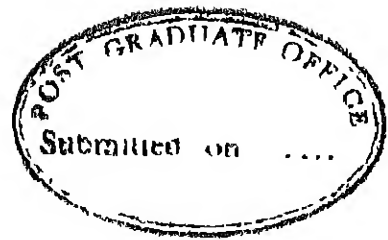
CENTRAL LIBRARY
I.I.T., KANPUR

Ref No. A 125692

CE- 1995-D-RAO-TIM

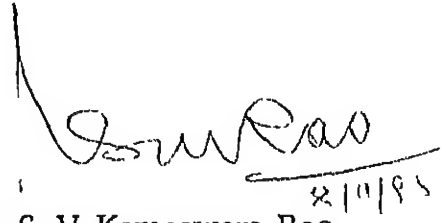


A125692



CERTIFICATE

It is hereby certified that the work contained in this thesis entitled **Time Domain Analysis of Three Dimensional Soil-Structure Interaction Problems** is an original research work carried out by **Mr. Ravu Venugopala Rao** under my supervision for the award of the Degree of Doctor of Philosophy, of Indian Institute of Technology, Kanpur, and the same has not been submitted elsewhere for the award of a degree or diploma.



8/11/95

Prof. N. S. V. Kameswara Rao

Kanpur

Department of Civil Engineering

November 8, 1995

Indian Institute of Technology Kanpur

ACKNOWLEDGMENTS

I wish to express my gratitude and regards to Prof. N. S. V. Kameswara Rao, for his guidance and encouragement throughout this investigation. I wish to record here that, I cherish my association with him since 1983. He has been a source of energy, and inspiration.

I wish to thank Prof. M. R. Madhav for his help and encouragement. I am grateful to Prof. P. K. Basudhar for all his encouragement and affection. I wish to record my thanks to Prof. Gokhale for all his help. Thanks are due to Prof. S. Chandra.

I wish to thank the Mr. Trivedi and Mr. Srivastav of Geotechnical lab and Mr. Bhatia of CE Office and other office staff

I am grateful to my friends, especially Hariprasad, Subbarao, Gopikrishna, Tirupathi, Nageswara Rao, Ravindra, Sitaram and Galagali for making this stay at IIT Kanpur pleasant and memorable. I thank my colleagues DNSingh and Kumar and juniors Ramakrishna, Sanjay and Sharma for their nice company. I wish express my thanks to DM, Jitendradas and Himanshu for their continued support. I thank my friend Mohan and his family members for their support and help.

I wish to thank my wife Sudha, and son Rahul for their support and love throughout the stay, inspite of the hardships of a rather long stay.

I wish to record my appreciation of the support of my mother and my father-in-law.

Venugopal

CONTENTS

CONTENTS	vii
LIST OF FIGURES	xi
NOTATION	xix
SYNOPSIS	xxv
1 INTRODUCTION	1
1.1 Brief Review of Existing Literature	2
1.2 Spatial and Temporal modeling	6
1.2.1 Absorbing boundaries	6
1.2.2 Boundary element methods	8
1.2.3 Temporal discretization	9
1.3 Scope of the Present Investigation	11
1.4 Organization of the Thesis	13
2 MODELING DYNAMIC SOIL-STRUCTURE INTERACTION	15
2.1 Introduction	15
2.2 Elastic Continuum Approach	17
2.3 Finite Element Method	18
2.3.1 Element Models and Approximating-Functions .	21

2.3.2	Formulation	31
2.3.3	Application of FEM to Dynamic problems	36
2.4	Lanczos Method	41
2.4.1	Introduction	41
2.4.2	Lanczos algorithm	42
2.4.3	Starting vector	45
2.4.4	Loss of orthogonality of Lanczos vectors	46
2.4.5	Number of Vectors	49
2.4.6	Coordinate transformation matrix	51
2.5	Direct Integration	52
2.5.1	Introduction	52
2.5.2	Θ method:	54
2.5.3	Θ Method with post-processing	55
2.6	Validation of the Model	57
2.6.1	Introduction	57
2.6.2	FEM implementation	58
2.6.3	Example 1. Elastic Half Space	61
2.6.4	Number of Lanczos Vectors	66
2.6.5	Size of the model	68
2.6.6	No of Elements	71
2.6.7	Spatial Variation of the load	72
2.6.8	Example 2. Elastic Half Space with a Vertical Trench	75
2.7	Summary	77
3	THREE DIMENSIONAL FOUNDATIONS	79
3.1	Introduction	79

3.2	Review of the Literature	81
3.3	Application of the Finite Element Method	84
3.3.1	Finite Element Model	85
3.4	Presentation of Results	91
3.4.1	Validation of the model	93
3.4.2	Effect of Embedment	98
3.4.3	Effect of Aspect Ratio (L/B)	103
3.4.4	Effect of Foundation Flexibility	108
3.4.5	Effect of Layered Soil	112
3.4.6	Effect of Linearly Varying Young's Modulus	120
3.4.7	Effect of Rigid Bedrock at Finite Depth	122
3.4.8	Summary	123
4	PILE FOUNDATION SOIL SYSTEMS	125
4.1	Introduction	125
4.2	Brief Literature Review	126
4.3	Present Model	128
4.4	Validation of the Model	128
4.5	Response of Single Piles	132
4.5.1	Effect of Slenderness Ratio	133
4.5.2	Effect of modular ratio	137
4.6	Response of Pile Foundations	139
4.6.1	Effect of Slenderness Ratio	141
4.6.2	Effect of Modular Ratio	145
4.6.3	Effect of Layered Soil	147
4.6.4	Effect of Number of Piles	149

4.7	Response of Machine Pile Foundation Systems With and Without Piles	151
4.7.1	Effect of Shear Modulus	153
4.7.2	Effect of Block/Pile Cap Thickness	156
4.8	Summary	158
5	ANALYSIS OF VIBRATION ISOLATION PROBLEMS	161
5.1	Introduction	161
5.2	Present Model	164
5.3	Presentation of The Results	165
5.3.1	Comparison of The Model	166
5.3.2	Effect of Trench/Barrier Depth	169
5.3.3	<i>Effect of Trench/Barrier Width</i>	172
5.3.4	Effect of Layered Soils	174
5.3.5	Effect of Frequency Ratio	177
5.4	Summary	180
6	CONCLUSIONS AND SCOPE FOR FUTURE STUDY	181
6.1	Introduction	181
6.2	Conclusions	181
6.3	Scope for Future Study	186

LIST OF FIGURES

2.1	Typical One-dimensional Elements	24
2.2	Typical Two-dimensional Elements	27
2.3	Half Space Loaded by Vertical Rickers's Wavelet	61
2.4	Half Space Loaded by Horizontal Rickers's Wavelet	62
2.5	A Typical FE Mesh	63
2.6	Effect of Number of Vectors on Rel. Error Norm	64
2.7	Effect of Number of Vectors on Vertical Displacement	65
2.8	Effect of Number of Vectors on Horizontal Displacement	65
2.9	CPU time for various stages of computation	68
2.10	Comparison of Vert. Displacements with Von Estorff's Values .	69
2.11	Effect of Mesh Size on Vertical Displacements	70
2.12	Comparison of Hor. Displacements with Von Estorff's Values .	70
2.13	Effect of Mesh Size on Horizontal Displacements	71
2.14	Effect of Number of Elements	72
2.15	Spatial Variation of the load – Different Load Cases	73
2.16	Effect of Spatial Variation of the Load with 20 Vectors	74
2.17	Effect of Spatial Variation of the Load with 40 Vectors	75
2.18	Half Space with trench Loaded by Vertical Rickers's Wavelet .	76
2.19	Effect of Trench on Vert. Displacements due to Vert Load	76
2.20	Effect of Trench on Hor. Displacements due to Hor Load	77

3.1	8 Noded Hexahedron Element in Global and Local Coordinate System	86
3.2	Problem Definition for 3dimensional Embedded foundation	95
3.3	Finite Element Discretization for 3dimensional Embedded foundation	95
3.4	Comparison of Vertical Compliance Function Values with Mita's Values	96
3.5	Comparison of Horizontal Compliance Function with Mita's Values	96
3.6	Comparison of Rotational Compliance Function with Mita's Values	97
3.7	Comparison of Torsional Compliance Function with Mita's Values	97
3.8	Effect of Embedgment on Vertical Compliance Function for Square Foundation	99
3.9	Effect of Embedgment on Vertical Compliance Function for Rectangular Foundation ($L/B = 2$)	99
3.10	Effect of Embedgment on Vertical Compliance Function for Rectangular Foundation ($L/B = 3$)	100
3.11	Effect of Embedgment on Horizontal Compliance Function for Square Foundation	100
3.12	Effect of Embedgment on Horizontal Compliance Function for Rectangular Foundation ($L/B = 2$)	101
3.13	Effect of Embedgment on Horizontal Compliance Function for Rectangular Foundation ($L/B = 3$)	101
3.14	Effect of Embedgment on Rotational Compliance Function for Square Foundation	102
3.15	Effect of Embedgment on Rotational Compliance Function for Rectangular Foundation ($L/B = 2$)	102

3.16 Effect of Embedment on Rotational Compliance Function for Rectangular Foundation ($L/B = 3$)	103
3.17 Effect of Aspect Ratio on Vertical Compliance Function for Embedded Foundation ($h/B = 0.5$)	104
3.18 Effect of Aspect Ratio on Vertical Compliance Function for Embedded Foundation ($h/B = 1.0$)	105
3.19 Effect of Aspect Ratio on Vertical Compliance Function for Embedded Foundation ($h/B = 1.5$)	105
3.20 Effect of Aspect Ratio on Horizontal Compliance Function for Embedded Foundation ($h/b = 0.5$)	106
3.21 Effect of Aspect Ratio on Horizontal Compliance Function for Embedded Foundation ($h/B = 1.0$)	106
3.22 Effect of Aspect Ratio on Horizontal Compliance Function for Embedded Foundation ($h/B = 1.5$)	107
3.23 Effect of Aspect Ratio on Rotational Compliance Function for Embedded Foundation ($h/B = 0.5$)	107
3.24 Effect of Aspect Ratio on Rotational Compliance Function for Embedded Foundation ($h/B = 1.5$)	108
3.25 Effect of Foundation Flexibility on Absolute Vertical Amplitude .	110
3.26 Foundation Flexibility <i>vs</i> Normalized Vertical Amplitude . .	110
3.27 Embedment <i>vs</i> Normalized Vertical Amplitude	111
3.28 Effect of Foundation Flexibility on Absolute Horizontal Amplitude	111
3.29 Effect of Foundation Flexibility on Normalized Horizontal Amplitude	112
3.30 Thickness Ratio <i>vs</i> Vertical Compliance Function ($M_r = 0.5$) .	114
3.31 Thickness Ratio <i>vs</i> Vertical Compliance Function ($M_r = 2.0$) .	114

3.32 Thickness Ratio <i>vs</i> Vertical Compliance Function ($M_r = 4.0$)	115
3.33 Modular Ratio <i>vs</i> Vertical Compliance Function ($l_r = 2.0$)	115
3.34 Modular Ratio <i>vs</i> Vertical Compliance Function ($l_r = 8.0$)	116
3.35 Thickness Ratio <i>vs</i> Horizontal Compliance Function ($M_r = 0.5$)	117
3.36 Thickness Ratio <i>vs</i> Horizontal Compliance Function ($M_r = 2.0$)	117
3.37 Thickness Ratio <i>vs</i> Horizontal Compliance Function ($M_r = 4.0$)	118
3.38 Modular Ratio <i>vs</i> Horizontal Compliance Function ($l_r = 2.0$)	118
3.39 Modular Ratio <i>vs</i> Horizontal Compliance Function ($l_r = 8.0$)	119
3.40 Thickness Ratio <i>vs</i> Rotational Compliance Function ($M_r = 0.5$)	119
3.41 Thickness Ratio <i>vs</i> Rotational Compliance Function ($M_r = 2.0$)	120
3.42 Effect of Linearly Varying Modulus on Vertical Compliance Function	121
3.43 Effect of Linearly Varying Modulus on Horizontal Compliance Function	121
3.44 Effect of Rigid Bedrock at Finite Depth on Vertical Compliance Function	122
3.45 Effect of Rigid Bedrock at Finite Depth on Horizontal Compliance Function	123
4.1 Triangular Pulse Excitation	130
4.2 Triangular Pulse Excitation	131
4.3 Vertical Displacement History of Pile Head Due to Triangular Pulse Load	131
4.4 Horizontal Displacement History of Pile Head Due to Triangular Pulse Load	132
4.5 Vertical Compliance Function of Pile Head ($E'_p/E_s = 10^4$)	133
4.6 Vertical Compliance Function of Pile Head ($E'_p/E_s = 10^4$)	134

4.7	Horizontal Compliance Function of Pile Head ($E_p/E_s = 10^3$)	135
4.8	Horizontal Compliance Function of Pile Head ($E_p/E_s = 10^4$)	135
4.9	Rotational Compliance Function of Pile Head ($E_p/E_s = 10^3$)	136
4.10	Rotational Compliance Function of Pile Head ($E_p/E_s = 10^4$)	137
4.11	Vertical Compliance Functions of Pile Head for Different Modular Ratios	138
4.12	Horizontal Compliance Functions of Pile Head for Different Modular Ratios	138
4.13	Rotational Compliance Functions of Pile Head for Different Modular Ratios	139
4.14	Plan Showing the Arrangement of Piles	140
4.15	Vertical Compliance Functions of Pile Cap ($E_p/E_s = 10^3$)	141
4.16	Vertical Compliance Functions of Pile Cap ($E_p/E_s = 10^4$)	142
4.17	Horizontal Compliance Functions of Pile Cap ($E_p/E_s = 10^3$)	143
4.18	Horizontal Compliance Functions of Pile Cap ($E_p/E_s = 10^4$)	143
4.19	Rotational Compliance Functions of Pile Cap ($E_p/E_s = 10^3$)	144
4.20	Rotational Compliance Functions of Pile Cap ($E_p/E_s = 10^4$)	144
4.21	Effect of Modular Ratio on Vertical Compliance Functions of Pile Cap	145
4.22	Effect of Modular Ratio on Horizontal Compliance Functions of Pile Cap	146
4.23	Effect of Modular Ratio on Rotational Compliance Functions of Pile Cap	146
4.24	Effect of Layer Thickness on Vertical Compliance Functions of Pile Cap	147

4.25 Effect of Layer Thickness on Horizontal Compliance Functions of Pile Cap	148
4.26 Effect of Layer Thickness on Rotational Compliance Functions of Pile Cap	148
4.27 Effect of Number of Piles on Vertical Compliance Functions of Pile Cap	149
4.28 Effect of Number of Piles on Horizontal Compliance Functions of Pile Cap	150
4.29 Effect of Number of Piles on Rotational Compliance Functions of Pile Cap	150
4.30 Horizontal and Rotational Excitation	152
4.31 Torsional Excitation	152
4.32 Machine Pile Foundation System	153
4.33 Effect of Shear Modulus on Horizontal Response	154
4.34 Effect of Shear Modulus on Rotational Response	155
4.35 Effect of Shear Modulus on Torsional Response	155
4.36 Effect of Pile Cap/Block Thickness on Horizontal Response	156
4.37 Effect of Pile Cap/Block Thickness on Rotational Response	157
4.38 Effect of Pile Cap/Block Thickness on Torsional Response	157
5.1 Open Trench Surrounding Machine Foundation	167
5.2 Cross section of Vibration Isolation System	167
5.3 Comparison of Amplitude Reduction Ratio Contours	169
5.4 Effect of Trench Depth on Amplitude Reduction Ratio	171
5.5 Effect of Barrier Depth on Amplitude Reduction Ratio	172
5.6 Effect of Trench Width on Amplitude Reduction Ratio	173
5.7 Effect of Barrier Width on Amplitude Reduction Ratio	174

5 8 Effect of Top Layer Thickness on Amplitude Reduction Ratio for $M_t = 0.5$	175
5 9 Effect of Top Layer Thickness on Amplitude Reduction Ratio of an Open Trench with $M_t = 2.0$	176
5 10 Effect of Top Layer Thickness on Amplitude Reduction Ratio of Barrier with $M_t = 2.0$	177
5 11 Effect of Frequency Ratio on Amplitude Reduction Ratio of an Open Trench	179

NOTATION

The following Notation has been used in this Thesis

a	Average acceleration
a	Slope of the linear of the variation of modulus
a^*	Acceleration at time t during a step
a_n	Acceleration at $n^i h$ step
a_0	Frequency ratio
a_1, a_2, \dots	Coefficients of the approximating polynomial
A	Amplitude reduction ratio
B	Half-width of the foundation block
$[B]$	Matrix relating strains to nodal displacements
$[C]$	Damping matrix
$[\bar{C}]$	Damping matrix in transformed space
C_{xx}	Horizontal compliance function in x direction
C_{yy}	Vertical compliance function
$C_{\psi yy}$	Torsional compliance function
$C_{\psi zz}$	Rotational compliance function
$C_{\psi zx}$	Rotational compliance function due to horizontal load
d	Thickness of footing
	Side of square pile
	Depth of the trench

D	Thickness of compressible layer
	Nondimensional trench depth
$\ err\ $	Error norm
$\ e\ r_{rel}$	Relative error norm
e	Relative error norm of load representation
E	Error vector in load representation
E_b	Young's modulus of top layer
E_p	Young's modulus of foundation material
E_s	Young's modulus of soil
E_t	Young's modulus of bottom layer
$[E]$	Elasticity matrix
f	Body force vector
f^e	Body force vector of an element
G_s	Shear modulus of soil
h	Depth of foundation
	Step size
h_n	New step size
I	Identity matrix
J	Jacobian of the transformation
$[J]$	Jacobian matrix
$[K]$	Stiffness matrix
$[K^e]$	Element stiffness matrix
$[K_m]$	Stiffness matrix in Lanczos space
$[\tilde{K}]$	Stiffness matrix in transformed space
l	Length of pile
	Trench location
L	Half length of the foundation

	Nondimensional trench location
	Lower triangular matrix
L ,	Rayleigh wave length
$[L]$	Matrix relating strains and displacements
M_r	Modular Ratio
$[M]$	Mass matrix
$[M^e]$	Element mass matrix
$[M_m]$	Effective mass matrix
$[\bar{M}]$	Mass matrix in transformed space
N_1, N_2, \dots	Shape function
$[N]$	Shape function matrix
N_i^e	Basis function for element e of node i
nel	Number of elements
$nnod$	number of nodes
$\{p^e\}$	Element load vector
P	Potential energy
$\{P\}$	Global load vector
$\{P_m\}$	Global load vector in original space
$\{P_n\}$	Load vector at n^{th} step
$\{\bar{P}_m\}$	Global load vector
$\{\bar{P}_j\}$	j^{th} participation factor in transformed space
q_j	j^{th} normalized Lanczos vector
$[Q]$	Lanczos subspace
r_j	j^{th} pure orthogonal vector
\bar{r}_j	j^{th} orthogonal vector in Krylov subspace
R	Residue over the domain
R^e	Residue over the element

t	Time
	Thickness of top layer
t_n	Time at n^{th} step
T	Kinetic energy
T_r	Nondimensional top layer
u	Dependent function
	Horizontal displacement in x direction
n	Displacement vector
u^e	Approximating function over the element
u_1, u_2, \dots	Nodal variables
$\{U\}$	Nodal displacements vector
v	Vertical displacement
v_n	Velocity vector at n^{th} step
v_{n+1}	Velocity vector at $n+1^{\text{th}}$ step
\bar{v}_{n+1}	Predicted velocity vector at $n+1^{\text{th}}$ step
w	Horizontal displacement x direction
	Width of the trench
w_f	Half width of footing
W	Nondimensional trench width
W_f	Nondimensional half width of footing
x_1, x_2, \dots	Nodal Coordinates
$x_h, x_{h/2}$	Displacements obtained with step sizes h and $h/2$ respectively
\mathbf{x}	Vector of nodal coordinates
\mathbf{X}	Vector of generalized (transformed) displacements
y_1, y_2, \dots	Ritz vectors
\mathbf{Y}	Matrix whose columns are Ritz vectors

z	Eigen vectors of the original system
α, β	Rayleigh damping coefficients
$\alpha_j, \beta_j, \gamma_j$	Amplitudes of the previous Lanczos vectors contained in vector \bar{r}_j
	Off-diagonal and diagonal entries of the tridiagonal Lanczos matrix
δa	Change in acceleration during one time step
ϵ	Strain
	Relative error norm of the load vector
	Relative error tolerance
	Semi-orthogonality level
ϵ^e	Strain over the element
Γ	Surface of the domain
Γ^e	Surface of the element
κ	Level of orthogonality among Lanczos vectors
λ	Eigen vectors of original system
ω	Frequency of excitation
ω_{ij}	Level of orthogonality between Lanczos vectors referred by its subscripts
Ω	Volume of the domain
Ω^e	Volume of the element
ν	Poisson's ratio
ν_p	Poisson's ratio of block/pile material
ν_s	Poisson's ratio of soil
ϕ	Transformation matrix
ψ	Random number
ρ	Mass density

ρ_p	Mass density of block/pile material
ρ_s	Mass density of soil
σ	Stress
σ^e	Stress over the element
τ	Surface force
θ_0, θ_1	Integration parameters of Theta Method
ζ, η, ξ	Natural coordinate system
\mathcal{C}	Differential operator describing the boundary conditions
\mathcal{L}	Differential operator describing the behaviour
	Langrangian of the whole domain

SYNOPSIS

The dynamic soil-structure interaction deals with response of structures and/or ground subjected to time-dependent loads. The loads could be applied directly on to the structure (arising from rotating machinery, wind, *etc.*) or through soil in the form of incident waves (arising out of earthquake or an explosion or unbalanced machinery *etc.*).

Analytical methods available for dynamic soil structure interaction are applicable only to highly idealized geometric representations and to linear elastic material behaviour in frequency domain. Numerical methods which need domain discretization can be not be applied directly as soil exists as a half-space. The discretization of finite (computational) domain coupled with boundary conditions on the finite domain to account for energy radiation (approximately) can be used to model the problems.

The Present investigation addresses the problems of dynamic soil-structure interaction in time domain. The computational schemes involves the use of FEM to discretize a *large* computational domain and a load dependent Lanczos transformation procedure to reduce the number of degrees of freedom obtained from the FEM. The resulting dynamic equilibrium equations are integrated using an adaptive strategy devised for a second order integration method. The computational scheme developed has the following capabilities – 1. No need for

energy absorbing boundaries, 2. Retains all the advantages of FEM, 3. An integrated analysis of soil, structure and foundation is possible, 4. Can analyze all modes simultaneously, 5. Can handle several arbitrary nature, 6. Can be used for transient as well as for steady state responses, 7. Error estimates and adaptive error control strategies are available for temporal discretization as well as for transformation process.

The study covers the areas of flexible and rigid foundation response to various types excitations. Effect of shape and embeddment of the foundation have been investigated. Soil has been idealized as linear isotropic continuum. Non-homogeneity of the soil has been considered in terms of continuously varying modulus and as a layered system. Response of foundation on finite thick soil stratum has also been investigated.

Response of pile foundation soil system has been investigated for various modes of excitation. Effect of various parameters like embeddment of pile cap, slenderness ratio relative rigidity and spacing of individual piles have been studied.

Vibration isolation has been investigated with open and filled trenches. Various parameters affecting the amplitude reduction like material properties of the trench fill, the geometry and location of the trench and excitation frequency.

In Chapter 1 a brief introduction to the problems is presented. The literature available is discussed and the need and scope of the present investigation is highlighted. Chapter 2 introduces the computational model utilized in this investigation. The validity of the elastic continuum theory of the soil has been discussed. A brief introduction

to finite element method has been presented, and the application of the finite element method to dynamic problems is presented. A large computational domain has been used to represent semi-infinite soil medium, and the system has been discretized. Load dependent Lanczos vectors have been utilized for coordinate transformation. Apriori error estimates have been used to asses the quality of the coordinate transformation and number of vectors or order of reduced system have been estimated by specifying error tolerance. The resulting dynamic equilibrium equations in reduced space have been solved in time domain. A variant of Newmark β method called Θ method, which retains second order accuracy with controllable numerical damping has been utilized. An adaptive time stepping strategy has been devised by post processing the solutions with specified local truncation error tolerance. The solutions (responses of required degrees of freedom) are obtained in original space.

An extensive validation has been carried out to verify the accuracy of the numerical model in time domain. An half-space and half-space with vertical trench have been chosen. To simulate transient excitation Ricker's Wavelet loading has been prescribed. Both vertical and horizontal excitations have been investigated in two dimensions. Excellent agreement with published results is observed. Effect of number of Lanczos vectors, model size, number of elements on the accuracy of the results has been brought out. Different spatial variation of the loads have been considered for generation of Lanczos vectors and found that reduced system matrices can be used to analyze the problems whose spatial loading patterns are similar to the one used to generate Lanczos vectors. Computational times required for each

stage of the computation is reported for different number of Lanczos vectors. The present model has been found to represent non convex domains in time domain with good accuracy. The solutions obtained are found to obey causality conditions for half-space and half-space with vertical trench problems.

In Chapter 3, results of the detailed parametric studies carried out on *embedded foundations* have been presented in terms of the compliance functions. The results obtained with present model are compared with existing time-domain boundary element model solution for vertical, horizontal, rotational and torsional modes. The agreement is found to be satisfactory. Effect of depth of embedment, aspect ratio of the footing, relative flexibility on the compliance functions for different modes at different frequency ratios have been investigated. Behaviour of flexible foundations at different embedments are presented to bring out the change in the response. Effect of linearly varying modulus, presence of rigid bedrock at finite depth and presence of layering in the soil system have been investigated. It has been found that effect of these parameters differ from vertical mode to horizontal mode of vibration. Linearly increasing modulus shows stronger effect on horizontal mode than vertical mode. It increases the resonant frequency for horizontal mode of vibration. Presence of hard rock is strongly influences the vertical compliance functions. The compliance functions are influenced by small thickness (usually 10 times the halfwidth of the foundation) of the top layer of the soil. As frequency of excitation increased the thickness of the soil layer influencing the behaviour decreases.

In Chapter 4 results obtained for pile foundations in homogeneous and

layered soils have been presented. Analysis of piles and pile cap has been carried out in an integrated manner along with soil medium. The study has been carried out in such a way that the effect of presence of piles in foundation system has been brought out. The responses in different modes of vibration in terms of compliance functions for pile cap are presented. A few parametric studies on the behaviour of single piles are carried out to. The response of single piles for transient excitation is investigated for validation and the behaviour predicted by the present model agrees well with those reported.

In case of single piles, increase in slenderness ratio substantially reduces compliance functions for vertical mode of vibration. Whereas for horizontal and rotational modes of vibration the effect of slenderness ratios is felt at higher modular ratios only.

The effect of group of piles on compliance functions of pile foundation (of the pile cap) is different in different modes of vibration. The presence of piles (four) reduces the compliance functions for vertical and rotational modes substantially (by a factor of 4), whereas the reduction is of the order of 1.5 for horizontal mode of vibration, and by a factor of 10 for rotational modes. The effect of modular ratio on compliance functions of the pile cap has been investigated. It is found that modular ratio does not have a significant effect on vertical and horizontal modes, but has strong influence on rotational response. Effect of stiffer stratum below has been investigated. The presence of stiffer soil influences the vertical mode strongly and increases the resonant frequencies. Unlike the block foundation considerable thickness of top layer influences the pile group behaviour. Increase in number of piles (reducing the pile spacing) reduces the compliances considerably in

vertical and rotational modes.

A parametric study on machine pile foundation soil system (MPFS) transmitting periodic but not harmonic excitations simultaneously is presented to study real life situations. The parameters considered for the study are the slenderness ratio of the piles, shear modulus of the soil and pile cap/block thickness. The machine consists of a diesel generating set, and is transmitting horizontal force and rocking moment with one period, and torsional moment with another period. These excitations are arbitrary except that they are periodic individually. The maximum displacements at the center of gravity of the foundation has been used to present the results.

Increasing the shear modulus reduces the response drastically at low shear modulii. The responses do not significantly reduce due to increase of the modulus beyond a value of 6 MPa . Presence of piles reduces the horizontal displacement by about 60% at low modulii and by a small fraction at higher modulii. For rotational and torsional modes the reduction is of the order of 100% due to presence of piles at low modulii. Increasing the slenderness ratio beyond a value of 20 in horizontal and rotational modes, and beyond a value of 10 in torsional mode, does not reduce the responses. The pile cap/block thickness has very little effect on horizontal and rotational modes. Increasing the pile cap thickness beyond 1.0m increases the responses in some of the situations.

In Chapter 5 a brief study has been carried out on the vibration isolation systems. Open and filled trenches as well as concrete wall barriers are considered for the study. The effect of width, depth and location of the trench/barrier on vibration isolation efficiency, in terms

of amplitude reduction, has been carried out for vertical and horizontal modes. Effect of layering of soil has also been investigated.

In Chapter 6 conclusions drawn from the present study are summarized. The highlights of the computational scheme *viz* the advantages of rational and integrated analysis for transient as well as steady state responses with small computational resources are reported. Possible extensions of the present scheme for non-linear analysis have been indicated.

Chapter 1

INTRODUCTION

The dynamic soil-structure interaction deals with response of structures and/or ground subjected to a specified time-varying loads. The loads could be applied directly on to the structure (arising from rotating machinery, wind etc.) or through soil in the form of incident wave (arising out of earthquake or an explosion).

Dynamic soil-structure interaction includes analysis of machine foundation soil systems, which is an important area of study. The Dynamic analysis of foundation soil systems have received a lot of attention of researchers recently. This is partly attributed to recognition of the importance of earthquake hazards which warrants dynamic analysis of structural systems including *substructures* (foundations), and availability of digital computers with lot of memory and computing power required for dynamic analysis. The dynamic soil-structure interaction unlike structural dynamics counterpart is quite complicated and involved because of its infinite extent (domain) and uncontrollable variations of the characteristics (non homogeneity etc.). Any realistic analysis of dynamic soil structure interaction needs three dimensional

idealization of the geometry.

Analytical methods available for dynamic soil structure interaction are applicable only to highly idealized geometric representations and to linear elastic material behaviour in frequency domain. Numerical methods which need domain discretization can not be applied directly as soil exists as a half-space. The discretization of finite (computational) domain coupled with appropriate boundary conditions on the finite domain to account for energy radiation can be used to model the problems.

The study of dynamic soil-structure interaction can be classified in to two distinct approaches – frequency domain approach and time domain approach. The frequency domain approach is suitable for linear elastic problems with periodic excitations. The time domain approach can handle all type of excitations and non-linear material behaviour. It also provides responses in a natural way (i.e. as events occur).

1.1 Brief Review of Existing Literature

Early investigations of soil-structure interaction dealt with response of soil idealizing it as linear, homogeneous, semi-infinite elastic half-space. Lamb (1904) initiated study of response of elastic half-space subjected to dynamic loads. Reissner (1936) making use of Lamb's solution, obtained the response of harmonic disc load on the surface of an elastic half-space. He assumed a uniform distribution of stresses under the disc. Quinlan (1953) derived the equations for obtaining the responses with contact pressures which vary across the diameter

with parabolic distribution, with uniform distribution and with the distribution corresponding to a rigid base. He gave solutions for rigid base approximations. Sung (1953) developed solutions for circular contact area with three pressure distributions, namely, 1. uniform, 2. parabolic, and 3. pressure distribution corresponding to rigid base. He gave solutions for different Poisson's ratios. These solutions can be used to compute the compliance functions of rectangular footing making use of the equivalent circular area. This equivalent area method provides solutions of reasonable accuracy for aspect ratios up to two (F E Richart, 1960). He also developed mathematical expressions for rectangular footing resting on half-space. Kobori (1962), Thomson and Kobori (1962) obtained compliance functions for uniformly distributed load over rectangular surface area. Arnold, Bycroft and Warburton (1955) and Bycroft (1956) obtained the solution for rocking vibrations of a circular footing.

A mixed boundary value problem, with prescribed displacements under a rigid footing and zero tractions over the remaining surface, was studied by Luco and Westmann (1971), employing boundary integral equations. Luco (1976) obtained impedance functions of a rigid foundation on layered viscoelastic medium using integral equations approach.

Finite Element Method along with different absorbing boundaries were employed by several investigators to obtain solutions to dynamic soil-structure interaction problems. Lysmer and Kuhlemeyer (1969) developed an absorbing boundary, called standard viscous boundary (SVB), consisting of discrete viscous dampers. Later they devised another boundary approximation called Rayleigh wave boundary (RWB)

which was recommended to be used along the vertical boundaries to achieve better absorption of Rayleigh waves. They obtained compliance functions for strip and axisymmetric foundations. Dasgupta and Kameswara Rao (1978) extended the methodology to study plane, axisymmetric and three dimensional problems. They incorporated non-linear material behaviour and non-homogeneity of the soil in the formulation. Lysmer and Waas (1972) developed an absorbing boundary for plane strain problems which transmits Love and Rayleigh waves. This boundary was applicable in frequency domain for layered media with horizontal layers extending to infinity resting on hard stratum. Kausel (1974) extended the same for axisymmetric problems and obtained impedance functions for different modes. Cohen and Jennings (1984) developed a transmitting boundary, which they called *paraxial boundary*, by solving wave equation propagating in one direction only. This boundary was successfully employed along with finite elements for obtaining solutions in time domain. Underwood and Geers (1978) developed a boundary approximation called *doubly asymptotic boundary element* analysis, which is an exact one for very low and high frequencies. Higdon (1992) developed a mathematical approximation to boundary (Higdon boundary) absorption by employing wave absorbers which can absorb waves impinging at any angle. The Higdon boundary was employed with finite difference method to solve wave propagation problems in layered media also. Venugopala Rao and Kameswara Rao (1994) made use of infinite elements to obtain the response of strip and circular footings for low frequency excitation. Zhang and Zhao (1987b), Zhang and Zhao (1987a) developed an infinite element approximation in frequency domain to obtain the

response of strip and rigid foundations on layered media.

The Boundary Element Method (BEM)s which can automatically include infinite region in the modeling have been extensively used to study the soil-structure interaction problems. The frequency domain formulation was first used to obtain impedance functions of rectangular foundations resting on or embedded in a viscoelastic half-space by Dominguez (1978). Impedance functions of foundations resting on non-homogeneous and layered soils were obtained by Abascal and Dominguez (1986). Ahmad and Banerjee (1988) employed quadratic elements in frequency domain to obtain compliance functions Karabalis and Beskos (1984) and Karabalis and Beskos (1986) used a time-domain BEM and obtained impedance functions for rigid surface and embedded foundations. The response of flexible foundations was investigated making use of domain methods like Finite Element (FE) and Finite Difference (FD) for foundation and Boundary Element (BE) for soil. Iguchi and Luco (1981) obtained the response of rectangular foundations on elastic half-space. Karabalis and Beskos (1985) and Gaitanaros and Karabalis (1988) obtained response of surface and embedded flexible foundations using time domain boundary element method for soil and FEM for the foundation. Gucunski and Peek (1993) presented response of circular foundations using soil stiffness matrices for layered soils evaluated through Green's functions and stiffness matrices of plate using finite difference method.

Gazetas and Tassoulas (1987b), Gazetas and Tassoulas (1987a) developed approximate models for stiffness and damping parameters for horizontal and rocking vibrations based on results obtained through numerical computation. Wolf (1988) developed approximate models

by adding an additional degree of freedom. He obtained stiffness, damping and mass parameters by curve fitting techniques to the results obtained through exact numerical computation. Similar models were reported by Barros and Luco (1990) with five parameters. They observed that these models represent elastic half-space better.

1.2 Spatial and Temporal modeling

As pointed out earlier, any realistic numerical model for dynamic soil-structure interaction has to discretize the spatial as well as time domains. Domain discretization methods (DDMs) like finite element and finite difference methods *etc.* can handle finite size domains, and these methods can easily incorporate spatial variation (non-homogeneity) of the material properties. The boundary discretization (like boundary element and boundary integral) methods (BDMs) can naturally address the infinite extent of the domain. These BDMs are usually global in space and time. They can not easily incorporate the non-homogeneity and non-linearity of the material. To model an infinite domain, by using a finite computational domain (in DDMs), an artificial boundary is to be created at a finite distance with appropriate boundary conditions to simulate smooth wave propagation (*i.e.* non reflecting) at the boundary.

1.2.1 Absorbing boundaries

Absorbing boundaries along with domain discretization was tried successfully by various researchers. The Lysmer's standard viscous and Rayleigh wave boundaries are local in space. The boundary scheme

is exact in one dimension but approximate in two and three dimensions *i.e.* it can fully absorb waves impinging in normal direction only. The boundary can be implemented in frequency domain only, since the Rayleigh wave boundary description contain frequency dependent parameters.

The paraxial boundary developed by Cohen and Jennings (1984) is a second order approximation to the waves traveling in one direction only. This boundary also reflects waves other than the ones impinging in normal direction. The paraxial boundary generates unsymmetric damping matrices, consequently, needs special solution procedures and special treatment to the boundary element. This boundary was not found to perform better than standard viscous boundary Wolf (1988). An absorbing boundary, called consistent energy absorbing boundary, for plane strain conditions was developed by Lysmer and Waas (1972). They solved wave propagation of Love and Rayleigh waves in a horizontally layered soil resting on rigid bed rock in wave number-frequency domain. Solving a quadratic eigenvalue problem for wave numbers, corresponding to waves propagating in one direction only, for a given frequency, a dynamic boundary stiffness matrix was developed. Kausel (1974), Kausel and Roesett (1975) extended the same for an axisymmetric formulation including unsymmetric modes. This boundary is more accurate than the previous ones, but, involves substantial computational effort and can be implemented in frequency domain only.

The doubly asymptotic approximation boundary developed by Underwood and Geers (1978) is exact only at zero and infinite frequencies.

The boundary approximation developed by Higdon (1992) consists

of simultaneous application of series of energy absorbing conditions, *i.e.* boundary condition is expressed as a product of first order wave absorbing conditions which absorb fully waves of particular velocity impinging at specific angle. The combined effect of such boundary conditions is to absorb wide range of waves with different velocities. This boundary introduces unsymmetric damping matrices, and consequently, numerical instabilities. These issues have to be properly taken care of in the implementation using suitable procedures like upwinding. The accuracy of the scheme improves with higher order boundary conditions and introduces more complexity and entails higher computational effort.

Givoli (1992) developed an absorbing boundary scheme which maps large domain (can be infinite also) to a finite domain with Dirichlet to Neumann (DtN) map on the boundary *i.e.* it maps Dirichlet boundary condition to a Neumann boundary condition, on the arbitrary boundary created. He gave expressions for DtN map for different class of problems in frequency domain and time domain. In time domain, DtN boundary being global in time, needs to store the time histories of the primary variable and its derivatives on the boundary for computation.

1.2.2 Boundary element methods

The boundary element methods (exterior problems) have the capability to handle infinite domains. The frequency domain formulations are computationally competitive to the DDMs. With availability of Green's function for layered media (Kausel and Peek, 1982) and with combination of FEM for Flexible foundations (Gucunski and Peek, 1993), they offer a computational framework for dynamic soil-structure interaction

problems in the frequency domain. The time-domain counterpart (of BEMs) has been successfully employed to study different class of problems like flexible foundations (Karabalis and Beskos, 1985) , vibration isolation (Ahmad and Al-Hussaini, 1991) and Pile foundations (Cheung, Tham and Lie, 1995) The BEMs suffer from following disadvantages. They are global in space and time. Incorporation of foundation flexibility and material nonlinearity is difficult to achieve. The time stepping needs nodal values to be available (both tractions and displacements) from initial step up to the previous step to compute the values for the current step (*i.e.* since time stepping is global) Hence step size can not be changed easily and prior knowledge of proper step size is essential to achieve acceptable accuracy. It was established that time-domain formulation of BEMs did not obey causality condition and modeling of non-convex domains needed special treatment like subdivision into multiple convex domains(Von Estorff, Pais and Kausel, 1990). Due to the global nature of time stepping, the computational requirements are enormous for time-domain formulation.

1.2.3 Temporal discretization

Spatial discretization of the domain in dynamic soil-structure interaction problems leads to a system of coupled second order ordinary differential equations with time as independent variable. These differential equations are to be integrated using numerical integration (time marching) schemes such as Newmark method, Runge-Kutta and central difference methods.

The accuracy of the schemes depends on the step size which is governed by the maximum eigenvalue (natural frequency) and it is to

be emphasized here that estimation of bounds of the eigenvalues for general finite element mesh is not easy. One should note that adaptive step size methods (*i.e.* the method which can predict the local truncation errors and suitably change the step size) are to be preferred due to their inherent higher levels of accuracy and possible savings in computational effort.

The desirable properties of any integration scheme are unconditional stability, flexibility to change the step size, high order of accuracy, flexibility for incorporation of algorithmic damping and its spectral radius should be close to unity for low frequencies and little less than unity for high frequencies (Hughes, 1984).

Newmark method is widely used in wave propagation and structural dynamics problems due to its unconditionally stability. But this method looses its order of accuracy (second) if algorithmic damping is introduced. Hilber, Hughes and Taylor (1977) introduced a second order method which retains the order of accuracy (second) and can incorporate desirable levels of numerical damping. Hoff and Pahl (1988) derived a second order method with one free parameter which can incorporate numerical damping. Zeng, Wiberg, *et al.* (1992) developed a post-processing technique to estimate local truncation errors in standard Newmark method and step size changing strategy. They found that this methodology improves accuracy and reduces the computational effort.

1.3 Scope of the Present Investigation

Based on the brief survey carried out, It can be pointed out that an accurate and feasible computational frame work for dynamic soil-structure interaction in time-domain is not available. The domain discretization methods along with various absorbing boundaries provide approximate solutions with different levels of accuracy in frequency domain. Some of the time domain boundaries like Higdon boundary, provide an improvement over others but are associated with undesirable properties such as generation of unsymmetric damping matrices. The time domain boundary element and DtN methods along with FEM accurately represent the semi-infinite extent of the domain, but the computational cost is enormous due to their global nature in time. A computational framework which will have the desirable properties of the domain methods like easy incorporation of non-homogeneity and non-linearity of the material(s), and an adaptive time integration scheme and with reasonable demand on computational resources, will be an appropriate strategy to solve dynamic soil-structure interaction problems in time domain.

To achieve such strategy the present investigation uses finite element model for spatial discretization (for both near and far field by considering a *large* mesh) circumventing the need for an energy absorbing boundary. Load dependent orthonormal (Lanczos) vectors (Wilson, Yuan and Dickens, 1979) have been utilized to transform the equation from original space to Lanczos space (to reduce the computational effort). An error monitoring technique is built in the algorithm to asses the loss of accuracy due the transformation. An adaptive time inte-

gration technique has been devised by post processing the Θ method proposed by Hoff and Pahl (1988) with specified error tolerance. The response of the system is obtained in time domain by direct time integration in the transformed space and required response quantities are computed in the original space. Apart from the general study of three dimensional foundations using 3D modelling in time domain, the effect of coupled modes of vibration of has not received enough attention. The effect of flexibility in different modes of vibration need to be established. The effect of embeddment for different aspect ratios of the foundation has to be quantified for different modes. Effect of layering of the soil system and variation of modulus with the depth need greater focus. Effect of hard rock at finite depth on the responses need to be investigated.

The available literature on the analysis of pile foundation soil system when modes of vibration are coupled is meagre. The effect of pile cap and its embeddment has not been incorporated in the analysis which effects the responses significantly. The continuity at the pile soil interface was enforced approximately in the past (*i.e.* continuity at the nodes only).

In case of vibration isolation using open trenches the effect of depth was investigated. The effect of operating frequency, width and location of the trench need to be addressed. The mode of vibration of the source is also needs focus. The effect of layering and material properties of the fill material of the infilled trench are to be investigated.

With the computational framework described above three dimensional block foundations have been investigated incorporating coupled modes, flexibility embeddment, layering *etc.* . Similarly the pile foun-

dation soil system including the effect of pile cap and its embeddment have been investigated for all modes of vibration. Vibration isolation with vertical and horizontal source have been investigated. The effect of operating frequency, width and location of the trench have been included in the analysis.

1.4 Organization of the Thesis

The work that has been carried out in this investigation is presented in the following manner.

Chapter 2 describes the formulation of the present computational frame work - basic concepts of finite element discretization, application of the FEM to dynamic soil-structure interaction problems, detailed exposition of the concept of load dependent Lanczos vector generation, generation of transformation matrices, inclusion of damping, detailed description of the time integration scheme, post processing technique and error control strategies. A thorough validation carried out on a two dimensional time domain test problem has also been presented. In Chapter 3, three dimensional embedded foundation have been investigated. Influence of various parameters such as aspect ratio, embedment depth, flexibility of the foundation, layering, linear variation of the modulus of the soil on the response of the foundation in vertical, horizontal and rotational modes are presented graphically. The results obtained with present investigation are compared with existing solutions.

In Chapter 4 vibrations of pile foundation are analyzed. Results of dynamic influence coefficient for pile group effect are shown graph-

ically. The response of the piles for transient excitation is computed and compared with existing solutions. The effect of velocity ratio, pile cap etc on the response is shown graphically. A real life problem of a machine foundation resting on block and pile foundation has been analyzed. The forces transmitted by the machine consists of arbitrary periodic excitations.

In Chapter 5 vibration isolation by open and filled trenches are investigated. The results are compared with existing ones. The effect of location of the trench, width, depth and material properties of the fill are investigated. Effect of layering of the soil is also investigated and the amplitude reduction is presented graphically.

Conclusions are summarized in Chapter 6. Possible extensions of the present work are indicated.

Chapter 2

MODELING DYNAMIC SOIL-STRUCTURE INTERACTION

2.1 Introduction

The dynamic soil-structure interaction deals with response of structure and/or ground subjected to a specified time-varying loads. The loads could be applied directly on to the structure (arising from rotating machinery, wind, *etc*) or through soil in the form of incident waves (arising out of earthquakes, explosions *etc*).

Analytical solutions for dynamic soil-structure interaction problems can be obtained for situations with highly idealized geometric representation of the problem, linear elastic material behaviour, and harmonic loading. Since soil exist as semi-infinite half-space, numerical methods have to incorporate the notion of infinity in the formulation. Numerical Methods like Integral Equation Method, Boundary Element Method can handle infinite domains naturally, whereas domain discretization methods like Finite Difference and Finite Element Methods can not

be applied to semi-infinite domains *per se*. A way out of handling such infinite domains is to consider a finite (computational) domain for discretization with an appropriate boundary conditions (energy absorbing) on the computational boundary, or a large domain with a boundary which reflects little energy. The later approach has been adapted in this investigation for its obvious reasons as discussed in the previous chapter.

The study of Dynamic Soil-Structure interaction can be classified into two distinct approaches - Frequency domain approach and Time domain approach. The frequency domain approach is suitable for linear elastic problems with periodic excitations. The Time domain approach can handle all types of excitations and non linear material behaviour. Domain discretization (large size model) coupled with time integration (time domain approach) has been utilized to analyze dynamic soil-structure interaction problems, in the present study.

In this chapter the computational model utilized in this investigation is presented. The Modeling consist of three stages - 1. Spatial discretization, 2. Lanczos vector transformation and 3. Temporal discretization. The validity of elastic continuum approach is discussed in Section 2.2. The Finite Element Method, which is used for spatial discretization, and its implementation is described in Section 2.3. The Lanczos vector transformation method, which is used reduce the problem size is described in Section 2.4. The temporal discretization needed to obtain the solution in time domain as implemented in this investigation is presented in Section 2.5. The methodology developed has been applied to few cases representing the range of problems to be addressed. The results along with published ones, wherever possible,

are presented in Section 2.6 for validation. A brief summary of the conclusions came out of the this numerical modeling are presented in Section 2.7

2.2 Elastic Continuum Approach

Soil is a complex material whose behaviour is difficult to describe in simple constitutive laws. It is a particulate medium with three phases namely solid phase (mineral), liquid phase (usually water) and gaseous phase. Moreover the soil is not perfectly elastic, whose properties depend with depth, in-situ (initial) stress and past loading history, *etc.* Hence a unified mathematical description of its behaviour is difficult. The behaviour could be elastic, plastic, viscoelastic or thixotropic depending on loading conditions and history. However for small stresses, which do not induce plastic flow, an elastic description of the material behaviour produces satisfactory results (Barkan, 1969). The soil as it occurs in nature is bounded by horizontal plane at the top and extends to infinity in lateral directions. It can be treated as semi-infinite body. The individual soil particles being small compared to the dimensions of the problem geometry, the soil is usually treated as a continuum.

In the absence of any theory which takes into account the special properties mentioned above, the elastic half-space theory is being used for analytical and computational modeling. The elastic continuum theory being rigorous (not empirical) in nature, it is suitable for experimental verification also. The material properties (here soil) needed to describe the linear elastic behaviour — such as Young's modulus E_s , Poisson's

ratio ν and mass density ρ can be determined easily.

In this investigation soil is modeled as elastic half-space. Non homogeneity of the material in terms of its Young's modulus is also considered.

2.3 Finite Element Method

Many of the engineering problems encountered in practice deal with systems with distributed (continuously) parameters. The application of physics to such systems (continua) often leads to a system of partial differential equations. In case the equations and the domain are simple, the solution can be obtained in a closed form (exact), often in the form of an infinite series, or using Fourier, Laplace transform methods etc. Exact solutions to general partial differential equations are difficult to obtain due to irregular and geometrically complicated domains and geometric and material nonlinearities. Consequently, various methods of finding suitable approximate solutions have been under continuous development. Finite Difference Method (FDM) and Variational methods are more popular ones. The classical variational methods (Ritz, Galerkin and Kantorovich methods) that are applicable to the whole domain, are based either on the minimization of a quadratic functional associated with the given problem or on minimization of error in the approximation. The difficulty in applying these methods lies in constructing approximating functions of the dependent variable, which need to satisfy the geometric boundary conditions on irregular domains. The finite element method (FEM) which is an offshoot of the classical methods overcomes this difficulty and gained wide popularity.



and acceptance (Reddy, 1984, Reddy, 1986)

In FEM the given domain is subdivided into a finite number of small subdomains. The subdomains, called *finite elements*, are of geometrically simple shapes, and permit a systematic construction of the approximating functions. Generally these approximating functions are algebraic polynomials developed using interpolation theory, hence called interpolation functions, and are independent of the specific boundary conditions and problem data. Since the approximating functions are defined element-wise, the accuracy of the approximation can be improved by increasing the number of elements. The minimum degree of the polynomial used for the interpolation functions depends on the order of the differential equation and/or the associated functional of the problem being solved. This in turn dictates the number of interpolation points, called *nodes* to be identified in the element. Generally the nodes are placed on the boundary of the element such that they uniquely define the element geometry (like vertices of a triangular element). Additional nodes, which may be required to define the interpolation functions can be placed either inside or on the boundary of the element. The boundary nodes also facilitate in connecting the adjacent elements together by ensuring the primary degrees of freedom (the variables that appear in essential boundary conditions) to be the same at the common nodes. The nodal values of the element uniquely defines the function values within the element and they form the basic unknowns of the problem.

Though the FEM was originally formulated based on physical (intuitive) approach, mathematical basis was developed later. The mathematical approach being elegant and rigorous, is generally employed. The FEM

formulations are illustrated with elasticity problems. The formulation of finite element method can be divided into the following steps (Schwarz, 1988).

Step1 The Problem domain is discretized by dividing the total domain into elements. The elements in general have straight edges, but curved elements produce better approximation to the region. The region is replaced by *union* of approximating elements for computational purposes.

Step2 For each of the elements a suitable approximation to the dependent variable which describes the problem has to be chosen. Rational functions of independent space variables are suitable. The form of approximation depends on the shape of the element and also on the type of problem being solved. These functions are evaluated using interpolation theory and have to satisfy continuity requirements which are generally obvious from purely physical considerations. The continuity requirements are also necessary mathematically because the set of approximating functions has to form an admissible class for either extremum principle or weighted residual method. If u represents displacement field of a continuous medium, u and often its derivatives (eg. for plate and beam problems) must be continuous across the boundary of two adjacent elements. Elements with approximating functions satisfying the continuity requirements are called *conforming* elements.

2.3.1 Element Models and Approximating-Functions

The subdomains or elements makeup the domain and they approximately represent the domain. The collection of the elements is called the finite element mesh. Each element in the mesh is a closed and non-empty one. The approximating functions as mentioned in earlier sections have to satisfy the continuity requirements of the variational statement of the problem. The approximating functions, depending upon their degree, could be linear, quadratic, cubic polynomial functions of the dependent variable. If u^e represents an approximation to the displacement field defined in the domain of the element, it can be expressed by a $(p-1)^{th}$ degree polynomial of the independent variable x as

$$u^e = a_1 + a_2x + a_3x^2 + \dots + a_p x^{p-1} \quad (2.1)$$

The coefficients a_1, a_2 etc can be evaluated using the function values at the nodes (i.e. *nodal variables*) of the element. Then the approximating function u^e can be expressed as a linear combination of *basis functions* N_i^e with nodal variables as coefficients as follows.

$$u^e = \sum_{i=1}^p u_i^e N_i^e(x) \quad (2.2)$$

where u_i^e denotes the nodal values of the dependent variable u^e , and N_i are algebraic functions of x and are of degree $p-1$. The above equation must be valid for any nodal variable u_i^e of node i ; the basis functions $N_i^e(x)$ must possess the interpolation characteristic that at

Convergence requirements :

In any numerical formulation, solutions obtained must converge or tend to the exact solutions of the problem. In displacement formulation the approximating functions have to satisfy certain requirements to ensure the convergence (Desai and Abel, 1972).

1. *The displacement models must include the rigid body modes.* This can be achieved by having constant terms in the model (like a_1 in equation 2.5).
2. *The displacement models should include the constant strain states of the element.* As element size approaches zero, the element strain approaches a constant value. To incorporate this behaviour the model must have terms associated with constant strain (like a_1 in equation 2.5).
3. *The displacement models must be continuous within the elements.* The continuity requirement can be met by choosing polynomial models for approximating functions.

Elements satisfying both second and third conditions are called complete elements.

Elements satisfying patch test will converge (Reddy 1986).

Element Models

The elements can be classified based on the degree of the approximating (interpolation) functions. They could be linear, quadratic, cubic *etc.* The interpolation functions can be constructed using Lagrange interpolation, Hermite interpolation, *etc.* The principles would be illustrated with a one-dimensional elements and the procedures for constructing the interpolation functions for two and three dimensional elements will be indicated.

1-dimensional Elements

A typical one-dimensional element family is shown in Figure 2.1. Let u^e be dependent variable and x the independent variable. For linear element of length h , u^e can be approximated as

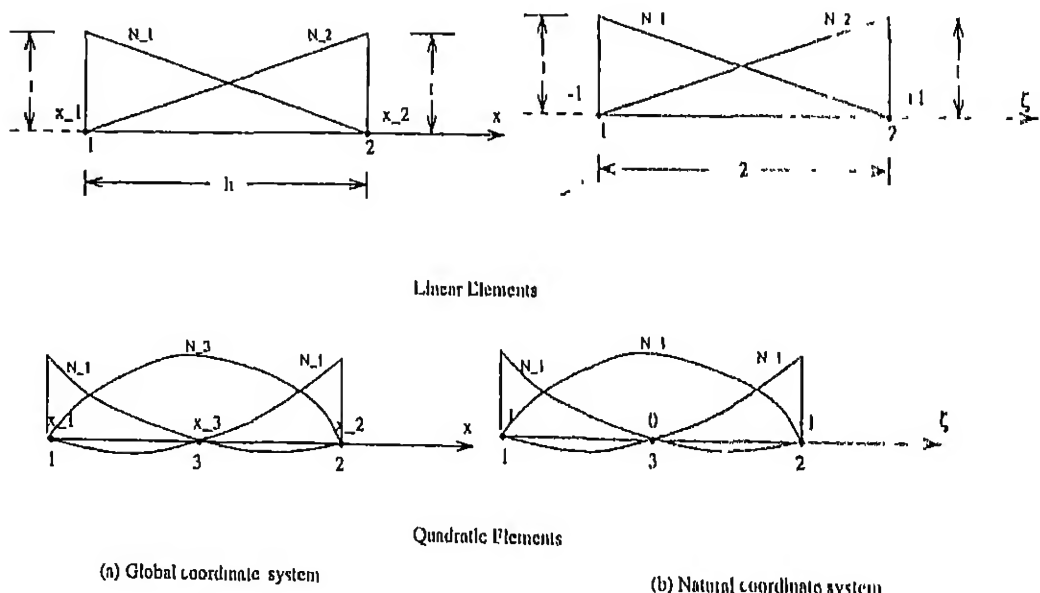


Figure 2.1: Typical One-dimensional Elements

$$u^e = a_1 + a_2 x \quad (2.5)$$

Constants a_1 and a_2 can be evaluated utilizing the nodal variables of u^e at nodes 1 and 2 in the above equation, i.e

$$\begin{aligned} x = 0, u = u_1 = a_1 \\ x = h, u = u_2 = a_1 + a_2 h \end{aligned} \quad (2.6)$$

Solving the above equation for coefficients a_1 and a_2 the (2.5) can be written as

$$u^e = N_1 u_1 + N_2 u_2 \quad (2.7)$$

Putting the same in matrix notation

$$u^e = [N_1, N_2] \begin{Bmatrix} u_1 \\ u_2 \end{Bmatrix} = [N^e] \{u^e\} \quad (2.8)$$

where

$$N_1 = 1 - x/h \text{ and } N_2 = x/h \quad (2.9)$$

N_1 and N_2 are called shape functions because they define the shape of the variation of u^e . $[N^e]$ is a row vector of shape functions containing N_1, N_2 and $\{u^e\}$ is a vector of nodal variables u_1, u_2 . As already mentioned in the earlier section, the shape functions can be constructed making use of interpolation theory (such as Lagrange's).

For example for a three noded element, the approximating function can be written as

$$u^e = [N_1, N_2, N_3] \begin{Bmatrix} u_1 \\ u_3 \\ u_2 \end{Bmatrix} \quad (2.10)$$

Now the shape functions N_1, N_2, N_3 are quadratic functions of the independent variable x , and can be constructed using Lagrange's interpolation as follows

$$N_i = \prod_{j \neq i}^n \frac{(x - x_j)}{(x_i - x_j)} \quad (2.11)$$

Where \prod indicates product of all possible terms and n denotes number of nodes of the element.

2 and 3-dimensional Elements

Shape functions of two and three dimensional elements can be constructed as products of corresponding shape functions of one dimensional elements in each direction.

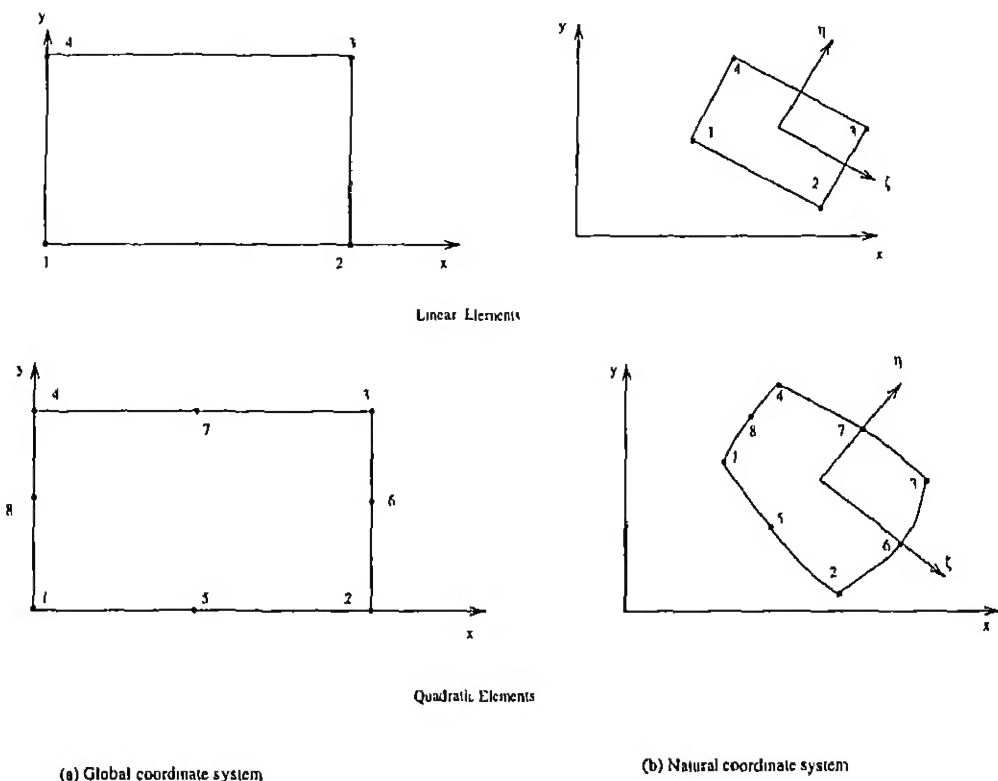


Figure 2.2 Typical Two-dimensional Elements

Typical rectangular elements of linear and quadratic interpolation are shown in Figure 2.2. The shape functions N_1 to N_4 for the linear element can be constructed from its 1-dimensional counterpart as follows:

$$N_1(x, y) = N_1(x) * N_1(y)$$

$$N_2(x, y) = N_2(x) * N_1(y)$$

$$N_3(x, y) = N_2(x) * N_2(y)$$

$$N_4(x, y) = N_1(x) * N_2(y) \quad (2.12)$$

Quadratic element shape functions can be constructed in a similar

fashion. The serendipity elements, which are special family of elements (Figure 2.2) will have nodes only on the boundary of the element. Construction of shape functions for the higher order (2 and above) serendipity elements need special treatment (see Hughes, 1987 for details).

Natural coordinates and isoparametric elements

To facilitate generalization of computation of the shape functions and element matrices a local (element) coordinate system will be beneficial. A natural coordinate system is a local coordinate system in which a point is specified in terms of dimensionless numbers whose magnitude does not exceed unity. A natural coordinate system for one-dimensional element is shown in Figure 2.1. The relationship between natural coordinate ζ and the physical coordinate x can be written as

$$\zeta = \frac{2x - (x_2 + x_1)}{x_2 - x_1} \quad (2.13)$$

As earlier pointed out the accuracy depends on the approximation of the domain by individual elements. To represent curved boundaries a coordinate mapping in which an element described in natural coordinate system is mapped on to a curved element described in physical (global) coordinate system. If the interpolation functions used for dependent variable approximation and the functions used for coordinate mapping are same then the elements are called isoparametric elements. The coordinate mapping in one dimension can be expressed as

$$x = [N_1 N_2] \begin{Bmatrix} \gamma_1 \\ \gamma_2 \end{Bmatrix} = [N] \{ \gamma \} \quad (2.14)$$

Now the interpolation (mapping) functions N_1 and N_2 can be rewritten in terms of natural coordinate ζ as

$$N_1 = \frac{1}{2}(1 - \zeta) \text{ and } N_2 = \frac{1}{2}(1 + \zeta) \quad (2.15)$$

Similar expressions can be developed for 2 and 3-dimensional elements analogously as follows. Typical isoparametric elements in 2-dimensions are shown in Figure 2.2. The coordinate mapping in two dimension can be expressed as

$$\begin{Bmatrix} x \\ y \end{Bmatrix} = \begin{bmatrix} N_1 & 0 & N_2 & 0 & N_3 & 0 & N_4 & 0 \\ 0 & N_1 & 0 & N_2 & 0 & N_3 & 0 & N_4 \end{bmatrix} \begin{Bmatrix} x_1 \\ y_1 \\ x_2 \\ y_2 \\ x_3 \\ y_3 \\ x_4 \\ y_4 \end{Bmatrix} \quad (2.16)$$

The above equation can be generalized for n -dimensional space as

$$\mathbf{x} = [\mathbf{N}_i] \{ \mathbf{x}_i \} \quad (2.17)$$

where \mathbf{x} and \mathbf{x}_i are the vectors of independent variables, and coordinates for the node i respectively; $[\mathbf{N}_i]$ is a diagonal sub matrix of order

equal to the number of space dimensions. Each of its entry equals to mapping function of the node. Expressing the same mathematically

$$\mathbf{x} = [x \ y \ z \ \dots]^T$$

$$[\mathbf{N}_i] = \begin{bmatrix} N_i & 0 & 0 & \dots & 0 \\ 0 & N_i & 0 & \dots & 0 \\ 0 & 0 & N_i & \dots & 0 \\ \dots & \dots & \dots & \dots & \dots \\ 0 & 0 & 0 & \dots & N_i \end{bmatrix}$$

$$\mathbf{x}_i = [x_i \ y_i \ z_i \ \dots]^T \quad (2.18)$$

The interpolation (mapping) functions N_1 to N_4 of the bilinear (linear in each direction) quadrilateral element (Figure 2.2) can be written from its one dimensional counter part (linear element) in natural coordinates as follows:

$$N_1 = \frac{1}{4}(1 - \zeta)(1 - \eta)$$

$$N_2 = \frac{1}{4}(1 + \zeta)(1 - \eta)$$

$$N_3 = \frac{1}{4}(1 + \zeta)(1 + \eta)$$

$$N_4 = \frac{1}{4}(1 - \zeta)(1 + \eta) \quad (2.19)$$

Since approximating functions are same as the mapping functions in isoparametric element scheme, the dependent variables can be written in terms of their nodal values as

$$\mathbf{u} = [\mathbf{N}_i] \left\{ \begin{array}{c} \mathbf{u}_i \end{array} \right\} \quad (2.20)$$

here u and u_n are arrays of dependent variables and it's nodal values respectively

2.3.2 Formulation

The basic formulation can be arrived at using different methods. Some of the popular methods are – 1. Ritz formulation and 2. Weighted Residual formulations. In Ritz formulation a suitable functional is constructed from the physics of the problem, whereas the differential equation governing the behaviour is used in weighted residual formulation.

For elasticity problems a suitable functional can be obtained using principles such as Principle of Minimum Potential energy (displacement formulation), Principle of Minimum Complimentary Energy (Stress formulation), Hamilton's Principle (dynamic problems) and Hellinger – Resissner Principle (Mixed formulation). The functionals so constructed using the above principles can be used with Ritz type formulation. Alternatively Differential equations governing the behaviour can be used with weighted Residual Formulation.

Ritz Formulation

In Ritz Formulation a functional with stationary properties is constructed by applying one of the above mentioned principles. The methodology is illustrated applying the principles for a static elasticity problem in the following paragraphs. Let Π denote the potential energy of an elastic body, it can be expressed as

$$\Pi = \frac{1}{2} \int_{\Omega} \epsilon^T \sigma dv - \int_{\Omega} u^T f dv - \int_{\Gamma} u^T \tau ds \quad (2.21)$$

The potential energy of the whole body can be expressed as the sum of the potential energies of the individual elements nel

$$\Pi = \sum_{i=1}^{nel} \left[\frac{1}{2} \int_{\Omega} \epsilon^{eT} \sigma^e dv - \int_{\Omega} u^{eT} f^e dv - \int_{\Gamma} u^{eT} \tau^e ds \right] \quad (2.22)$$

where u , ϵ , σ are vectors of displacements, strains and stresses; f and τ are the vectors of body forces and surface tractions respectively. Ω denotes the domain of the body and Γ is the boundary of the body. The variables with superscript e refers to the corresponding elemental quantities.

Using the linear constitutive relations, stresses can be expressed as

$$\sigma = [E]\epsilon \text{ and } \sigma^e = [E]\epsilon^e \quad (2.23)$$

where $[E]$ denotes elasticity matrix.

Assuming small strain theory, strains can be defined in terms of displacements using differential operator $[L]$ as

$$\epsilon = [L]u \quad (2.24)$$

The differential operator $[L]$ depends on the nature of the problem. For 2-Dimensional problems, it can be written as

$$[L] = \begin{bmatrix} \frac{\partial}{\partial x} & 0 \\ 0 & \frac{\partial}{\partial \tau} \\ \frac{\partial}{\partial y} & \frac{\partial}{\partial \tau} \end{bmatrix} \quad (2.25)$$

Similar relations hold for elemental quantities also, making use of the approximation (Equation 2.8) of the element displacements; element strains can be expressed as

$$\epsilon^e = [L]u^e = [L][N]\{u^e\} = [B]\{u^e\} \quad (2.26)$$

where matrix $[B]$ relates element strains to nodal displacement variables.

Substituting the expressions for stresses and strains in the (2.22) results

$$\Pi = \sum_{i=1}^{nel} \left[\frac{1}{2} \int_{\Omega^e} \{u^e\}^T [B]^T [E] [B] \{u^e\} dv - \int_{\Omega^e} \{u^e\}^T [N]^T \{f^e\} dv - \int_{\Gamma^e} \{u^e\}^T [N]^T \{\tau^e\} ds \right] \quad (2.27)$$

where Ω^e and Γ^e denote the domain and boundary of the element. Taking variation of both sides and setting it to zero (stationary condition) we get the algebraic equation governing the behaviour in terms of the nodal variables.

$$\delta \Pi = \sum_{i=1}^{nel} \{\delta u^e\} \left[\int_{\Omega^e} [B]^T [E] [B] \{\delta u^e\} dv - \int_{\Omega^e} [N]^T \{f^e\} dv - \int_{\Gamma^e} [N]^T \{\tau^e\} ds \right] = 0 \quad (2.28)$$

Since the variation $\{\delta u^e\}$ is arbitrary the expression inside the parenthesis should vanish, resulting in an algebraic equation in nodal variables, *i.e.*

$$[K]\{U\} = \{P\} \quad (2.29)$$

where

$$[K] = \sum_{i=1}^{nel} [K^e] \text{ and } [K^e] = \int_{\Omega^e} [B]^T [E] [B] dv \quad (2.30)$$

and

$$\{P\} = \sum_{i=1}^{nel} \{p^e\} \text{ and } \{p^e\} = \int_{\Omega^e} [N]^T \{f^e\} dv - \int_{\Gamma^e} [N]^T \{r\} ds \quad (2.31)$$

$[K^e]$ and $\{p^e\}$ are called *element* stiffness matrix and element load vector respectively; $[K]$ and $\{P\}$ are called *global* stiffness and load vector respectively. The summation sign in equations (2.30, 2.31) indicates assembly of the corresponding element quantities.

Weighted residual formulation

Weighted residual formulation can be used if construction of a functional is not obvious or difficult as in the case of nonlinear problems. This formulation makes use of the differential equations governing the behaviour. The approximating functions of the dependent variable (solution) are constructed as explained in the earlier section. This approximate solution is substituted in the differential equation and

the residue is minimized over the domain (each element). Depending upon the choice of weighting functions for minimization of the residue, different schemes are developed. In Galerkin's method interpolation functions are used as weighting functions. This method generates symmetric stiffness matrices for self adjoint differential operators. Let the equation governing the behaviour of the problem in the domain Ω with the boundary conditions on the boundary Γ , be

$$\mathcal{L}(u) = 0 \text{ in domain } \Omega \quad (2.32)$$

$$\mathcal{C}(u) = 0 \text{ on the boundary } \Gamma \quad (2.33)$$

Where \mathcal{L} and \mathcal{C} are differential operators.

The residue R over the whole domain Ω is the sum of the residues of each element of domain Ω^e which is obtained by substituting the approximate solution u^e defined over each of the elements in the above equation. i.e

$$R = \sum_{i=1}^{nel} R^e = \sum_{i=1}^{nel} \mathcal{L}(u^e) \quad (2.34)$$

Approximate solution can be obtained by minimizing the residue with respect to a set of weighting function. The weighting functions are chosen to be shape functions in Galerkin's method. Now the unknown nodal variables appearing in the approximate solutions can be obtained by solving the resulting algebraic equations,

$$\int_{\Omega} \{N_i\}^T R d\Omega = 0 \quad (2.35)$$

This can be expressed in terms of element quantities as

$$\sum_{i=1}^{ne} \int_{\Omega^e} [N]^T \mathcal{L}([N]) \{u^e\} d\Omega^e = 0 \quad (2.36)$$

The continuity requirements of the shape function (approximating functions) depend on the order of the operator \mathcal{L} . This can be reduced by carrying out the integration by parts. The above equation produces a set of simultaneous equations in unknown nodal variables.

2.3.3 Application of FEM to Dynamic problems

In this section the implementation of the Finite Element Method for spatial discretization is discussed. A displacement type formulation uses nodal displacements u, v, w as primary variables. Variational formulation has been utilized to develop the procedure for spatial discretization. Hamilton's principle has been used to construct the functional. The principle is stated as follows (Desai and Abel, 1972)

Among all possible time histories of displacement configurations which satisfy compatibility and the constraints or kinematic boundary conditions and which also satisfy conditions at time t_1 and t_2 , the history which is the actual solution makes the Lagrangian functional a minimum.

This can be stated as

$$\delta \int_{t_1}^{t_2} \mathcal{L} dt = 0 \quad (2.37)$$

where δ indicates the variation of the integral and \mathcal{L} is the Lagrangian which can be expressed as

$$\mathcal{L} = T - P - W \quad (2.38)$$

where T , P , and W are kinetic energy, strain energy and potential energy of the applied loads. Accordingly

$$\mathcal{L} = \frac{1}{2} \int_{\Omega} [u^T \rho u - \dot{\epsilon}^T \sigma] dv + \int_{\Omega} \dot{u}^T f dv + \int_{\Gamma} u^T \tau ds \quad (2.39)$$

where ρ is mass density of the material, dots denote the time derivative of the variables.

Lagrangian \mathcal{L} of the whole domain can be written as sum of the contributions over each of the elements, *i.e.*

$$\begin{aligned} \mathcal{L} = & \sum_{i=1}^{nel} \left[\frac{1}{2} \int_{\Omega^e} \left\{ u^e T \rho \dot{u}^e - \dot{\epsilon}^e T \sigma^e \right\} dv \right. \\ & \left. + \int_{\Omega^e} u^e T f^e dv + \int_{\Gamma^e} u^e T \tau^e ds \right] \end{aligned} \quad (2.40)$$

Substituting for the approximate displacement vector u^e defined over each of the element and stress strain relations in the above equation results

$$\begin{aligned} \mathcal{L} = & \sum_{i=1}^{nel} \left[\frac{1}{2} \int_{\Omega^e} \left(\rho \{u^e\}^T [N]^T [N] \{u^e\} - \{u^e\}^T [B]^T [E] [B] \{u^e\} \right) dv \right. \\ & \left. + \int_{\Omega^e} \{u^e\}^T [N]^T \{f^e\} dv + \int_{\Gamma^e} \{u^e\}^T [N]^T \{\tau^e\} ds \right] \end{aligned} \quad (2.41)$$

Hereafter the summation symbol is omitted for the sake of conciseness and wherever elemental quantities appear, usual summation (assembly)

over the elements is implied. Substituting the above expression for Lagrangian in (2.37) results

$$\int_{t_1}^{t_2} \left[\rho \{ \delta u^e \}^T \left(\int_{\Omega^e} [N]^T [N] \{ u^e \} dv \right) - \{ \delta u^e \}^T \left(\int_{\Omega^e} [B]^T [E] [B] \{ u^e \} dv \right. \right. \\ \left. \left. - \int_{\Omega^e} [N]^T \{ f^e \} dv - \int_{\Gamma^e} [N]^T \{ \tau^e \} ds \right) \right] dt = 0 \quad (2.42)$$

Integrating the first term

$$\int_{t_1}^{t_2} \left[\rho \{ \delta \dot{u}^e \}^T \int_{\Omega^e} [N]^T [N] \{ u^e \} dv \right] dt = \left[\rho \{ \delta u^e \} \left(\int_{\Omega^e} [N]^T [N] \{ u^e \} dv \right) \right]_{t_1}^{t_2} \\ - \int_{t_1}^{t_2} \left[\rho \{ \delta u^e \} \left(\int_{\Omega^e} [N]^T [N] \{ \ddot{u}^e \} dv \right) \right] dt \quad (2.43)$$

substituting this expression in the (2.42) results

$$\left[\{ \delta u^e \} \int_{\Omega^e} \rho [N]^T [N] \{ u^e \} dv \right]_{t_1}^{t_2} \\ - \int_{t_1}^{t_2} \{ \delta u^e \} \left[\int_{\Omega^e} \left(\rho [N]^T [N] \{ \ddot{u}^e \} + [B]^T [E] [B] \{ u^e \} \right) dv \right. \\ \left. - \int_{\Omega^e} [N]^T \{ f^e \} dv - \int_{\Gamma^e} [N]^T \{ \tau^e \} ds \right] dt = 0 \quad (2.44)$$

The first term in the right hand side (r.h.s) vanishes because because the displacement configurations should satisfy the boundary conditions at times t_1 , and t_2 (Hamilton's principle) *i.e.* the variation $\{ \delta u^e \}$ should be equal to zero at times t_1 , and t_2 . Rest of the expression inside the parenthesis should also vanish because the variation is arbitrary. The resulting equation can be written as

$$[M^e]\{u^e\} + [K^e]\{u^e\} = \{p^e\} \quad (2.45)$$

where $[M^e]$ is element mass matrix and is given by

$$[M^e] = \int_{\Omega^e} \rho [N]^T [N] dv \quad (2.46)$$

Assembling the element matrices results in a system of differential equations (equations of motion) governing the behaviour of the body as follows

$$[M]\{U\} + [K]\{U\} = \{P\} \quad (2.47)$$

Here the vectors U , and P are time dependent.

Mass Matrices

The mass matrix defined by the above equation is called consistent mass matrix because the same shape functions $[N]$ are used to generate the stiffness matrix. Often a diagonal form of the mass matrix is adopted assuming that the mass of the body is concentrated (lumped) only at the nodes of the body *i.e.* the continuum is discretized as particle *lumps*. This form of the matrix is diagonal and is called lumped mass matrix. The procedure is called adhoc lumping. Numerical integration (special) rules which produce a diagonal consistent mass matrix are possible for simple elements only. Usually it is recommended that consistent mass matrices be used for natural frequency computations and lumped mass matrices be used for wave propagation problems (Cook,

1974) Diagonal mass matrices are computationally advantageous and require less storage. In this investigation a *systematic lumping* method is adopted which performs better than both adhoc lumping and consistent mass matrices. In this method only diagonal entries of the consistent mass matrix are generated and they are scaled so that mass of the element is conserved.

Damping

Damping in dynamic soil-structure interaction is present in two forms – 1. Radiation damping and 2. Material damping. The radiation damping is due to the infinite extent of soil in which energy is lost in the form of outgoing waves. Analytical formulations can incorporate the infinite extent of the soil, but computational methods which work with finite domains like FEM can not incorporate the same. As already mentioned the concept of infinite extent can not be incorporated in FEM formulation and hence *A Large Mesh* is considered for discretization. The energy at large distances is negligibly small and the reflections do not influence the accuracy of the solutions. The material damping is due to hysteresis in the material. The treatment of the material damping in computational analyzes is often specified in terms of equivalent viscous damping. This is introduced by means of specified fractions of *critical damping*, or Rayleigh or proportional damping in which damping matrix is specified as a linear combination of mass and stiffness matrices. The former description is advantageous in frequency domain analysis, whereas the later form is used in time domain analysis. The Rayleigh damping is utilized in the present investigation. The damping matrix $[C]$ can be expressed as

$$[C] = \alpha[K] + \beta[M] \quad (2.48)$$

where α and β are called the stiffness and mass proportional damping constants respectively. Incorporating the damping defined as above the equation of motion becomes

$$[M]\{U\} + [C]\{U\} + [K]\{U\} = \{P\} \quad (2.49)$$

The above equation which describes the behaviour of the dynamical system is transformed to Lanczos space as explained in the next section. The transformed equations are used in time stepping scheme. The time histories of the generalized coordinates (of transformed domain) are projected on to the original space to obtain the displacement histories *etc.* Hereafter the parenthesis around a variable $[]$ indicating they represent a matrix will be omitted for conciseness.

2.4 Lanczos Method

2.4.1 Introduction

Lanczos method is originally devised to extract some (not all) eigen values and eigen vectors of an eigen system. It involves generation of orthonormal sequence of vectors known as Lanczos vectors iteratively from Krylov subspace. At each step the current vector is normalized with two previous vectors and build a tridiagonal matrix whose eigen values and eigen vectors are Rayleigh-Ritz approximations of the original system. This method (theoretically) terminates after n (order

of the system) iterations. But, in practice, due to finite precision of numerical computation, the Lanczos vectors loose their orthogonality and may need re-orthogonalization frequently (see Paige, 1976). The same procedure is extended to generalized eigen value problems. The loss of orthogonality of Lanczos vectors is investigated by Paige (1976). Different schemes – total re-orthogonalization (Wilson, Yuan and Dickens, 1979), selective re-orthogonalization (Parlett and Scott, 1979), and partial re-orthogonalization (Simon, 1984), are suggested to overcome the problem.

The Lanczos vectors which are orthonormal, can also be used to construct a coordinate transformation matrix to be used in the solution of dynamic equilibrium equations. Recently Wilson, Yuan and Dickens (1979) and Ibrahimbegovic, Harn, *et al.* (1990) developed a methodology to generate a set of orthogonal (Lanczos) vectors for use in coordinate transformation as an alternative to conventional mode super position method. Nour-Omid and Clough (1984) showed that Lanczos vectors can be used to solve structural dynamic problems in time-domain. The basic methodology as implemented in this investigation in generating Lanczos vectors is described here briefly.

2.4.2 Lanczos algorithm

The Lanczos vectors are generated spanning the Krylov sub space defined by the sequence of vectors r , $(K^{-1}M)^1 r$, $(K^{-1}M)^2 r$, $(K^{-1}M)^3 r$, ..., $(K^{-1}M)^m r$, given the pair of matrices K and M and r being an arbitrary vector. The sequence of vectors converges to an eigen vector corresponding to the smallest eigen value of the generalized eigen value problem defined by the equation.

$$(K - \lambda M)z = 0 \quad (2.50)$$

In dynamic response analysis the orthonormal sequence of vectors from Krylov subspace will be utilized for coordinate transformation. Different schemes (see Cullum and Willoughby, 1985) are available for generation of Lanczos vectors for eigen vector computation. In Lanczos algorithm, Gram-Schmidt orthogonalization (Cullum and Willoughby, 1985) will be employed at each step to normalize the current vector with respect to matrix M and the two previous vectors of the Krylov sequence. The result will be a set of m orthonormal vectors.

Let (q_1, q_2, \dots, q_j) be j Lanczos vectors generated and $j+1^{th}$ vector is to be found. Then q_{j+1} can be calculated by first computing a preliminary vector from the Krylov sequence

$$\bar{r}_j = K^{-1}Mq_j \quad (2.51)$$

Now the preliminary vector will be normalized with two preceding vectors q_{j-2} , q_{j-1} as

$$\bar{r}_j = r_j + \alpha_j q_j + \beta_j q_{j-1} + \gamma_j q_{j-2} + \dots \quad (2.52)$$

where r_j is pure vector orthogonal to two previous vectors and α_j , β_j and γ_j are the amplitudes of the previous vector contained in \bar{r}_j . The coefficients can be evaluated using the orthonormality of Lanczos vectors. Premultiplying the above equation by $q_j^T M$, and noting the M orthonormality of the vectors, except first term all other terms on the right hand side vanish, resulting in

$$\alpha_j = q_j^T M \bar{r}_j \quad (2.53)$$

Similarly β_j can be evaluated as

$$\beta_j = q_{j-1}^T M \bar{r}_j \quad (2.54)$$

Replacing \bar{r}_j by its expression from (2.52) we get

$$\beta_j = q_{j-1}^T M K - 1 M q_j = r_{j-1}^T M q_j \quad (2.55)$$

Expanding \bar{r}_{j-1} in terms of its pure vector r_{j-1} substituting in the transpose of (2.55) β_j becomes

$$\beta_j = q^T M r_{j-1} + \alpha_{j-1} q_j^T M q_{j-1} + \beta_{j-1} q_j^T M q_{j-2} + \dots \quad (2.56)$$

It is obvious that all terms except the first vanish on the right hand side of the above equation. Now q_j is the vector obtained by normalizing r_{j-1} with β_j , i.e.

$$q_j = \frac{1}{\beta_j} r_{j-1} \quad (2.57)$$

Substituting this expression in (2.56) results

$$\beta_j = \frac{1}{\beta_j} r_{j-1} M r_{j-1} \quad (2.58)$$

Then the value of β_j will be

$$\beta_j^2 = r_{j-1} M r_{j-1} \quad (2.59)$$

In a similar procedure it can be shown that γ_j and rest of the coefficient of the terms in (2.52) can be shown to zero

In summary, the process of generating the Lanczos vectors can be expressed as follows:

Choose $q_0 = 0$, a starting vector r_0 and $\beta_1 = (r_0^T M r_0)^{1/2}$. then,

For $j = 1, 2, \dots, m$ compute q_j

$$q_j = \frac{r_{j-1}}{\beta_j} \quad (2.60)$$

$$\bar{r}_j = K^{-1} M q_j \quad (2.61)$$

$$r_j = \bar{r}_j - \alpha_j q_j - \beta_j q_{j-1} \quad (2.62)$$

$$\alpha_j = \bar{r}_j^T M q_j \quad (2.63)$$

$$\beta_{j+1} = (r_j^T M r_j)^{1/2} \quad (2.64)$$

2.4.3 Starting vector

The starting vector r_0 , in general can be chosen arbitrarily. If the starting vector is related to loading amplitudes we may expect that the modes which are contributing to the response will be included. Thus the starting vector is taken to be static displacement vector given by

$$r_0 = K^{-1} P \quad (2.65)$$

where P is the vector of loading amplitudes. Inclusion of the static displacement vector (Wilson, Yuan and Dickens, 1979) avoids any possible need of applying static correction, because the static displacements are included in the coordinate transformation itself. More over for

small number of Lanczos steps, the basis vectors will be Rayleigh Ritz approximations of scattered eigen vectors non orthogonal to loading amplitudes in the Krylov sequence. The coordinate transformation matrix will contain approximations of eigen vectors of higher modes excited by the loading, resulting in a small number of basis vectors.

2.4.4 Loss of orthogonality of Lanczos vectors

As mentioned in earlier section the Lanczos vectors loose orthogonality due to the finite precision arithmetic. The simple Paige style algorithm (Paige, 1976) without re-orthogonalization may need large number of vectors ($m \gg n$) to isolate eigen vectors. However the use of Lanczos vectors can only be pursued in coordinate transformation if and only if few orthonormal vectors could produce results acceptable of accuracy. Hence re-orthogonalization of Lanczos vectors is essential in the application of coordinate transformation process.

The orthogonality of the Lanczos vectors can be maintained by re-orthogonalization. These methods can be categorized as - 1. Complete re-orthogonalization 2. Limited re-orthogonalization. In complete re-orthogonalization, the current vector is normalized with all previous vectors (Wilson, Yuan and Dickens, 1979). This process needs large core memory or secondary storage to store all previous vectors. Consequently the procedure is both I/O intensive and needs large computational resources. In the latter choice the re-orthogonalization is applied when found necessary. In limited re-orthogonalization the loss of orthogonality is monitored continuously (at the end of each step). Two variants of limited re-orthogonalization namely selective and partial re-orthogonalization schemes, which are useful in coordi-

nate transformation process are presented.

Selective re-orthogonalization

This method is suggested by Parlett and Scott (1979), wherein, re-orthogonalization is done against a few selected (not all previous) vectors when found necessary. It is suggested by Paige (1980) that loss of orthogonality is due to presence of components of converged Ritz vectors of the system in the Lanczos vectors. This fact is made use of in selective re-orthogonalization. The current vector is normalized with respect to all previously computed *converged* Ritz vectors. These Ritz vectors will be small in number, and they may be stored in core memory. A refined methodology is suggested Parlett and Nour-Omid (1985) to monitor the loss of orthogonality. The computation of Ritz vectors is carried out periodically rather than at the end of each step.

Partial re-orthogonalization

The aim of all re-orthogonalization schemes is to prevent loss of orthogonality *i.e.* to maintain a certain level of orthogonality among Lanczos vectors. We define level of orthogonality κ among the Lanczos vectors at j^{th} step as

$$\kappa = \max_{1 \leq k \leq j-1} q_j^T q_k \quad (2.66)$$

The full re-orthogonalization of q_j against all previous vectors maintains level of orthogonality κ a round of level ϵ . However numerical results suggest (Parlett and Scott, 1979, Simon, 1984) that semi-orthogonality *i.e.* $\kappa = \sqrt{\epsilon}$, among the Lanczos vectors is sufficient to prevent spurious

eigen values. This scheme suggested by Simon (1984), maintains semi-orthogonality among the Lanczos vectors. The monitoring of loss of orthogonality is done by updating an array consisting of levels of orthogonality. These levels of orthogonality are not computed explicitly, rather they are computed using a simple recurrence relation suggested by Simon (1984). Let ω 's refer to the level of orthogonality between the Lanczos vectors referred by its subscripts. Then

$$\begin{aligned}\omega_{k,k} &= 1 \text{ for } k = 1, \dots, j \\ \omega_{k,k-1} &= q_k^T q_{k-1} \text{ for } k = 2, \dots, j \\ \beta_{j+1} \omega_{j+1,k} &= \beta_{k+1} \omega_{j,k+1} + (\alpha_k - \alpha_j) \omega_{j,k} + \beta_k \omega_{j,k-1} - \beta_j \omega_{j-1,k} + \psi_{j,k}\end{aligned}\quad (2.67)$$

where $\psi_{j,k}$ is a random number to account for roundoff errors. It is suggested by Simon (1984) that $\psi_{j,k}$ can be taken to be random number with 0- mean and ϵ - standard deviation. Here it should be noted that the ω 's are estimated or computed levels of orthogonality but found to be very close to the actual ones (Simon, 1984).

At k^{th} stage, update the recurrence relation for $\omega_{j+1,k}$ and find the vectors whose levels of orthogonality exceeded the semi-orthogonality level. *i.e.*

$$\text{for } k = 1, 2, \dots, j \text{ find } j's \text{ such that } \|\omega_{j+1,k}\| \geq \sqrt{\epsilon} \quad (2.68)$$

The vectors which satisfy the above equation are re-orthogonalized with current and next vector and corresponding ω 's are reset to ϵ . It is found that both Selective and Partial reorthogonalizations require comparable computational effort (Simon, 1984). The Selective re-

orthogonalization is more suitable for eigenvalue computations since Ritz vectors are computed periodically for re-orthogonalization. Whereas Partial re-orthogonalization schemes is suitable in case Lanczos vectors are intended to be used for solution of simultaneous equations and coordinate transformation. Here, in this investigation Partial re-orthogonalization scheme is chosen because of its simplicity.

2.4.5 Number of Vectors

The number of vectors required to obtain the results with desired accuracy can be obtained as follows. According Bayo and Wilson (1984) and Coutinho, Landau, *et al.* (1987) a measure of error introduced in the the loading function in the transformed space can be used to gauge the accuracy of representation. It is expected that lower the error higher is the accuracy. Let the transformation matrix be ϕ be defined by the relation

$$U = \phi X \quad (2.69)$$

where X is the generalized displacement vector in the new coordinates space and $\phi = [\phi_1, \phi_2, \dots, \phi_m]$, $m < n$ is the coordinate transformation matrix. The dynamic response $U(t)$ is now approximated by a linear combination of generalized displacements $X(t)$. Substituting for U in (2.49), we get

$$\bar{M} \dot{X} + \bar{C} \dot{X} + \bar{K} X = \bar{P}(t) \quad (2.70)$$

where \bar{M} , \bar{C} , \bar{K} and are generalized mass, damping, and stiffness

matrices and $\bar{P}(t)$ is the generalized load vector respectively and are given by the following equations.

$$\bar{M} = \phi^T M \phi \quad (2.71)$$

$$\bar{C} = \phi^T C \phi \quad (2.72)$$

$$\bar{K} = \phi^T K \phi \quad (2.73)$$

$$\bar{P}(t) = \phi^T P(t) \quad (2.74)$$

Premultiplying the (2.71) by $M\phi$ and considering the spatial variation only, the load representation P_m in original space incorporated in the analysis can be expressed as

$$P_m = \sum_{j=1}^m M\phi_j \bar{p}_j \quad (2.75)$$

where p_j is j th participation factor and is given by

$$\bar{p}_j = \phi_j^T P \quad (2.76)$$

Now the error E in loading representation can be expressed as

$$E = P - P_m \quad (2.77)$$

It is convenient to express the error in suitable norm relative to the original load as

$$e = \frac{\|P^T E\|}{\|P^T P\|} \quad (2.78)$$

The relative error norm e will lie between 1 (for $m = 0$ i.e. 0 vectors are used) and 0 (for $m = n$ i.e. all vectors are used). A suitable value of error tolerance (relative viz. in terms of percentage) may be specified and the Lanczos vectors are generated till the relative error norm e falls below the error tolerance of the load vectors.

2.4.6 Coordinate transformation matrix

Coordinate transformation matrix can be derived as follows:

- Triangularize the stiffness matrix K , i.e

$$K = L^T D L \quad (2.79)$$

- choose static displacement vector as r_0 as explained in the previous section
- generate m Lanczos vectors which are orthonormal (apply partial re-orthogonalization where necessary). Check whether relative error norm of load representation is less than error tolerance
- Project the stiffness matrix in to Lanczos subspace as

$$K_m = Q^T K Q, \quad Q = [q_1, q_2, \dots, q_m] \quad . \quad (2.80)$$

- Solve the eigen problem in Lanczos subspace

$$K_m Y = I_m Y \Omega_m, \quad Y = [y_1, y_2, \dots, y_m] \quad (2.81)$$

- Compute coordinate transformation matrix

$$\phi = QY \quad (2.82)$$

CENTRAL LIBRARY
I. I. T., KANPUR

Call No. A 125692

2.5 Direct Integration

2.5.1 Introduction

Dynamic analysis of engineering systems require temporal and often spatial discretization (for continuous systems). The spatial discretization results in a system of coupled differential equations such as (2.49), describing the physical behaviour. These equations, in principle, can be solved by direct integration. The direct integration method will be efficient in case the excitation is either transient or periodic consisting of combination of several frequencies. For nonlinear dynamic problems the direct integration methods are the only tools readily applicable. Direct integration schemes can be broadly divided into two categories

1. Single step methods and 2. Multi-step methods. Single step methods have a number of advantages over multi-step methods. They are self starting and amenable to time step modification. These methods are more convenient for nonlinear systems.

Linear multi-step (including single step) methods can be classified into two broad categories with reference to stability. As per Dahlquist (1963)

- An explicit algorithm which is unconditionally stable does not exist.
- Unconditionally stable algorithm of order greater than two does not exist.

Thus one category of algorithms are implicit with unconditional stability of order one and two. Newmark methods (order two) fall under

this category Zienkiewicz, Wood, *et al.* (1984) have developed a unified set of single step integration methods which are unconditionally stable. These algorithms are derived by weighted residual approach. In structural dynamic analysis computations damping out higher frequencies (called numerical damping) is a desirable property in addition to unconditional stability. The spectral radius of higher frequencies should be less than 1.0, whereas for low frequencies it should be close to 1.0. This can be achieved by making $\gamma > 0.5$ in Newmark methods, but order of accuracy falls below two. Hilber, Hughes and Taylor (1977) developed second order accurate method which they call α method with an additional parameter α . This method has the property of controllable damping (specified in terms of α). Another method (called Θ method) based on weighted residual technique is presented by Hoff and Pahl (1988) which has better order of accuracy and controllable numerical damping. The Θ method has only one free parameter θ , which controls numerical damping.

The other category falls under conditionally stable multi-step algorithms of order greater than two. Because of conditional stability and increase of the order of matrices by a factor of two, this class of algorithms are not investigated for use in structural dynamics. The higher order algorithms, because of higher accuracy, are viable alternatives if stability is ensured, produce more accurate solutions with less computational effort. However, as mentioned earlier, the desirable property of numerical damping, can not be incorporated in higher order methods like 4th order Runge-Kutta method and Adam-Moulton methods (Stoer and Bulirsch, 1980).

2.5.2 Θ method:

The Θ method of Hoff and Pahl (1988) which has been used in this investigation, is described briefly.

The dynamic equilibrium may be described by the original (Equation 2.49) or by the transformed (2.70) with the given initial conditions.

If x_n , v_n , a_n and P_n are the displacement, velocity, acceleration and force vectors at n th step respectively; then the corresponding quantities at $(n+1)^{th}$ step (with step size h) can be obtained as

$$a_{n+1} = a_n + \delta a \quad (2.83)$$

$$v_{n+1} = v_n + ha_n + (1.5 - \theta)h\delta a \quad (2.84)$$

$$x_{n+1} = x_n + hv_n + 0.5h^2a_n + \frac{1}{4\theta_1^2}h^2\delta a \quad (2.85)$$

$$M_m \delta a = \bar{P}_{n+1} - Ma_n - C\bar{v}_{n+1} - Kx_{n+1} \quad (2.86)$$

where

$$M_m = M + (1.5 - \theta_1)hC + \frac{1}{4\theta_1^2}h^2K$$

$$\bar{P}_{n+1} = P_n + \theta_1(P_{n+1} - P_n)$$

$$\bar{v}_{n+1} = v_n + \theta_1 ha_n$$

$$\bar{x}_{n+1} = x_n + \theta_1 hv_n + 0.5h^2a_n$$

with $0.95 \leq \theta_1 \leq 1.0$

The matrices K , C , M are the stiffness, damping and mass matrices of the system. P_n is the load vector at n th step. These quantities refer to the *transformed* system.

Since this is a second order method, the step size adjustment can be incorporated using Richardson extrapolation (Stoer and Bulirsch, 1980).

That is, compute the solution at time $t + h$ with step size h , and $h/2$. Then the difference of the solutions gives an estimate of error as

$$err = \left\| \frac{7}{8} (x_h - x_{h/2})^{1/3} \right\| \quad (2.87)$$

Where err is a measure of local truncation error, x_h and $x_{h/2}$ are displacement vectors at time $t+h$ with step sizes h and $h/2$ respectively. The symbol $\| \cdot \|$ here denotes a maximum norm.

2.5.3 Θ Method with post-processing

This method differs from the earlier one only in computation of local error. The post-processing of solution is done at the end of each step to estimate the error and consequently the step size required for prescribed error tolerance. In this method acceleration is assumed to be constant in each step. If a continuous (viz. linear) valued function of time is utilized for approximation of acceleration, more accurate results could be obtained (see Zeng, Wiberg, *et al.*, 1992). If a^* is the acceleration at any time t during the n^{th} step, it can be expressed as

$$a^* = a_n + \frac{t}{h} \delta a \quad (2.88)$$

where $t_n \leq t \leq t_{n+1}$ and $h = t_{n+1} - t_n$

Now the error in acceleration during the n^{th} step can be written as

$$e = a^* - a \quad (2.89)$$

where \mathbf{a} is the average acceleration vector during the n^{th} step and can be expressed as

$$\mathbf{a} = \left(1 - \frac{1}{2\theta_1^2}\right) \mathbf{a}_n + \frac{1}{2\theta_1^2} \mathbf{a}_{n+1} \quad (2.90)$$

The local truncation error in displacements is obtained by integrating the error in accelerations two times. A norm of error in displacements $\|err\|$ can be expressed as

$$\|err\| = \left(\frac{1}{6} + \frac{1}{4\theta_1^2}\right) h^2 \|\delta\mathbf{a}\| \quad (2.91)$$

Since the above norm is an absolute quantity and problem dependent specifying an absolute value is not feasible always. A relative error norm $\|err_{rel}\|$ which is the ratio of error norm $\|err\|$ and norm of the displacements at the current step is used for step size correction. *i.e.*

$$\|err_{rel}\| = \frac{\|err\|}{\|x\|} \quad (2.92)$$

Select the step size economically such that for each step, the local error roughly equals the prescribed error tolerance. This can be achieved as follows:

Define two parameters γ_1 and γ_2 such that $0 < \gamma_1 < 1$ and $\gamma_2 < 1$ and

$$\gamma_1 \epsilon \leq \|err_{rel}\| \leq \gamma_2 \epsilon \quad (2.93)$$

Accept the step if (2.93) is satisfied. In practice the step size adjustment is carried out if

1. Error is more than the upper limit of the tolerance ($\gamma_2 \epsilon$) or
2. Error falls below the lower limit of tolerance ($\gamma_1 \epsilon$) for *fixed number* of times (say 5–10) consecutively. This is to avoid costly factorization frequently needed whenever step change is made.

New step size can be calculated as

$$h_{new} = h * \left(\frac{\epsilon}{\epsilon \gamma_{rel}} \right)^{1/3} \quad (2.94)$$

2.6 Validation of the Model

2.6.1 Introduction

Before actually applying the model to three dimensional soil–structure interaction problems which this investigation aimed to address, it is considered appropriate to validate the model with two-dimensional problems of similar kind. The set problems considered by Von Estorff, Pais and Kausel (1990) are chosen for validation purposes. The problem set consist of 1. A half space and 2. A half space with a vertical trench. To simulate transient loading a fast decaying Ricker's wavelet (Von Estorff, Pais and Kausel, 1990) has been chosen. The effect of model parameters such as number of Lanczos vectors (Section 2.4.5) considered, size of the mesh, element size (number of elements) have been studied and reported here. The implementation of the model for these problems has been discussed in the following sections. The effect of different (from that of the problem to be solved) spatial distributions of the load is also considered for the generation of Lanczos vectors.

It will be useful to understand the effect of spatial variation of the load on the accuracy, and to evolve a simpler computation model for infinite domain independent of the loading.

2.6.2 FEM implementation

A 2-dimensional finite element model with 4 noded isoparametric elements is used in this implementation. A graded mesh (Figure 2.5) with ratio of maximum element size minimum element size (length/width) of 3.1 has been used. Since the problem is plane strain one, the elasticity matrix $[E]$ becomes

$$[E] = \frac{E}{(1+\nu)(1-2\nu)} \begin{bmatrix} 1-\nu & \nu & 0 & 0 \\ \nu & 1-\nu & 0 & 0 \\ 0 & 0 & 1-2\nu & 0 \\ 0 & 0 & 0 & 2 \end{bmatrix} \quad (2.95)$$

and the strain displacement matrix $[L]$ is defined in (2.25). The shape functions can be written as

$$[N]^T = \begin{Bmatrix} (1-\zeta)(1-\eta) \\ (1+\zeta)(1-\eta) \\ (1+\zeta)(1+\eta) \\ (1-\zeta)(1+\eta) \end{Bmatrix} \quad (2.96)$$

Substituting these expression in (2.30) and integrating over the domain (area) of the element, stiffness matrix $[K^e]$ can be written as

$$[K^e] = t \int_{A^e} [B]^T [E] [B] dx dy \quad (2.97)$$

where t is the thickness of the element (taken to be unity) and A^e is the area of the element. In 2-dimensional domain each node will have 2 degrees of freedom namely u , and v . The matrix B in this case can be written as (it will be of order of 3x8)

$$[B] = [L] \begin{bmatrix} N & 0 \\ 0 & N \end{bmatrix} \quad (2.98)$$

In isoparametric formulation the physical domain is mapped onto parametric domain using the same shape functions used for displacement approximation. The matrix operator $[L]$ contains derivatives of dependent variables (u, v) with respect to physical coordinates (x, y). Since the shape functions are expressed in natural coordinates ζ , and η , derivatives with respect to physical coordinates have to be computed using Jacobian transformation from natural coordinate space to physical coordinate space.

The derivatives with respect to natural coordinates can be expressed using chain rule as

$$\begin{aligned} \frac{\partial}{\partial \zeta} &= \frac{\partial x}{\partial \zeta} \frac{\partial}{\partial x} + \frac{\partial y}{\partial \zeta} \frac{\partial}{\partial y} \\ \frac{\partial}{\partial \eta} &= \frac{\partial x}{\partial \eta} \frac{\partial}{\partial x} + \frac{\partial y}{\partial \eta} \frac{\partial}{\partial y} \end{aligned} \quad (2.99)$$

The above equation can be expressed in matrix form as

$$\begin{Bmatrix} \frac{\partial}{\partial \zeta} \\ \frac{\partial}{\partial \eta} \end{Bmatrix} = \begin{bmatrix} \frac{\partial x}{\partial \zeta} & \frac{\partial y}{\partial \zeta} \\ \frac{\partial x}{\partial \eta} & \frac{\partial y}{\partial \eta} \end{bmatrix} \begin{Bmatrix} \frac{\partial}{\partial x} \\ \frac{\partial}{\partial y} \end{Bmatrix} = [J] \begin{Bmatrix} \frac{\partial}{\partial x} \\ \frac{\partial}{\partial y} \end{Bmatrix} \quad (2.100)$$

where matrix $[J]$ is called Jacobian of the transformation

Now the derivatives with respect to physical coordinates can be obtained as

$$\begin{Bmatrix} \frac{\partial}{\partial x} \\ \frac{\partial}{\partial y} \end{Bmatrix} = [J]^{-1} \begin{Bmatrix} \frac{\partial}{\partial \zeta} \\ \frac{\partial}{\partial \eta} \end{Bmatrix} \quad (2.101)$$

The Jacobian in the above equation can be evaluated from (2.16) as follows

$$[J] = \begin{bmatrix} \sum N_{i,\zeta} x_i & \sum N_{i,\zeta} y_i \\ \sum N_{i,\eta} x_i & \sum N_{i,\eta} y_i \end{bmatrix} \quad (2.102)$$

Where , indicates differentiation with respect to variable following it and \sum indicates summation over the number of nodes of the element, *viz*

$$\sum N_{i,\zeta} x_i = \frac{dN_1}{d\zeta} x_1 + \frac{dN_2}{d\zeta} x_2 + \frac{dN_3}{d\zeta} x_3 + \frac{dN_4}{d\zeta} x_4 \quad (2.103)$$

Replacing the physical coordinates x and y by their natural coordinates, the stiffness matrix can be expressed as

$$[K^e] = t \int_{-1}^{+1} \int_{-1}^{+1} [B]^T [E] [B] \|J\| d\zeta d\eta \quad (2.104)$$

where $\|J\|$ denotes the determinant of Jacobian.

Similarly the element mass matrix can be expressed as

$$[M^e] = t \int_{-1}^{+1} \int_{-1}^{+1} \rho [N]^T [N] \|J\| d\zeta d\eta \quad (2.105)$$

The integration is carried out using Gaussian quadrature. The element load and damping matrices are not computed, rather global load vector in terms of global variables are computed since loading exists only at one node. Since proportional (Rayleigh) damping is used the damping matrix is generated in the transformed (after applying the Lanczos transformation) domain.

A value of $\theta_1 = 0.988$ which produces small numerical damping is used in time integration. The values of damping parameters α and β are taken to be 4% and 2% respectively.

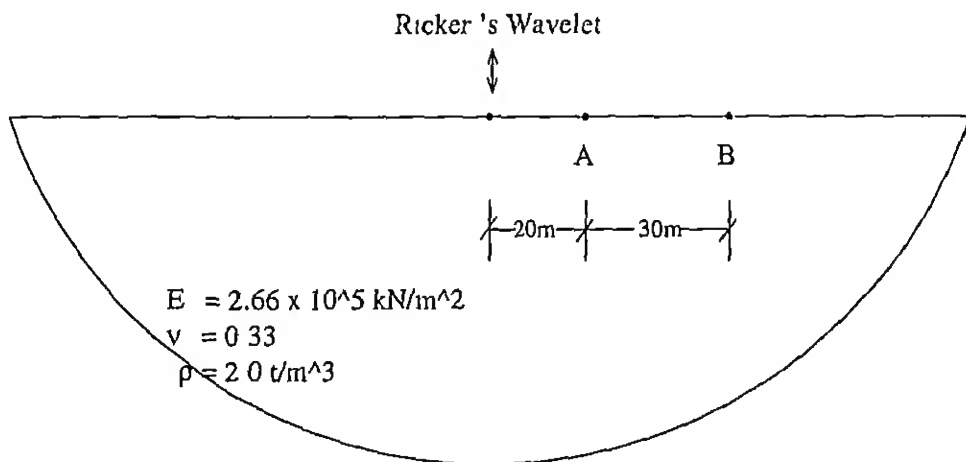


Figure 2.3 Half Space Loaded by Vertical Ricker's Wavelet

2.6.3 Example 1. Elastic Half Space

In this example an elastic half-space (see Von Estorff, Pais and Kausel, 1990) subjected to a Ricker's wavelet (transient excitation) in vertical and horizontal directions is investigated. The displacement histories at points 'A' and 'B' which are located at a distance of 20m, and 50m

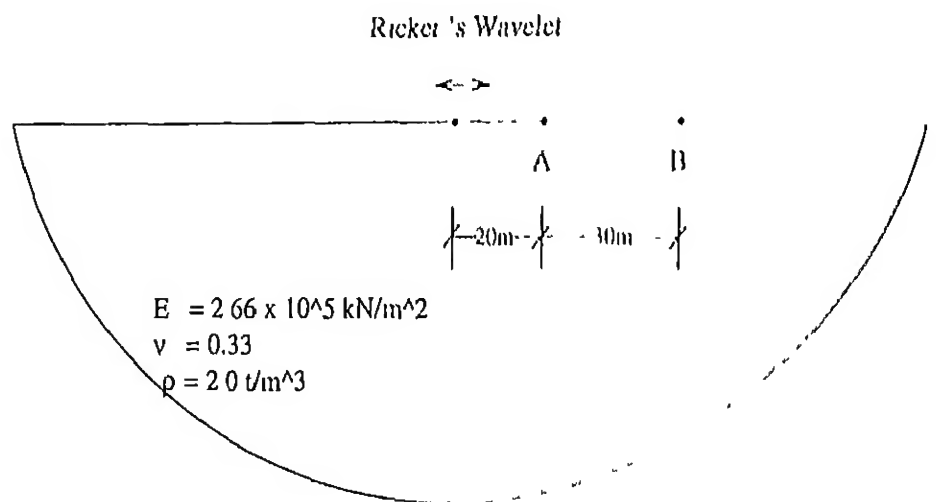


Figure 2.4: Half Space Loaded by Horizontal Ricker's Wavelet

on the surface from the load are monitored.

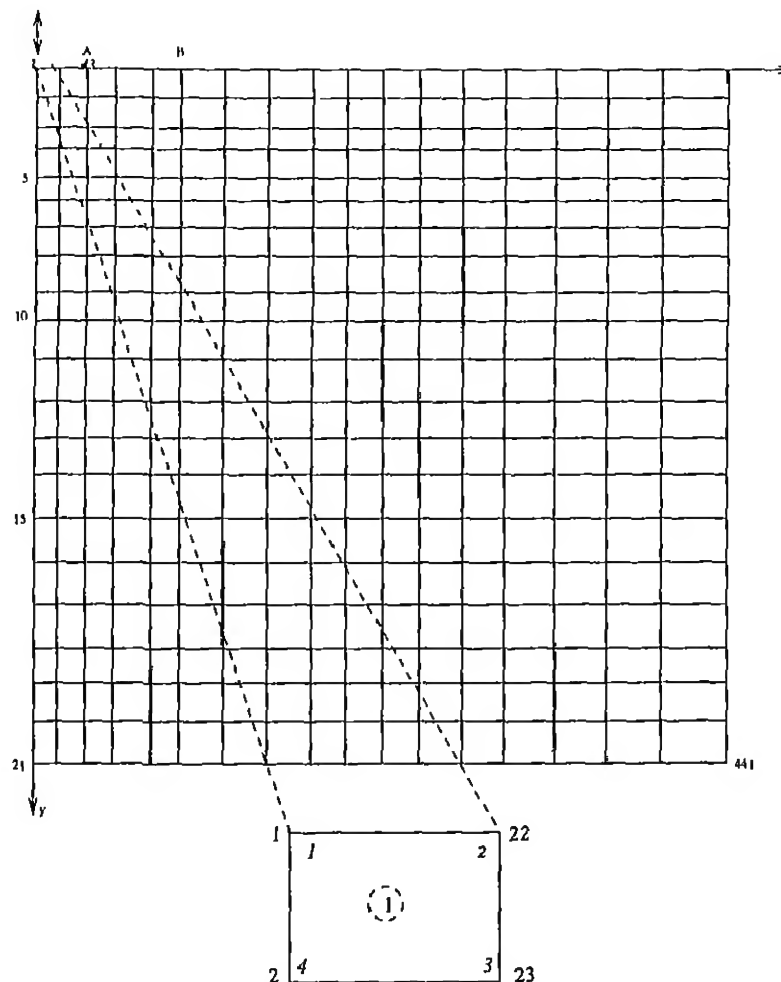


Figure 2.5. A Typical FE Mesh

A schematic diagrams of the problem considered are shown in Figures 2.3, 2.4. Only one half of the domain is discretized for vertical loading and full domain is used for horizontal loading. A typical graded mesh with 20 number of elements in each direction shown in Figure 2.5, is utilized for vertical loading case.

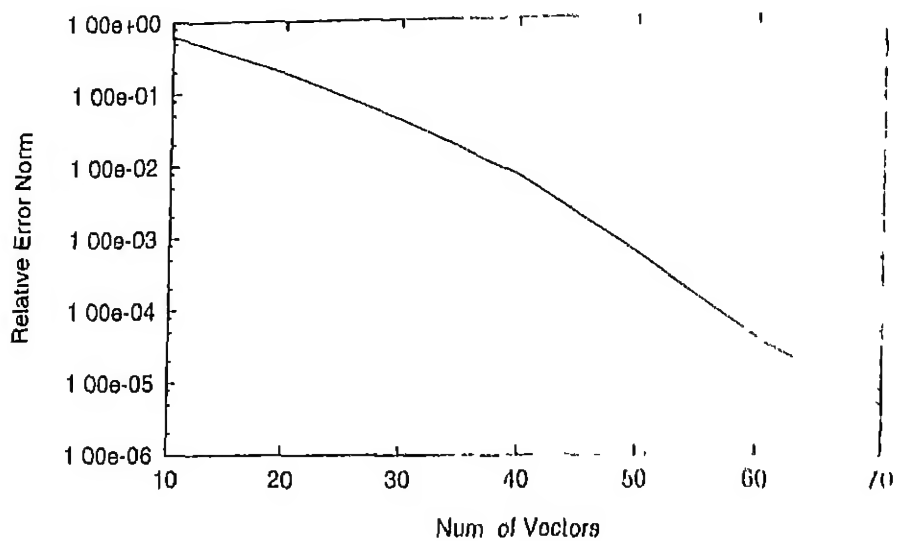


Figure 2.6: Effect of Number of Vectors on Rel. Error Norm

The parameters of the soil are as follows - Young's Modulus = $2.66 \times 10^5 kN/m^2$, Poisson's ratio = 0.33, and density = $20 t/m^3$. The load function $f(t) = (1 - 2\tau^2)e^{-\tau^2}$, where $\tau = t/\pi$.

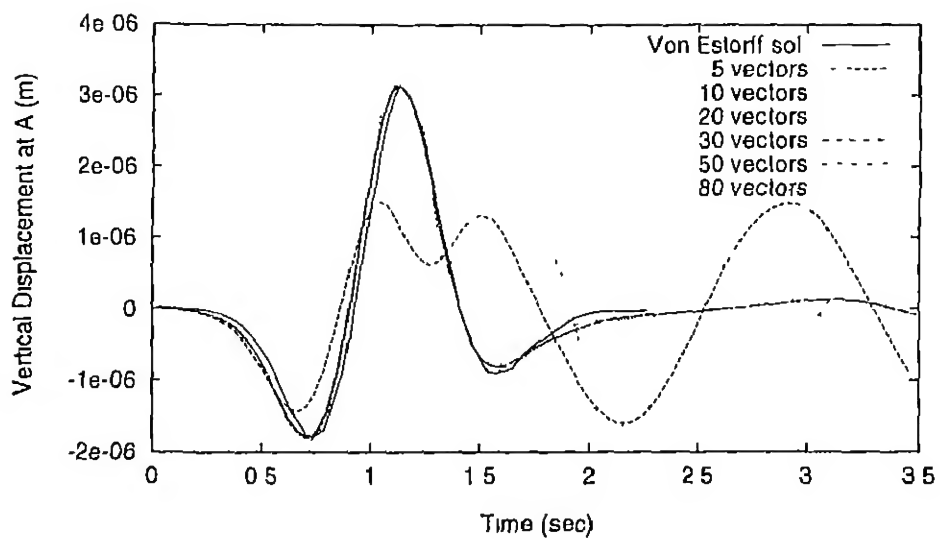


Figure 2.7: Effect of Number of Vectors on Vertical Displacement

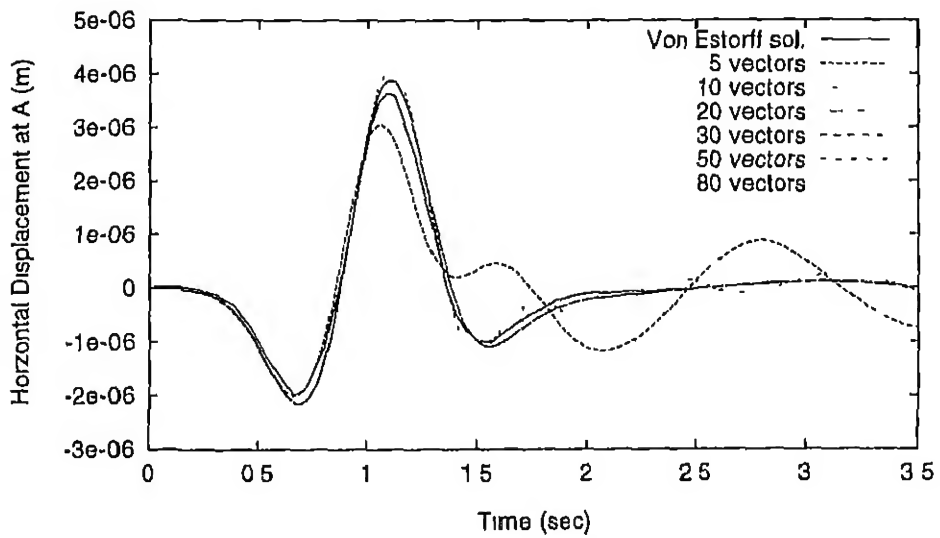


Figure 2.8: Effect of Number of Vectors on Horizontal Displacement

2.6.4 Number of Lanczos Vectors

To study the effect of *number of Lanczos vectors* considered for coordinate transformation, the error norm in load representation as defined by equation (2.78) is computed. Both absolute and relative norms are shown in Figure 2.6. The effect of number of Lanczos vectors on the accuracy of the results are shown in terms of vertical displacement history at point 'A' in Figure 2.7. The effect can be seen in the case of horizontal displacement of half-space loaded by horizontal Ricker's wavelet in Figure 2.8. As expected error norm in load representation reduces rapidly with increase in number of Lanczos vectors. Similarly accuracy of the results improves rapidly as number of vectors increases (reported in the following sections). It can be observed that 20 Lanczos vectors could produce solutions of desired accuracy.

Computational time

To asses the computational resources required for the first two stages of the modeling scheme (Section 2.1), CPU times are logged in and analyzed in this section. The first two stages of the scheme (Section 2.1) namely the spatial discretization and Lanczos vector transformation can be divided into the following steps ~ 1. FE Assembly, 2. Lanczos Vector generation, 3. Transformation matrix generation, 4. Writing transformed system matrices and Lanczos vectors (I/O) to disk. CPU times required for each of these steps obtained on DEC ALPHA 3000s600 are given in Table 2.1. The same information is shown in Figure 2.9. CPU time required for step 1 (FE assembly) remains constant with number of Lanczos vector because this step is independent

of Lanczos vector generation. The CPU time required for each step per vector (slope of the lines in Figure 2.9) remains same for steps 2 and 4; whereas for step 3 which involves Ritz vector computation (Equation 2.81) increases. However, it can be observed that Total CPU time per vector (column 7) does not vary much.

No. of Vectors	FE Assembly	Lanc. vect generation		Transform matrix		I/O	Total	Total time per vector
		(1)	(2)	(3)	(4)			
5	0.5232	0.3867	0.1376	0.3670	1.4145		0.2829	
10	0.5231	0.6900	0.3338	0.7837	2.3306		0.2331	
20	0.5241	1.2171	0.8042	1.5460	4.0914		0.2046	
30	0.5339	1.8954	1.8641	2.3327	6.6261		0.2209	
50	0.5348	3.6246	4.5193	3.9138	12.5925		0.2519	
80	0.5290	7.5308	10.2294	6.3624	24.6516		0.3081	

Table 2.1: CPU times for various stages of computation in sec

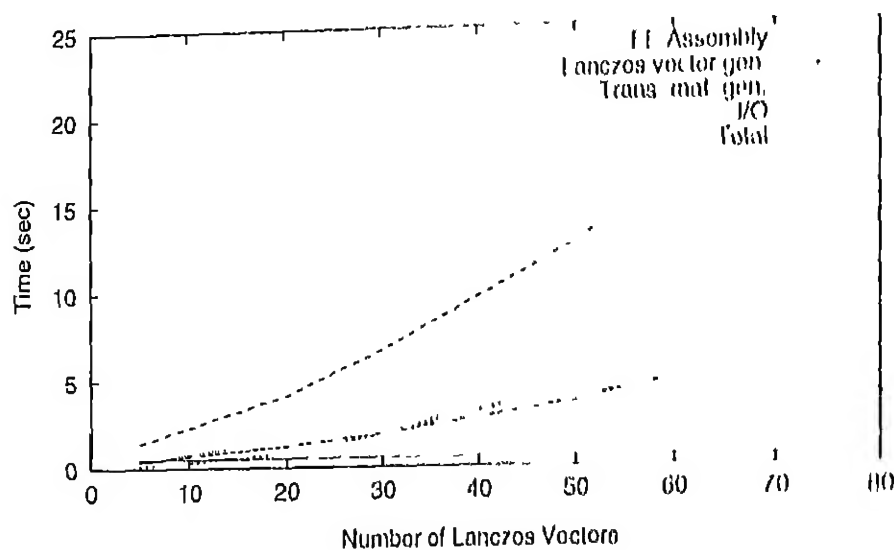


Figure 2.9: CPU time for various stages of computation

2.6.5 Size of the model

To investigate the effect of the size of the model (computational domain), four models of sizes 400x400m (small), 400x600m (small1), 600x600m (medium) and 800x800m (large) are considered in case of vertical loading. Number of elements in each direction are taken to be 20. The time step is monitored carefully so that *Courant* criterion (Higdon, 1992) is not violated. Lumped mass method is adopted for the analysis. Time integration is carried out for 3sec. The vertical displacement at point 'A' obtained with these models are shown in Figure 2.11. The results obtained with the models compare very well with those of Von Estorff, Pais and Kausel (1990) obtained using boundary element methods. Only in small models, the displacements beyond 1.5 seconds do not match well, which could be due to the influence of reflected waves.

Similar study has been carried out with models 800x400m (small), 1200x400m (small1), 1200x600m (medium) and 1600x800m (large) for horizontal excitation. The number of elements used in horizontal and vertical directions are 40 and 20 respectively. Horizontal displacements at point 'A' obtained with these three models are shown in Figure 2.13. The results agree very well those reported by Von Estorff, Pais and Kausel (1990) (see Figure 2.12) except for those obtained with small meshes at times beyond 15secs

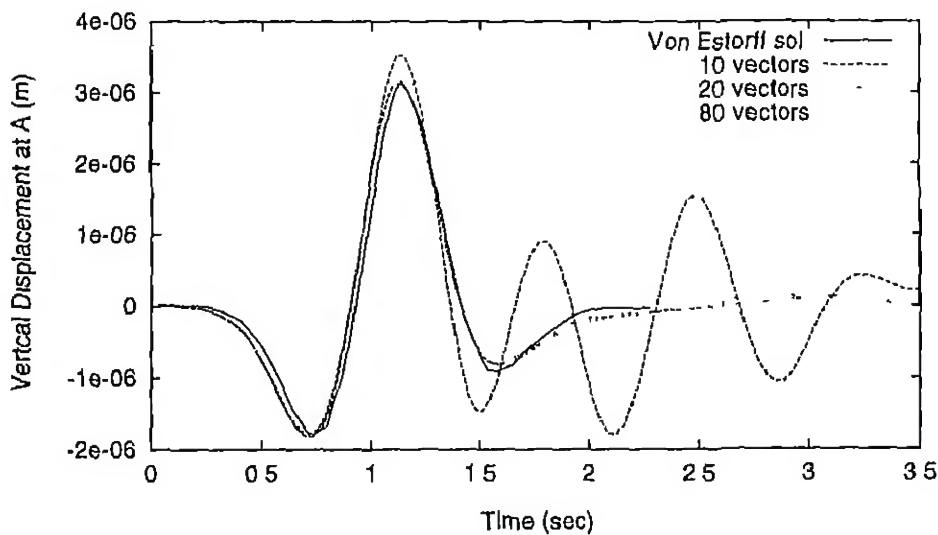


Figure 2.10: Comparison of Vert. Displacements with Von Estorff's Values

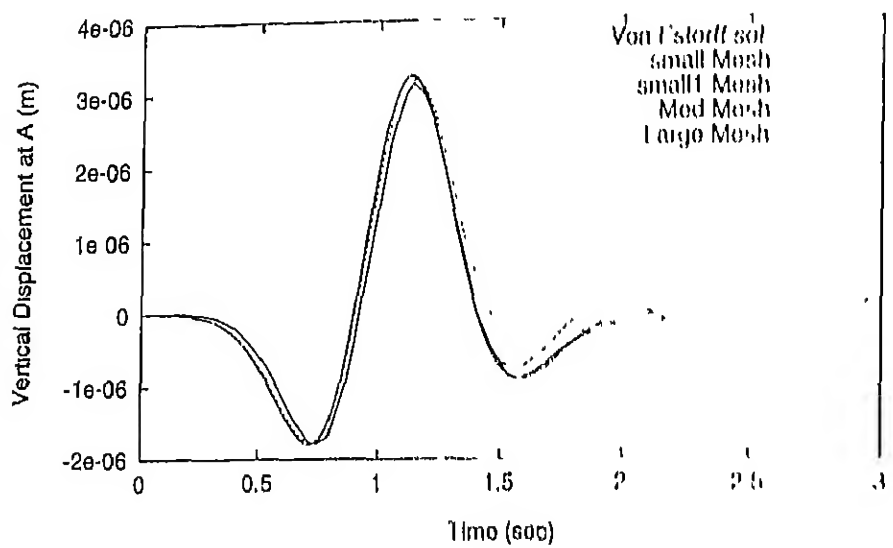


Figure 2.11: Effect of Mesh Size on Vertical Displacements

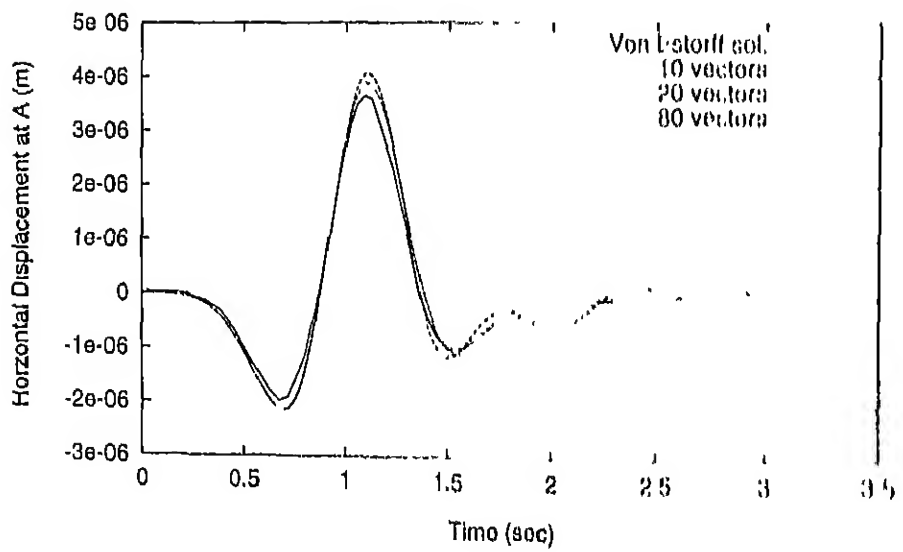


Figure 2.12: Comparison of Hor. Displacements with Von L'storti's Values

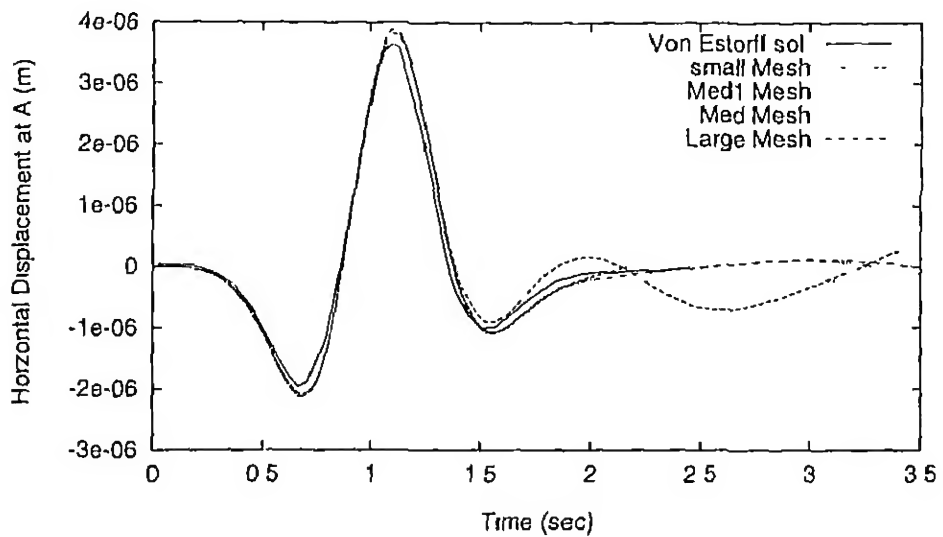


Figure 2.13 Effect of Mesh Size on Horizontal Displacements

2.6.6 No of Elements

In this section the effect of number of elements (element size) on the accuracy is reported. The computational domain of 800x800m size is discretized with varying no of elements from 20 to 40 in both the directions. The vertical displacement history at point 'A' subjected to a vertical load is obtained with these three mesh schemes and plotted in Figure 2.14. It can be observed that all the three models produced results of almost same accuracy and agree well with those reported by Von Estorff, Pais and Kausel (1990).

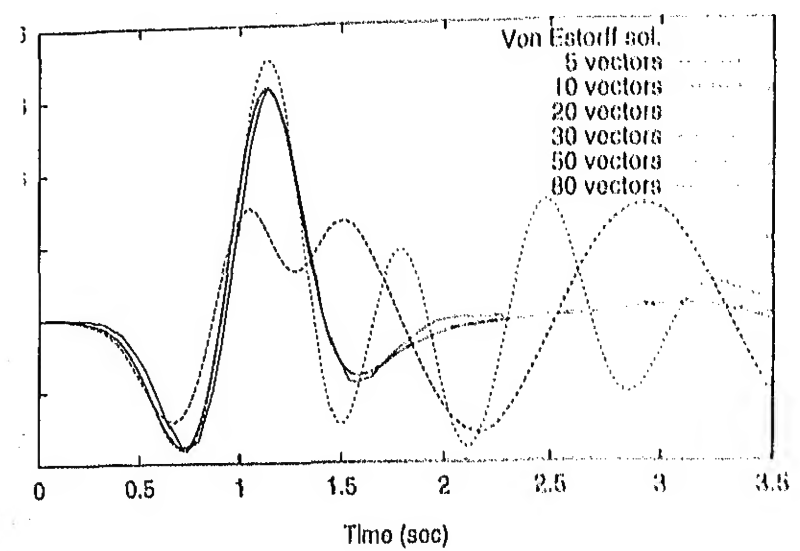


Figure 2.14: Effect of Number of Elements

Initial Variation of the load

in different loading schemes (shown in Figure 2.15), are rate the Lanczos vectors only namely

at 10m right (node 22) of original position (node 1)

at 10m down (node 2) the original position (node 1)

at 50m right (node 85) of original position (node 1)

at 50m down (node 4) the original position (node 1)

at 100m right (node 127) of original position (node 1)

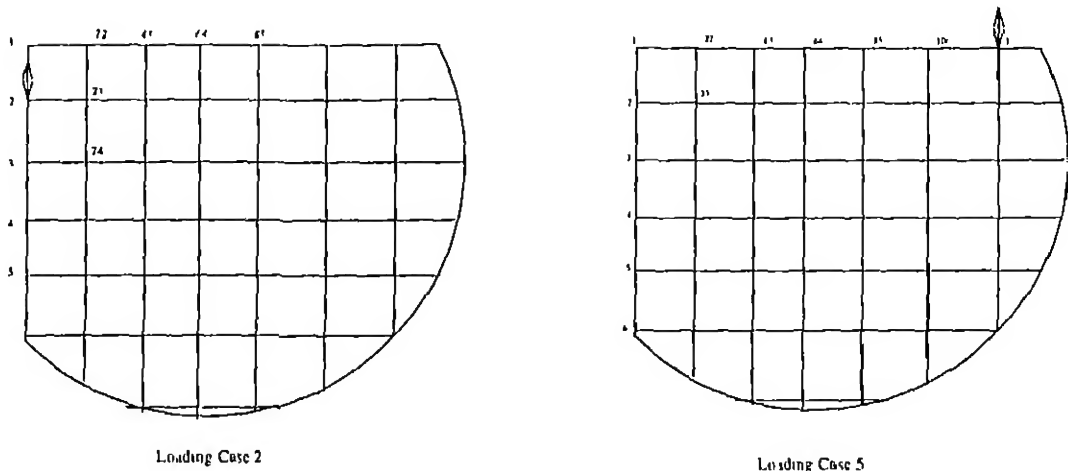


Figure 2.15 Spatial Variation of the load – Different Load Cases

Large mesh with 20 elements in each direction is utilized for the study. Displacement histories at points 'A' and 'B' are obtained with 20 and 40 Lanczos vectors. Vertical displacement history at point 'A' for vertical loading with 20 and 40 number of Lanczos vectors are shown in Figures 2.16, 2.17. It can be observed that results obtained with loading cases 2 and 4 match well; whereas the ones obtained with other schemes do not match well with those obtained with actual loading scheme; It may be observed that if the loading scheme used for generation of Lanczos vectors is spatially farther (loading cases 3 and 5) yields poor results and increase of vectors improves the accuracy. If the loading considered is close to the observation region, results obtained will be overestimated (loading case 1).

It may be inferred that spatially different loading schemes can be used to generate Lanczos vectors and system matrices keeping in mind the following points.

- The loading scheme should not be very different (like loading cases 3 and 5) from actual loading.
- The loading scheme should not close to the observation region (like loading case 2)

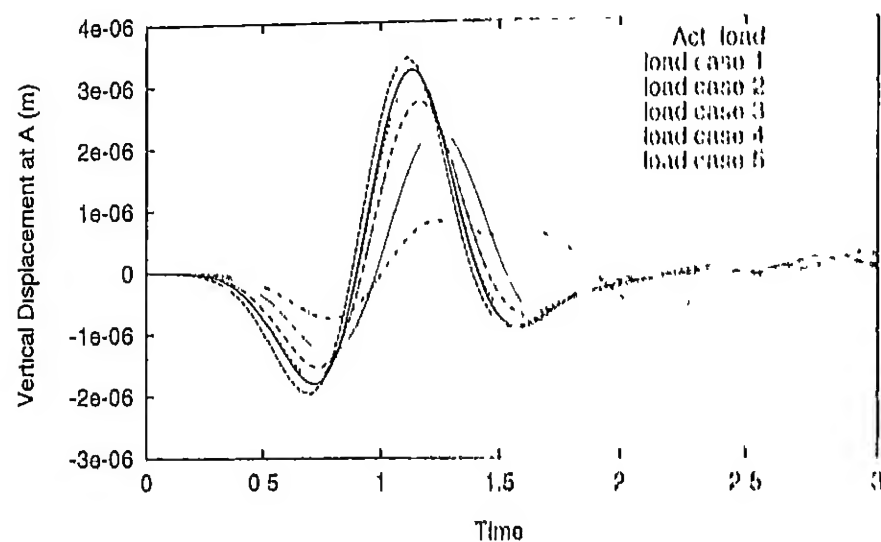


Figure 2.16: Effect of Spatial Variation of the Load with 20 Vectors

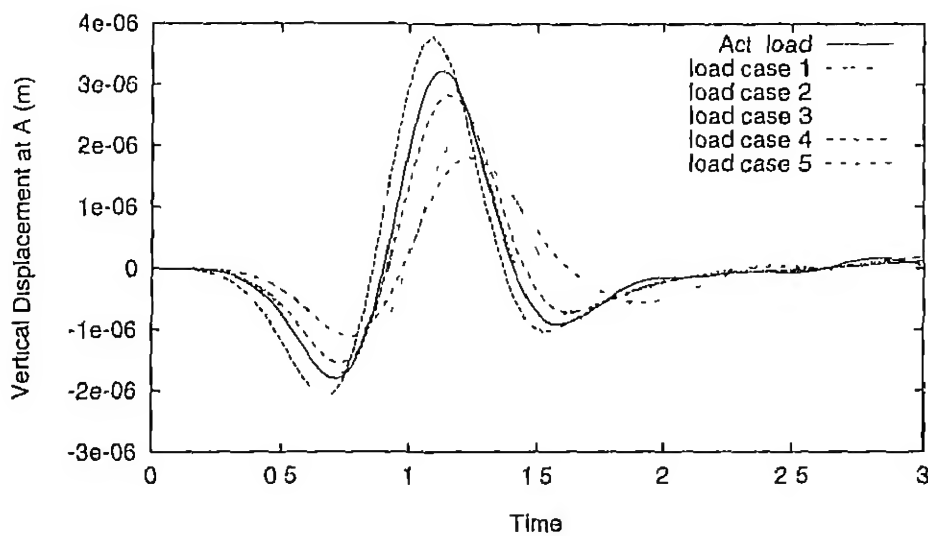


Figure 2.17 Effect of Spatial Variation of the Load with 40 Vectors

2.6.8 Example 2. Elastic Half Space with a Vertical Trench

This example helps in understanding the behaviour and applicability of the scheme for non convex domains. A schematic diagram of half space with vertical trench adjacent to the load is shown in Figure 2.18. The geometry of the problem is same as in earlier example except that a vertical trench of 50m deep and 10m wide is located at 5m to right of the load. In this example also both vertical and horizontal loading schemes are considered. The displacement history at point 'A' for both vertical and horizontal loading are shown along with those reported by Von Estorff, Pais and Kausel (1990) in Figures 2.19, 2.20. It can be observed that the results obtained by the present model agree well those obtained by Von Estorff, Pais and Kausel (1990).

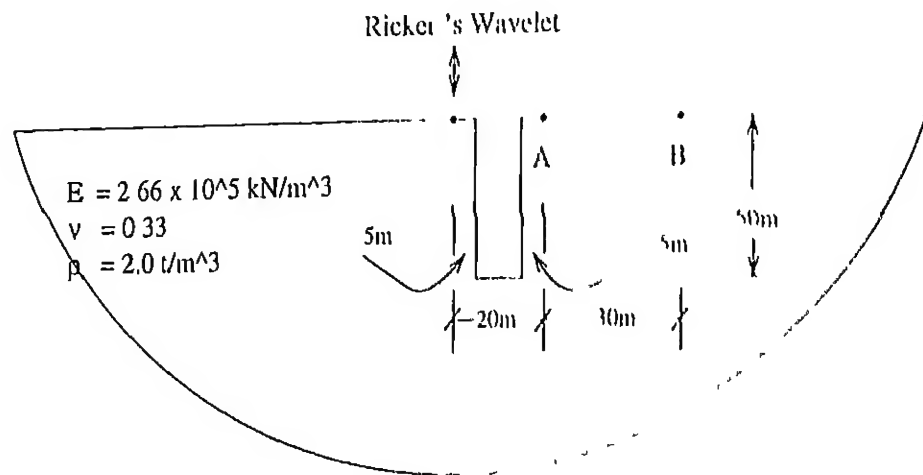


Figure 2.18: Half Space with trench Loaded by Vertical Ricker's Wavelet

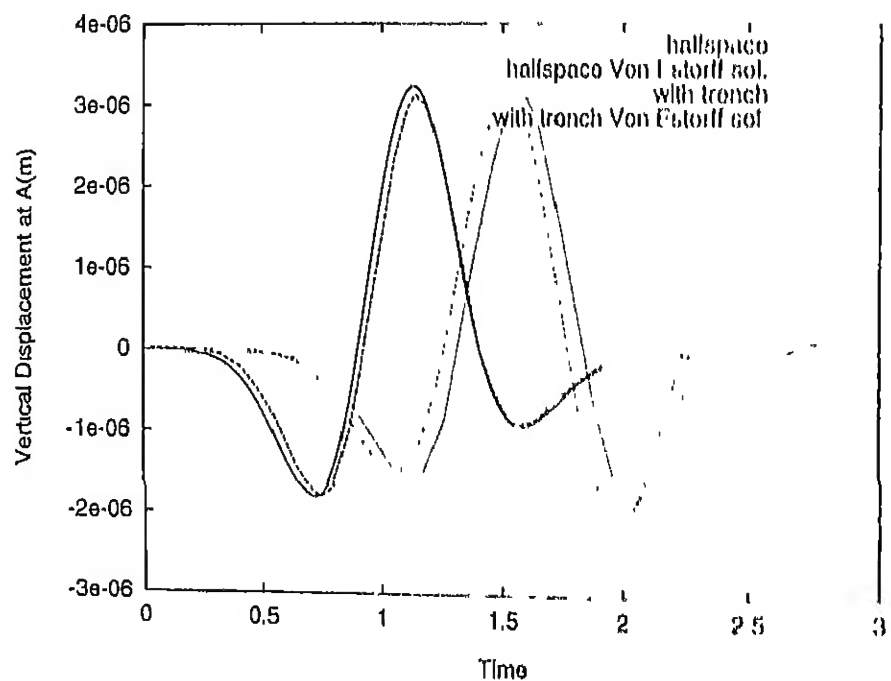


Figure 2.19. Effect of Trench on Vert. Displacements due to Vert. Load

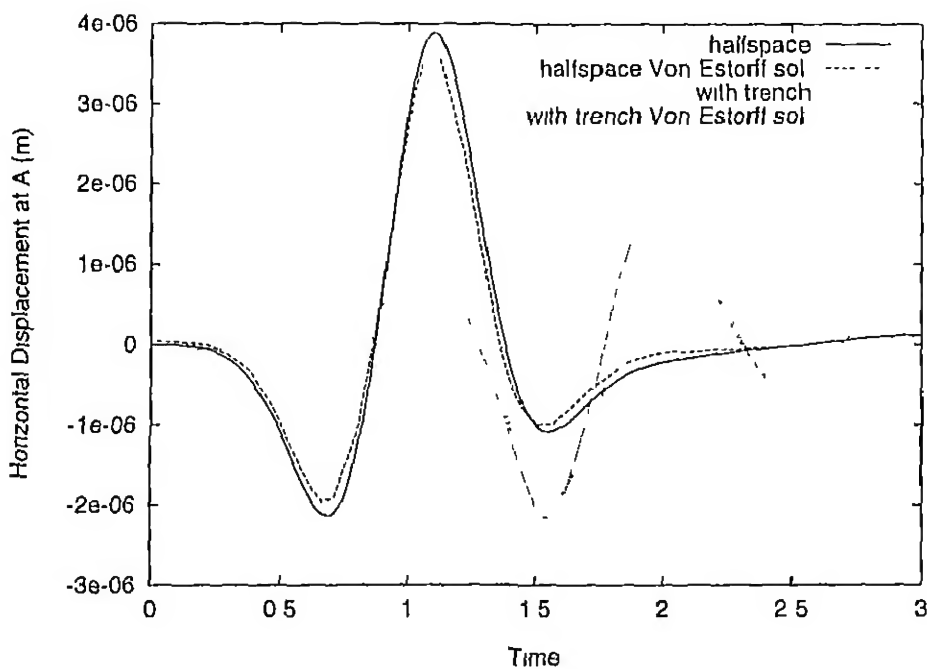


Figure 2.20: Effect of Trench on Hor. Displacements due to Hor Load

It would be important to mention that the solutions obey the causality conditions in all the situations investigated. This could be verified directly from the displacement histories reported. More over solutions obtained by Von Estorff, Pais and Kausel (1990) found to satisfy this requirement and the present solutions agree well with them

2.7 Summary

Based on the limited numerical investigation carried out the following conclusions can be drawn.

1. A large mesh coupled with Lanczos vector transformation could represent semi infinite soil mass for computational purposes.

2. The present numerical scheme can effectively handle transient loading in time domain.
3. The model can estimate errors due to coordinate transformation as well as temporal discretization and control them.
4. The error introduced due to coordinate transformation exponentially decreases (see Figure 2.6) with increase in number of Lanczos vectors. The computational cost per vector remains almost constant and desired level of accuracy can be obtained with sufficient number of Lanczos vectors.
5. The system (transformed) matrices generated with a particular spatial variation of the load can be used to analyze for other loading conditions if the loading schemes are similar (see Section 2.6.7)
6. A transformed model with few degrees of freedom (about 20-40) could simulate a physical model with large (about 840) degrees of freedom.
7. The present model can effectively analyze non-convex domains also (vertical trench problems).
8. The solutions obtained with present model obey the causality condition.
9. With relatively small computational effort semi-infinite half-space problems with transient loading could be analysed in *time domain*.
10. It would be important to emphasize that the present scheme is local both space and time.

Chapter 3

THREE DIMENSIONAL FOUNDATIONS

3.1 Introduction

Dynamic soil-structure interaction is concerned with study of structures founded on soils and subjected to dynamic loads directly applied to the structure or transmitted through the soil. In its early stages, dynamic soil-structure interaction dealt with external excitation problems like vibrations of machine foundations. More recently, important structures, like nuclear reactor containment structures, tall buildings etc. excited through the motion of the soil in seismic areas, have received lot of attention of the researchers. The flexibility of the foundation has a significant effect on the response of the structures and must be taken into account in the analysis.

Soil structure interaction effects are studied usually in the frequency domain assuming linear elastic behaviour of the soil. In this method the dynamic behaviour (responses) of the foundation (massless) along

with the soil is studied first, then the responses along the foundation structure interface are incorporated in the analysis of the structure. Soil-structure interaction problems, where non linear effects are important, require a time domain analysis. Non-linear contact conditions, partial uplift, non-linear material behaviour, and arbitrarily varying loads, are some of the usual situations which require a direct time domain analysis.

Foundations are usually massive, rectangular in shape and embedded in the soil. The usual concept of rigid foundation may not apply to the whole range of frequencies of interest. Consequently the force displacement relationship of the foundation, treating it to be rigid, through an impedance matrix may not describe the behaviour accurately.

The foundation soil system response depends on the shape and embedment of the foundation, the relative flexibility of soil and foundation, spatial variation of the material properties of the soil (non homogeneity and layering), and excitation. Because of the embedment and finite rigidity of the foundation, in real life problems, the responses in the principal coordinated directions will be coupled. Any comprehensive study of the foundation soil system should be able to incorporate the above mentioned parameters in the model. A brief review of the literature pertaining to the dynamic analysis of 3-dimensional foundations is presented in the next section.

3.2 Review of the Literature

During the early part of this century machine foundations were designed by empirical models treating the system as single degree of freedom systems (Balkan, 1969). Lamb (1904) initiated study of response of elastic half-space subjected to dynamic loads. Reissner (1936) obtained the response of harmonic disc load on surface. He assumed a uniform distribution of stresses under the disc. Quinlan (1953) reported solutions for varying contact pressure across the diameter. He gave solutions for rigid base approximations. Sung (1953) developed solutions for circular contact area with three pressure distributions, namely, 1. uniform, 2. parabolic, and 3. pressure distribution corresponding to rigid base. He gave solutions for different Poisson's ratios. These solutions can be used to compute the compliance functions of rectangular footing making use of the equivalent circular area. This equivalent area method provides solutions of reasonable accuracy for aspect ratio of two (F. E. Richart, 1960). Sung (1953) developed mathematical expressions for rectangular footing resting on half-space. Kobori (1962), Thomson and Kobori (1962) obtained compliance functions for uniformly distributed load over rectangular surface area. Arnold, Bycroft and Warburton (1955) and Bycroft (1956) obtained the solution for rocking vibrations of a circular footing. Actual stress distribution beneath a footing does vary with operating frequency, and is not known apriori. A mixed boundary value problem, with prescribed displacements under a rigid footing and zero tractions over the remaining surface, was studied by Luco and Westmann (1971). Luco (1976) obtained impedance functions of rigid foundation on layered

viscoelastic medium using integral equations approach. Finite Element Method along with different absorbing boundaries were employed by several investigators to obtain the impedance functions of surface and embedded foundations. Lysmer and Kuhlemeyer (1969) developed an absorbing boundary consisting of discrete viscous dampers and Rayleigh wave dampers. They obtained compliance functions for strip and axisymmetric foundations. Dasgupta and Kameswara Rao (1978) extended the methodology to study plane, axisymmetric and three dimensional problems. They considered non-linear material behaviour and non-homogeneity. Lysmer and Waas (1972) developed an absorbing boundary which transmits Love and Rayleigh waves. This boundary was applicable for layered media with horizontal layers extending to infinity in lateral directions resting on hard stratum in frequency domain. Kausel (1974) extended the same for axisymmetric problems and obtained impedance functions for different modes.

The Boundary Element Method (BEM) which automatically includes infinite region in the modeling have been extensively used to study the soil-structure interaction problems. The frequency domain formulation was first used by Dominguez (1978) to obtain impedance functions of rectangular foundations resting on or embedded in a viscoelastic half-space. Impedance functions of foundations resting on non-homogeneous and layered soils were obtained by Abascal and Dominguez (1986). Ahmad and Banerjee (1988) employed quadratic elements in frequency domain to obtain compliance functions. Karabalis and Beskos (1984) and Karabalis and Beskos (1986) used a time-domain BEM and obtained impedance functions for rigid surface and embedded foundations. The response of flexible foundations was investigated

making use of domain methods like Finite Element (FE) and Finite Difference (FD) for foundation and Boundary Element (BE) for soil. Iguchi and Luco (1981) obtained the response of rectangular foundations on elastic half-space. Karabalis and Beskos (1985) and Gaitanaros and Karabalis (1988) obtained response of surface and embedded flexible foundations using time domain boundary element method and FEM for the foundation. Gucunski and Peek (1993) presented response of circular foundations using soil stiffness matrices for layered soils evaluated through Green's functions and stiffness matrices of plate using finite difference energy method.

Gazetas and Tassoulas (1987b), Gazetas and Tassoulas (1987a) developed approximate models for stiffness and damping parameters for horizontal and rocking vibrations based on results obtained through numerical computation. Wolf (1988) developed approximate models by adding an additional degree of freedom. He obtained stiffness, damping and mass parameters by curve fitting techniques to the results obtained through exact numerical computation.

The existing methodologies to solve the 3dimensional foundation soil systems fall in one of the categories.

1. Finite element discretization with energy absorbing boundaries to model the far field.
2. Boundary element method in frequency domain ignoring the foundation flexibility.
3. Boundary element method in time domain.
4. Hybrid methods - FE discretization for foundation and BE for the rest of the domain.

Category 1 methods account the energy radiation approximately. Most of these models, like those of Kausel (1974) and Lysmer and Kuhlemeyer (1969), can be used in frequency domain only. Category 2, 3 and 4 methods can model the infinite extent exactly. The time domain variants of these BE methods, being global in space and time, need enormous computational resources. They can not handle flexible foundations directly. Category 4 methods also suffer the disadvantages of the BEMs in time domain.

The present investigation uses a finite element model for spatial discretization (both near and far field) circumventing the need for an energy absorbing boundary. The response of the system is obtained in time domain by direct time integration after transforming the equations from original space to Lanczos space. The investigation thus uses an integrated approach to solve coupled motion wherein all modes could be present.

3.3 Application of the Finite Element Method

Analytical solutions to dynamic soil-structure interaction problems can be obtained for situations with idealized geometry of the foundation, linear material behaviour and periodic loading. Numerical techniques, with advent of high speed computers, provide methodology to solve complex field problems. The Finite Element Method (FEM) and Boundary Element Method (BEM) are some of the powerful methods which employ discretization of the domain. The FEM, as pointed out in Chapter 1, is ideally suited for problems with flexible foundation systems, non-homogeneous and nonlinear material behaviour and for

time domain analysis, if the effect of far field is incorporated properly. In this investigation the spatial discretization is carried out using FEM considering a *large domain* of the half-space. Lanczos transformation techniques (described in Section 2.4) are applied to system of equations of motion resulting from the spatial discretization. The transformed equations are solved in time domain with an adaptive direct integration method described in Section 2.5.3.

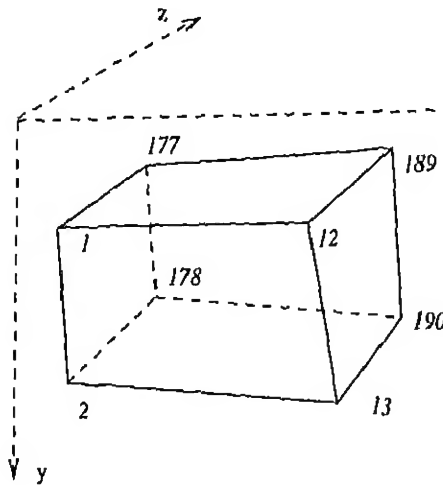
3.3.1 Finite Element Model

An eight noded hexahedron isoparametric element is considered as basic element. Considering the range of foundation thickness and displacement continuity with underlying soil, it has also been discretized with same eight noded elastic elements. The governing equation of motion ((2.49)) in which the system matrices $[M]$, $[C]$ and $[K]$ are assembled from the individual element matrices. The elements mass, damping and stiffness matrices are obtained as described in the following section.

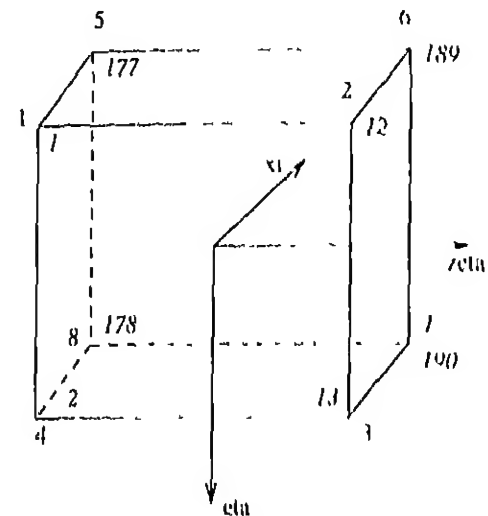
Element stiffness matrix

An eight noded isoparametric element is shown in global and local coordinate systems in Figure 3.1. Global node numbers of a typical element are shown in italics and local node numbers for isoparametric element are shown in roman numerals. Since the local coordinates range from -1 to +1, the element is a cube with a side of 2 units long and origin of the system at its centroid. The actual element could be of any shape with six-faces. The coordinate mapping which relates

the two coordinate system can be expressed as (Equation 3.2)



(a) Global coordinate system



(b) Local coordinate system

Figure 3.1 8 Noded Hexahedron Element in Global and Local Coordinate System

$$\mathbf{x} = [\mathbf{N}_i] \{x_i\} \quad (3.1)$$

where \mathbf{x} and \mathbf{x}_i are the vectors of independent variables, and coordinates for the node i respectively; $[\mathbf{N}_i]$ is a diagonal sub matrix of order equal to the number of space dimensions (3). Each of its entry equals to mapping function of the node. The subscript i varies from 1 to 8.

In (3.1),

$$\begin{aligned} \mathbf{x} &= [x \ y \ z]^T \\ [\mathbf{N}_i] &= \begin{bmatrix} N_i & 0 & 0 \\ 0 & N_i & 0 \\ 0 & 0 & N_i \end{bmatrix} \\ \mathbf{x}_i &= [x_i \ y_i \ z_i]^T \end{aligned} \quad (3.2)$$

The mapping functions can be written as

$$N_i = (1 + \zeta_i \zeta)(1 + \eta_i \eta)(1 + \xi_i \xi) \quad (3.3)$$

where ζ_i , η_i , and ξ_i are coordinates of the node i and take either +1 or -1

The displacement vector \mathbf{u} can be expressed in terms of its nodal values using the shape function expressed in the local coordinate system of the element. Since isoparametric formulation is being adapted the shape functions are same as the coordinate mapping functions of the element. Hence,

$$\mathbf{u} = [\mathbf{N}_i]\{\mathbf{u}_i\} \quad (3.4)$$

The differential operator defining the stress strain relations can be expressed as

$$[L] = \begin{bmatrix} \frac{\partial}{\partial x} & 0 & 0 \\ 0 & \frac{\partial}{\partial x} & 0 \\ 0 & 0 & \frac{\partial}{\partial z} \\ \frac{\partial}{\partial y} & \frac{\partial}{\partial x} & 0 \\ 0 & \frac{\partial}{\partial z} & \frac{\partial}{\partial y} \\ \frac{\partial}{\partial z} & 0 & \frac{\partial}{\partial x} \end{bmatrix} \quad (3.5)$$

The strain nodal displacement matrix B is given by

$$[B] = [L][N] \quad (3.6)$$

The differential operator $[L]$ contains derivatives with respect to physical coordinates. The derivatives have to be computed using Jacobian

transformation from natural coordinate space to physical coordinate space. The Jacobian can be expressed as (detailed description is given in Section 2.6.3),

$$[J] = \begin{bmatrix} \sum N_{i,\zeta} x_i & \sum N_{i,\zeta} y_i & \sum N_{i,\zeta} z_i \\ \sum N_{i,\eta} x_i & \sum N_{i,\eta} y_i & \sum N_{i,\eta} z_i \\ \sum N_{i,\xi} x_i & \sum N_{i,\xi} y_i & \sum N_{i,\xi} z_i \end{bmatrix} \quad (3.7)$$

The ' , ' indicates differentiation with respect to the variable following the symbol and the symbol \sum indicates summation over the number of nodes of the element (8 here), *viz.*

$$\begin{aligned} \sum N_{i,\zeta} x_i = & \frac{dN_1}{d\zeta} x_1 + \frac{dN_2}{d\zeta} x_2 + \frac{dN_3}{d\zeta} x_3 + \frac{dN_4}{d\zeta} x_4 \\ & + \frac{dN_5}{d\zeta} x_5 + \frac{dN_6}{d\zeta} x_6 + \frac{dN_7}{d\zeta} x_7 + \frac{dN_8}{d\zeta} x_8 \end{aligned} \quad (3.8)$$

The elasticity matrix $[E]$ for three dimensional solid can be expressed as,

$$[E] = \frac{E}{(1+\nu)(1-2\nu)} \begin{bmatrix} 1-\nu & \nu & \nu & 0 & 0 & 0 \\ \nu & 1-\nu & \nu & 0 & 0 & 0 \\ \nu & \nu & 1-\nu & 0 & 0 & 0 \\ 0 & 0 & 0 & \frac{1}{2}\nu & 0 & 0 \\ 0 & 0 & 0 & 0 & \frac{1}{2}\nu & 0 \\ 0 & 0 & 0 & 0 & 0 & \frac{1}{2}\nu \end{bmatrix} \quad (3.9)$$

The stiffness matrix of the element now can be expressed

$$[K^e] = \int_{-1}^{+1} \int_{-1}^{+1} \int_{-1}^{+1} [B]^T [E] [B] \|J\| d\zeta d\eta d\xi \quad (3.10)$$

where $\|J\|$ denotes the determinant of Jacobian. The stiffness matrix is evaluated using a (2x2x2) Gaussian quadrature.

Element mass matrix

Element mass matrix can be expressed as

$$[M^e] = \int_{-1}^{+1} \int_{-1}^{+1} \int_{-1}^{+1} \rho [N]^T [N] \|J\| d\zeta d\eta d\xi \quad (3.11)$$

As already mentioned, *systematic lumping* method is adopted for mass matrix. Only the diagonal entries of the element mass matrix are evaluated using $(2 \times 2 \times 2)$ quadrature and they are scaled so that the element mass is conserved.

Damping matrix

Element damping matrices are not evaluated since Rayleigh damping (proportional) is used, the damping matrices (global) in the transformed domain are computed directly.

Force vector

Since very few elements are loaded, element load vectors are not computed, rather the global load vector is computed. Most of the computations are done using point loads.

Linearly varying Young's modulus

Soil medium with linearly varying Young's modulus has also been considered for the analysis. The stiffness matrices of the elements are computed using an effective Young's modulus. Young's modulus in each element is assumed constant and its magnitude is taken to be its value at the centroid of the element. The variation of Young's modulus with depth (y coordinate) may be expressed as

$$E_y = E_t \left(1 + a * \frac{y}{B}\right) \quad (3.12)$$

where E_t , E_y are the modulii at the surface (i.e. $y = 0$) and at depth y ; a is a constant which equals to the slope of the variation. Responses are obtained for different values of a .

Layered soil

Horizontally layered soils have been considered for the analysis. Young's modulus of each layer can have different values. The discretization is done such that the element boundaries lie along the interface between the layers. The stiffness matrices of the elements are computed using the Young's modulus of the layer in which they lie. A two layer system is investigated with different ratios of Young's modulii and different top layer thickness. The ratio of the thickness of the top layer to halfwidth of footing and ratio of Young's modulus of bottom soil to that of top soil are used to present the responses. Poisson's ratio and density of the layers are kept same for all layers as they do not significantly effect the responseDasgupta and Kameswara Rao (1978).

Rigid Bedrock at Finite Depth

Soil of finite thickness lying on a rigid bedrock is also investigated. The displacements at bottom of the soil stratum are restrained in this analysis. A non-dimensional thickness parameter, which is defined as the ratio of the thickness of the soil layer to the halfwidth of the footing is used to present the responses.

Footing embedgment

In general footings are embedded in the soil. To study the effect footings at different embedgments are considered. Loading is applied on the top surface of the foundation. A non-dimensional ratio of depth of embedgment to halfwidth of footing is used to present the responses.

Foundation flexibility

Foundation flexibility has significant effect on responses. A non-dimensional flexibility ratio (reciprocal of rigidity) is used to characterize the relative flexibility of the foundation. Varying the Young's modulus of the foundation material, different flexibility ratios are obtained. The effect of foundation flexibility in terms of the variation of the displacements along width and/or length of the foundation is used to present the results. The effect of embedgment of the foundation on flexibility is also investigated.

3.4 Presentation of Results

Amplitudes for vertical, horizontal and rocking (rotation about z) modes of vibration are obtained by applying harmonic loads/momenta in each of the direction independently. Integration is carried out till the transients die and steady state is reached. It is found that if the integration is carried out for about 8 to 9 times the periods of the load, steady state could be achieved. The amplitudes are obtained from the displacement histories. Compliance functions for rigid foundation

are computed for vertical, coupled horizontal and rotational modes of vibration for frequency ratios ranging from 0.0 to 2.0. A non dimensional compliance function is defined for each mode of the vibration for any given frequency ratio a_0 as,

$$\begin{aligned} C_{yy} &= \frac{G_s L}{P_y} v \\ C_{xx} &= \frac{G_s L}{P_x} u \\ C_{\psi_{zz}} &= \frac{G_s L B^2}{M_z} \psi_z \\ C_{\psi_{yy}} &= \frac{G_s L B^2}{M_y} \psi_y \end{aligned} \quad (3.13)$$

and

$$a_0 = \frac{\omega B}{V_s} \quad (3.14)$$

where C_{yy} , C_{xx} , $C_{\psi_{zz}}$ and $C_{\psi_{yy}}$ are the compliance functions for vertical, horizontal along x direction, rotation about z axis and torsional directions respectively; v is the vertical amplitude due to vertical load P_y , u is the horizontal displacement along x axis due the load P_x acting along x direction, ψ_z is the rotation about z axis due to the moment M_z about z axis. ψ_y is the torsional displacement (about y axis) due to the torsional moment M_y about y axis. ω is the frequency of excitation. Torsional compliance functions are obtained only for the comparison purposes

$$V_s = \sqrt{\frac{G_s}{\rho_s}} \quad (3.15)$$

where ρ_s is the mass density of the soil.

Compliance functions for coupled horizontal and rocking modes are also obtained for rigid foundation

$$C_{\psi_{zz}} = \frac{G_s LB}{P_x} \psi_z$$

$$C_{x\psi_z} = \frac{G_s LB}{M_z} u$$

$$C_{\psi_{zx}} = C_{x\psi_z} \quad (3.16)$$

Here the compliance functions $C_{\psi_{zx}}$ is the compliance relating the rotation ψ_z about z axis due to Horizontal load P_x along x axis, similarly $C_{x\psi_z}$ relates the the horizontal displacement u along x axis due to moment M_z about z axis.

3.4.1 Validation of the model

A typical 3-dimensional foundation excited by harmonic loads and moments in vertical, and coupled horizontal and rotational modes independently, is analyzed with the present model. Problem definition and a part of the discretized domain used for vertical mode are shown in Figures 3.2, 3.3 respectively. Node numbers are shown in roman numerals and element numbers are in italics. L , B and d are length, width and thickness of the foundation respectively; and h is the depth of embeddment. Due to symmetry one quarter of the model for vertical mode and one half of the model for horizontal mode is chosen for discretization. The geometry and the material properties of the problems analyzed are as follows—

Vertical Mode:

Size of the model = 30x30x30m

Number of Elements	=	12x10x12
Young's Modulus of Soil E_s	=	47.09MPa
Poisson's Ratio Soil ν_s	=	0.33
Unit weight of Soil ρ_s	=	23.52 kN /m ³
Half Length of Footing L	=	2.0m
Half Width of Footing B	=	2.0m
Thickness of Footing d	=	1.0m
Depth of Embeddment h	=	1.0m

Horizontal Mode:

Size of the model	=	60x30x30m
Number of Elements	=	24x10x12
Young's Modulus of Soil E_s	=	47.09MPa
Poisson's Ratio Soil ν_s	=	0.33
Unit weight of Soil ρ_s	=	23.52 kN /m ³
Half Length of Footing L	=	2.0m
Half Width of Footing B	=	2.0m
Thickness of Footing d	=	1.0m
Depth of Embeddment h	=	1.0m

Compliance functions obtained with present model are compared with those reported by Mita and Luco (1989) and are shown in Figures 3.4, 3.5, 3.6 and 3.7. The results obtained compare well with those reported by Mita and Luco (1989)

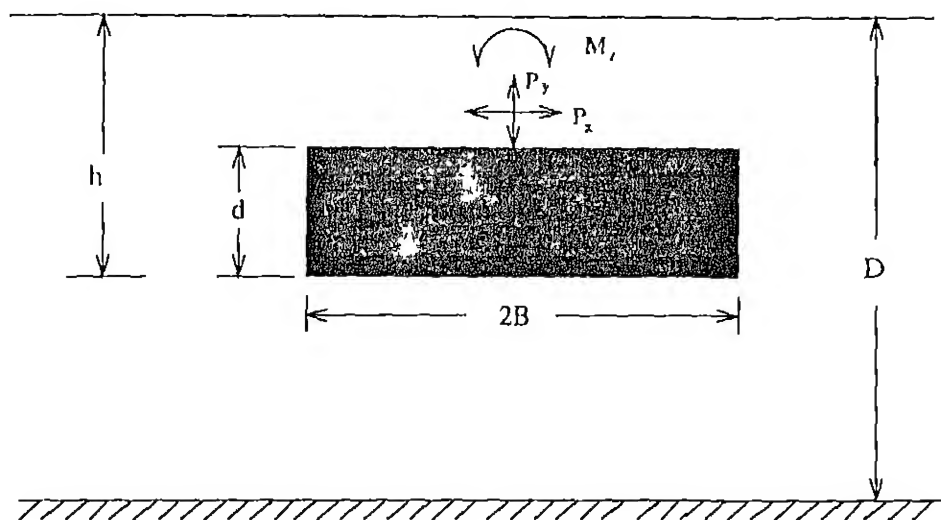


Figure 3.2 Problem Definition for 3dimensional Embedded foundation

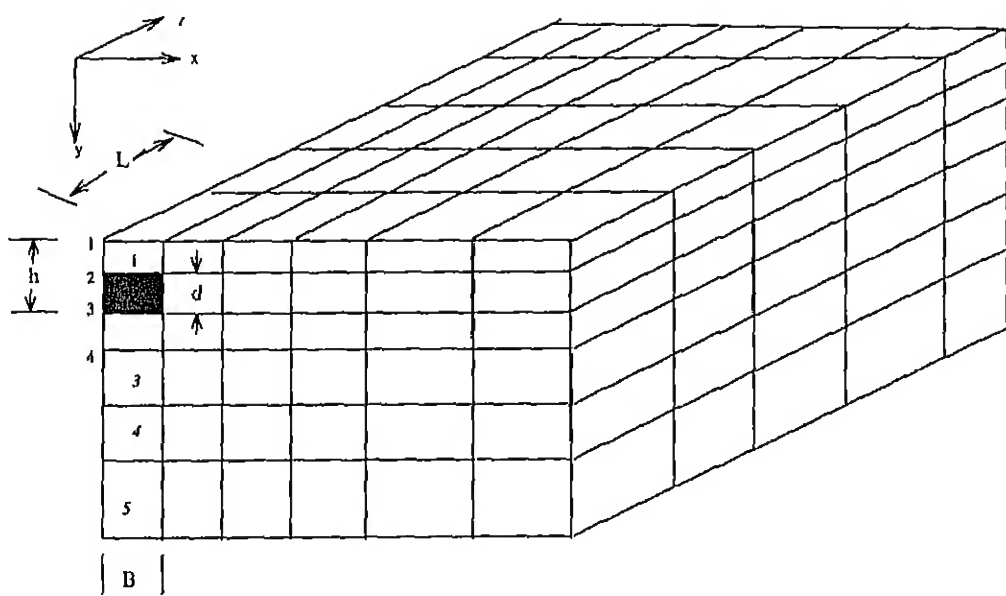


Figure 3.3: Finite Element Discretization for 3dimensional Embedded foundation

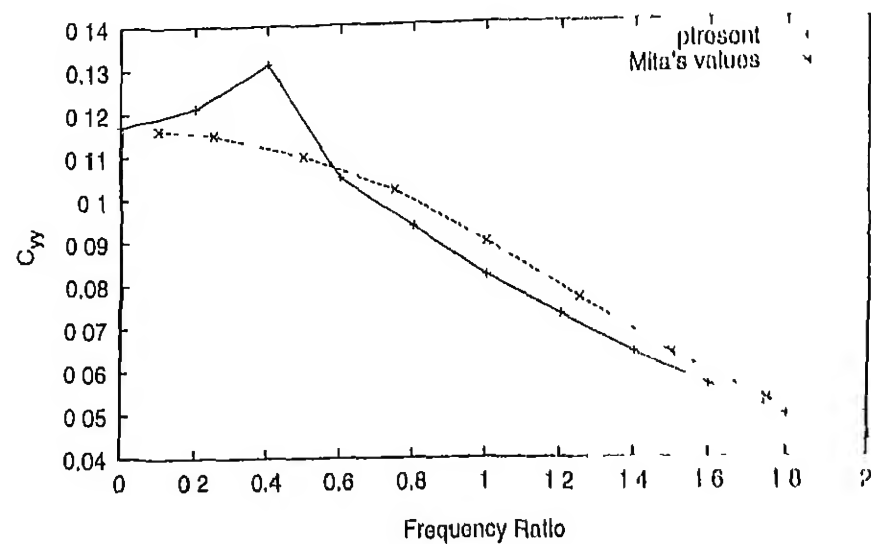


Figure 3.4: Comparison of Vertical Compliance Function Values with Mita's Values

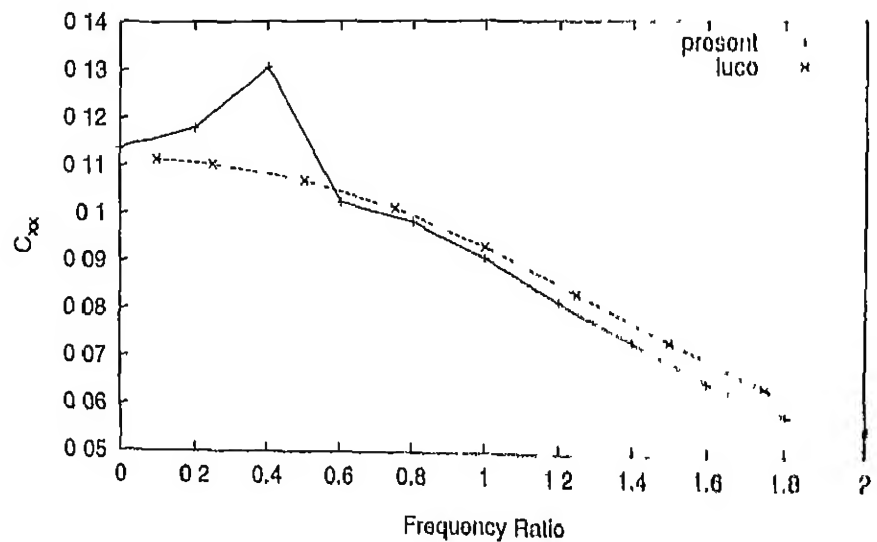


Figure 3.5: Comparison of Horizontal Compliance Function with Mita's Values.

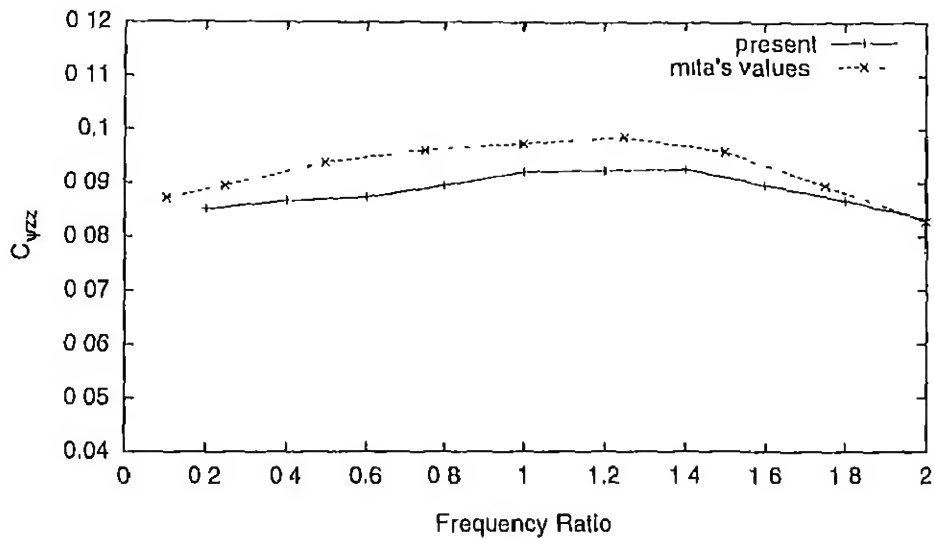


Figure 3.6. Comparison of Rotational Compliance Function with Mita's Values

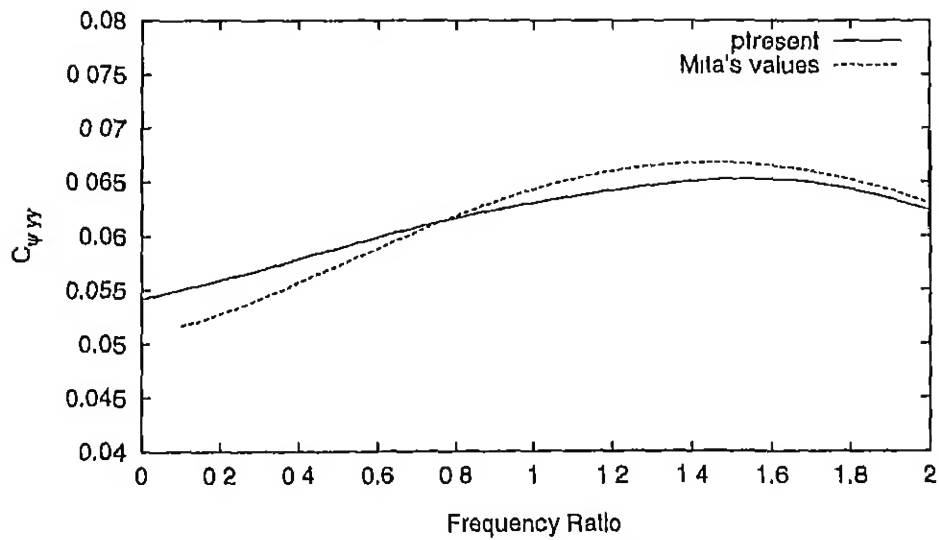


Figure 3.7: Comparison of Torsional Compliance Function with Mita's Values.

3.4.2 Effect of Embedment

Compliance for vertical, horizontal and rocking modes for various embedment ratios ranging from 0.5 to 1.5 (ratio of depth of foundation to halfwidth of footing h/B) are computed and presented in Figures 3.8 to 3.16. It can be observed that with increase in embedment ratio, the compliance functions decrease throughout the frequency range. However the reduction in the compliance functions varies with mode and aspect ratio of the foundation. The reduction in the values of compliance functions for vertical modes with embedment is small (of the order of 10%) except for static case (Figures 3.8 to 3.10). In case of horizontal mode the reduction is of the order of 50% (Figures 3.11 to 3.13). Similar order of reduction can be observed for rotational mode of vibration (Figures 3.14 to 3.16).

For vertical mode of vibration the reduction in compliance function with increase in embedment ratio is more for square foundation than for rectangular one (Figures 3.8 to 3.10). Similar behaviour is observed for horizontal mode of vibration (Figures 3.11 to 3.13). For rotational mode of vibration reduction in compliance function is more for rectangular foundation than square one (Figures 3.14 to 3.16).

Embedment of the foundation does not significantly alter the resonant frequencies for any of the modes of vibration.

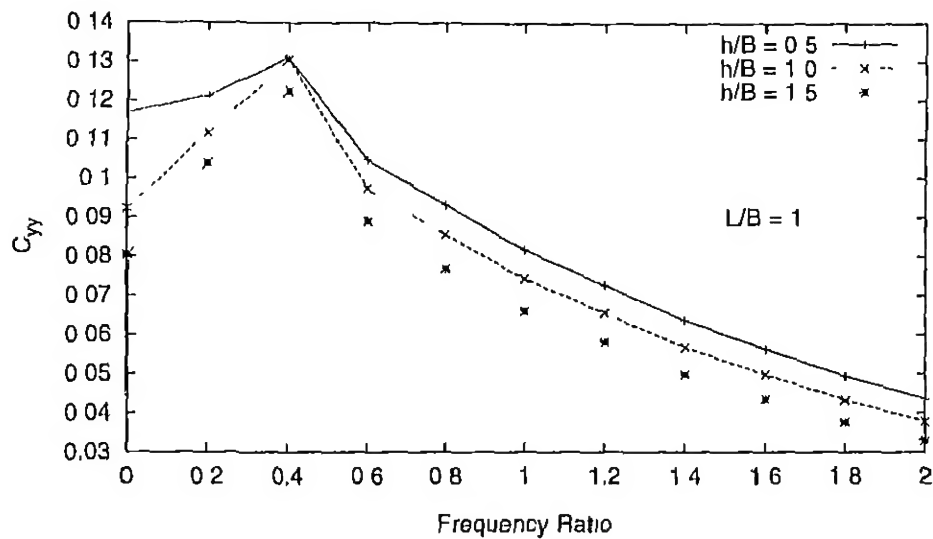


Figure 3.8 Effect of Embedment on Vertical Compliance Function for Square Foundation

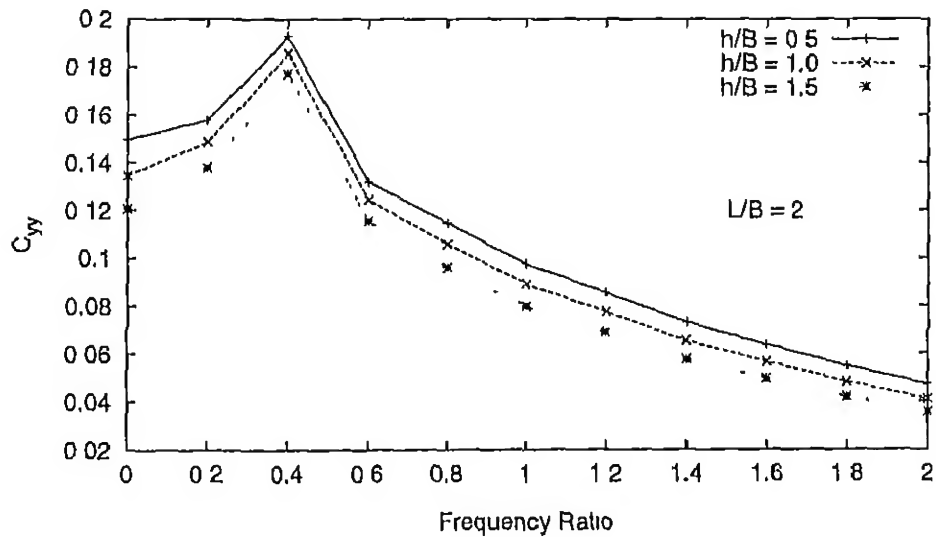


Figure 3.9: Effect of Embedment on Vertical Compliance Function for Rectangular Foundation ($L/B = 2$)

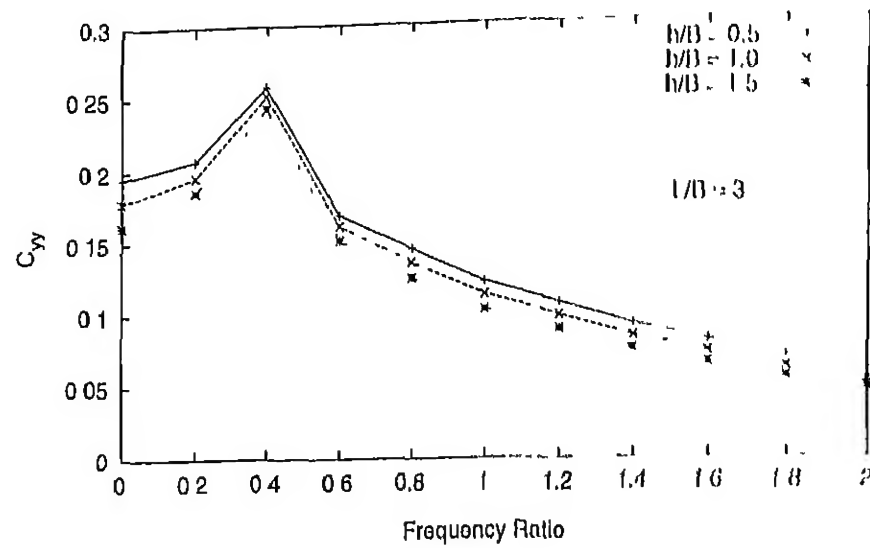


Figure 3.10. Effect of Embedment on Vertical Compliance Function for Rectangular Foundation ($L/B = 3$)

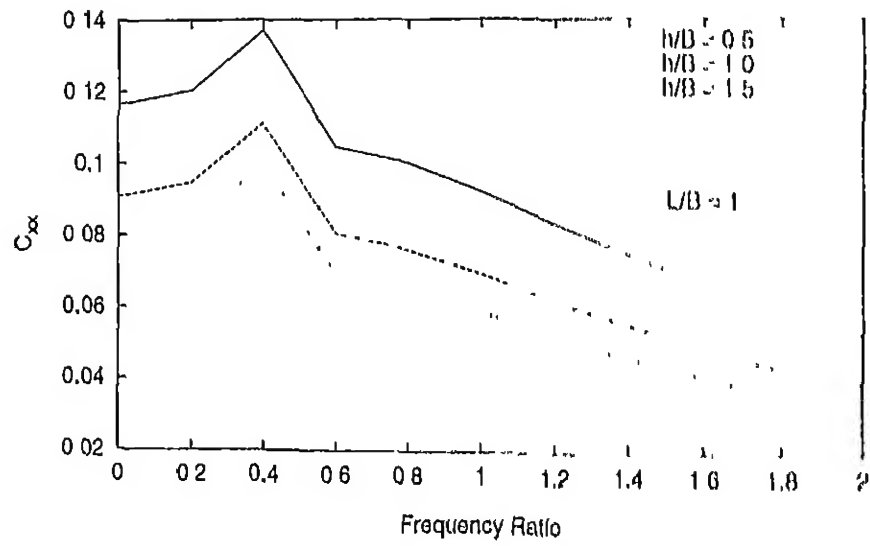


Figure 3.11 Effect of Embedment on Horizontal Compliance Function for Square Foundation

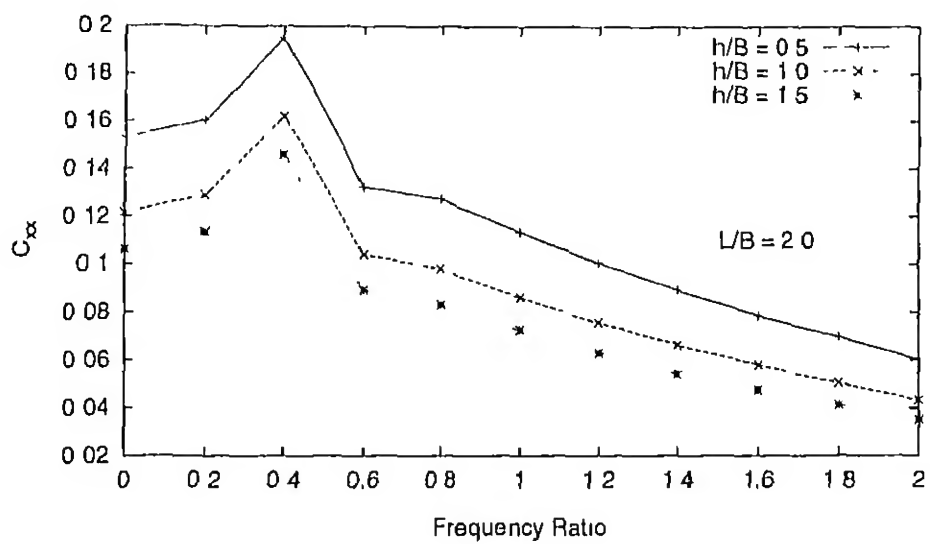


Figure 3.12 Effect of Embedment on Horizontal Compliance Function for Rectangular Foundation ($L/B = 2$)

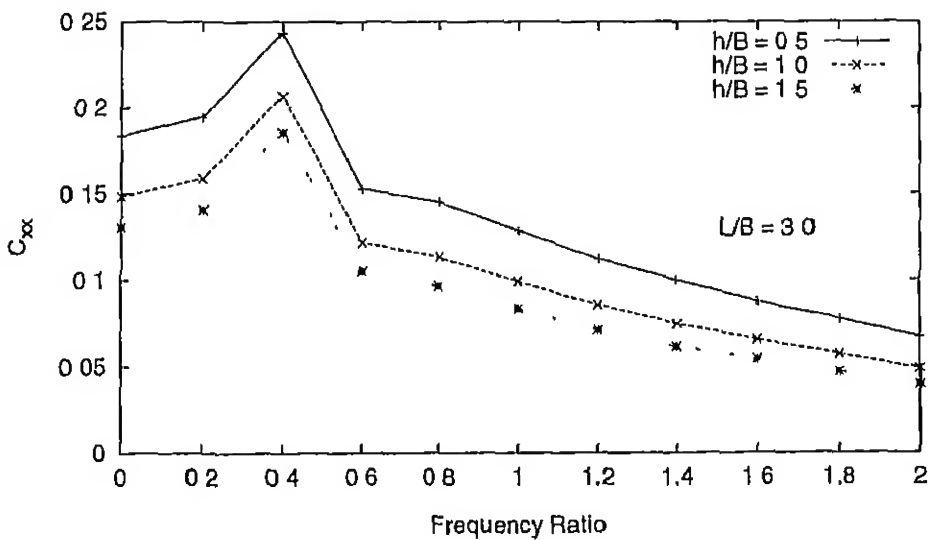


Figure 3.13 Effect of Embedment on Horizontal Compliance Function for Rectangular Foundation ($L/B = 3$)

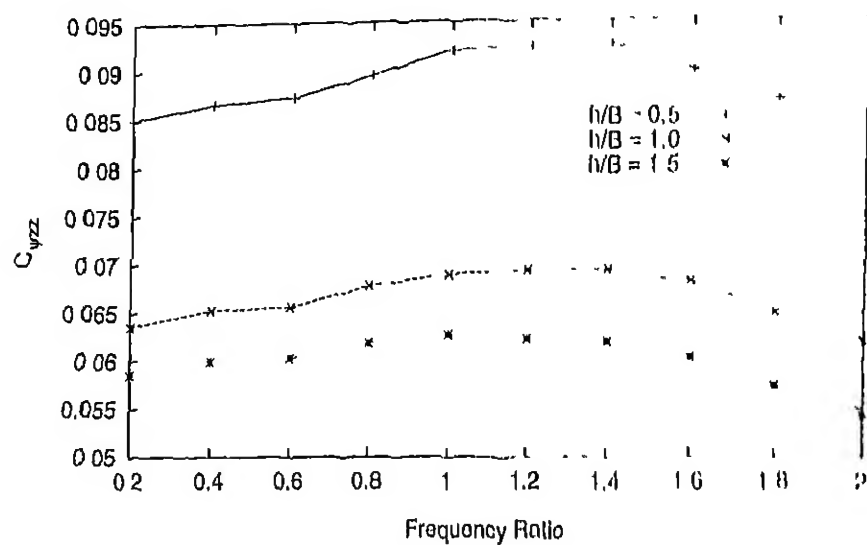


Figure 3.14 Effect of Embedment on Rotational Compliance Function for Square Foundation

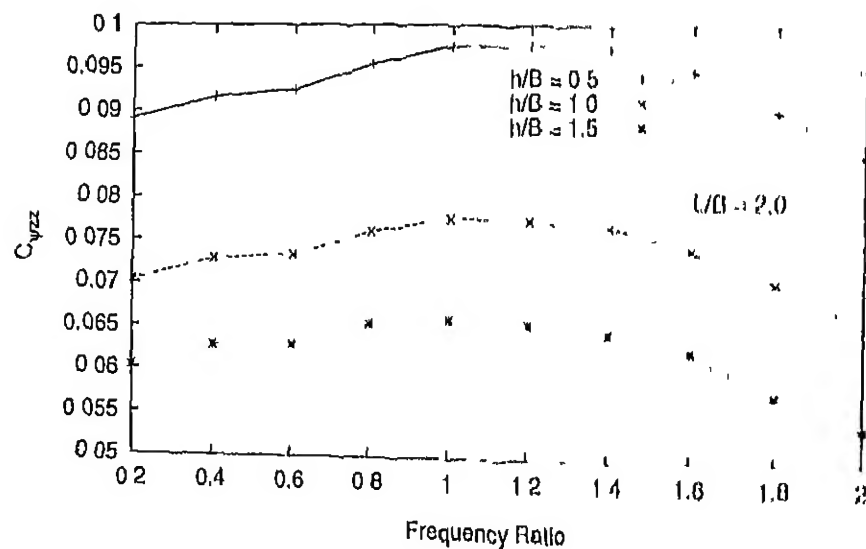


Figure 3.15 Effect of Embedment on Rotational Compliance Function for Rectangular Foundation ($L/B = 2$)

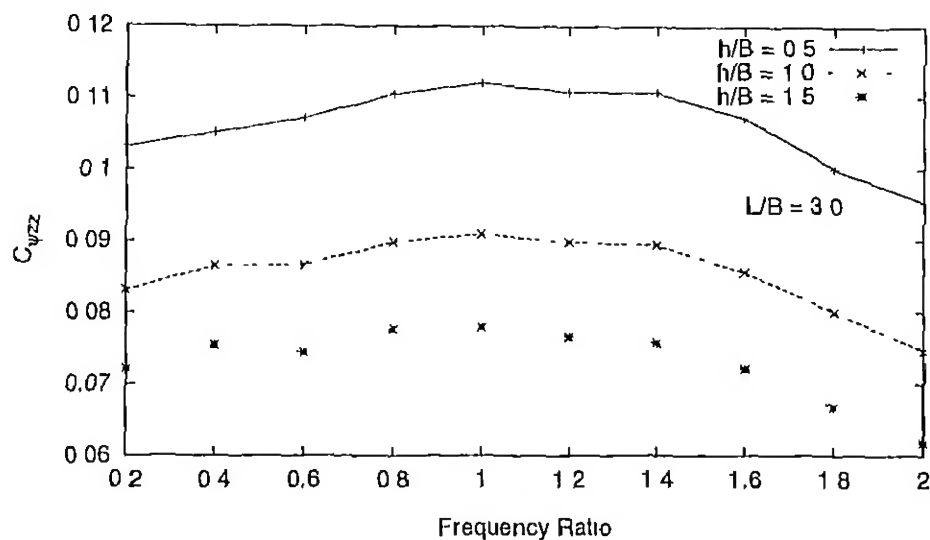


Figure 3.16 Effect of Embedment on Rotational Compliance Function for Rectangular Foundation ($L/B = 3$)

3.4.3 Effect of Aspect Ratio (L/B)

The Effect of Aspect ratio of the foundation on the compliance function at different embedment ratios are investigated. Compliance functions for vertical, horizontal and rocking modes are shown in Figures 3.17 to 3.24.

It can be noted from Figures 3.17 to 3.24 that aspect ratio does not alter the resonant frequencies in all three modes of vibration. For vertical mode of vibration, compliance function (Figures 3.17 to 3.19) increases with aspect ratio by more than 100% from square foundation to rectangular foundation with $L/B = 3$ at resonance. At high frequencies the effect of aspect ratio is small. For horizontal mode of vibration compliance function (Figures 3.20 to 3.22) increase with aspect ratio by about 90% from square foundation to rectangular foundation with

$L/B = 3$ at resonance. In case of rotational vibration the aspect ratio does not have significant effect (Figures 3.23 to 3.24 as in case of other modes. Maximum increase in the compliance function is of the order of 20%.

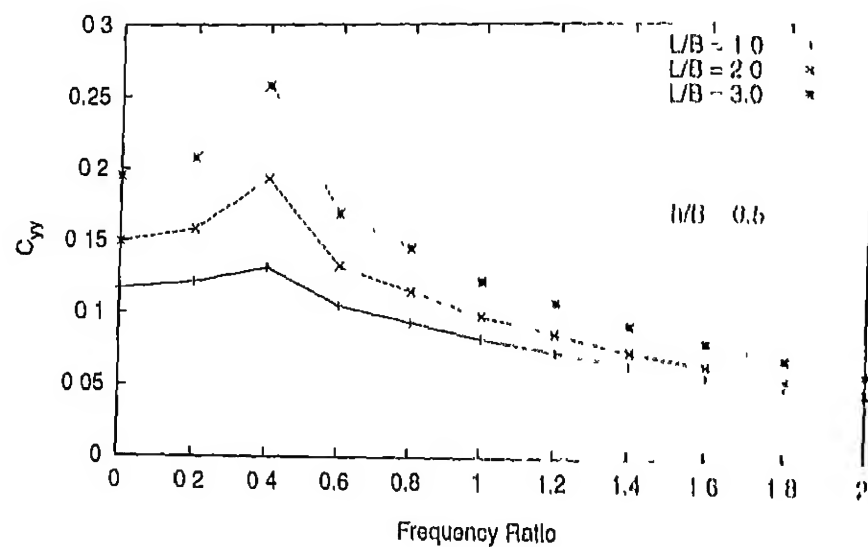


Figure 3.17: Effect of Aspect Ratio on Vertical Compliance Function for 1 mbedded Foundation ($h/B = 0.5$)

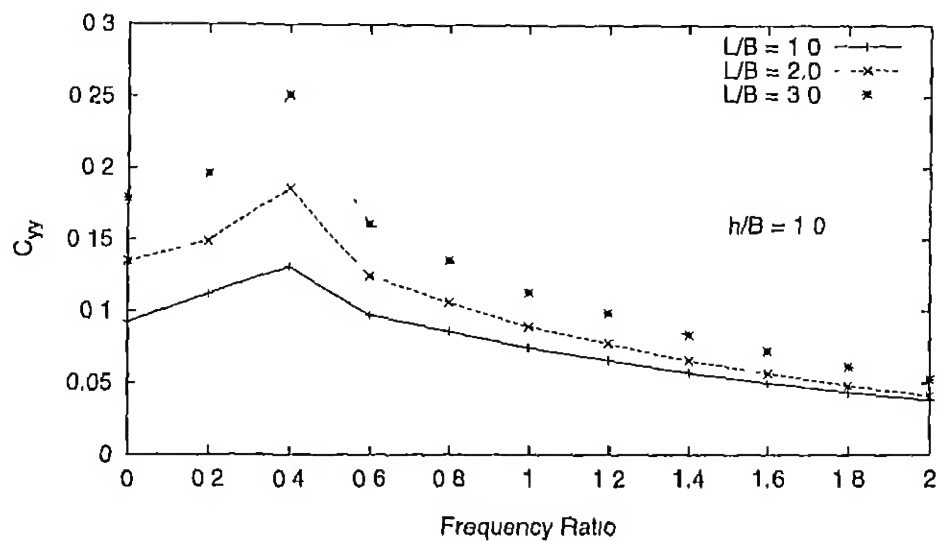


Figure 3.18 Effect of Aspect Ratio on Vertical Compliance Function for Embedded Foundation ($h/B = 1.0$)

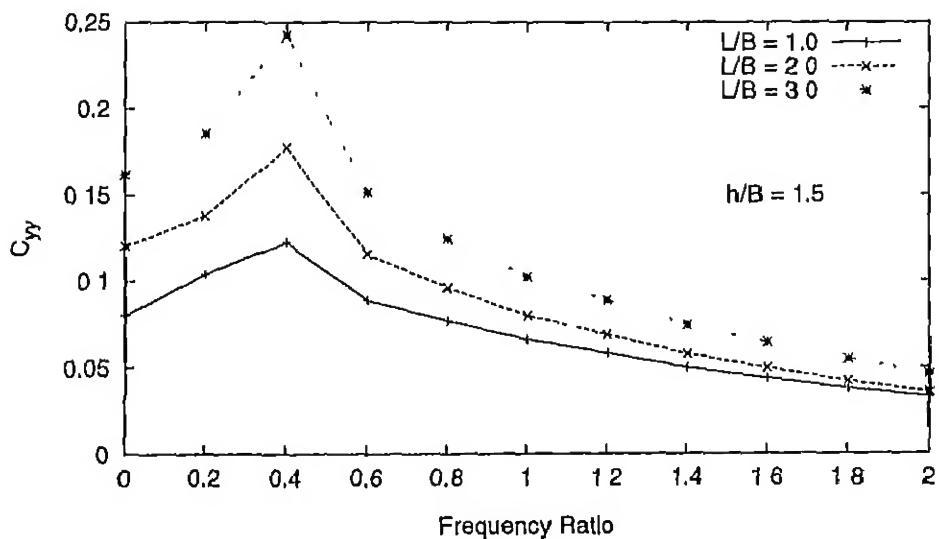


Figure 3.19 Effect of Aspect Ratio on Vertical Compliance Function for Embedded Foundation ($h/B = 1.5$)

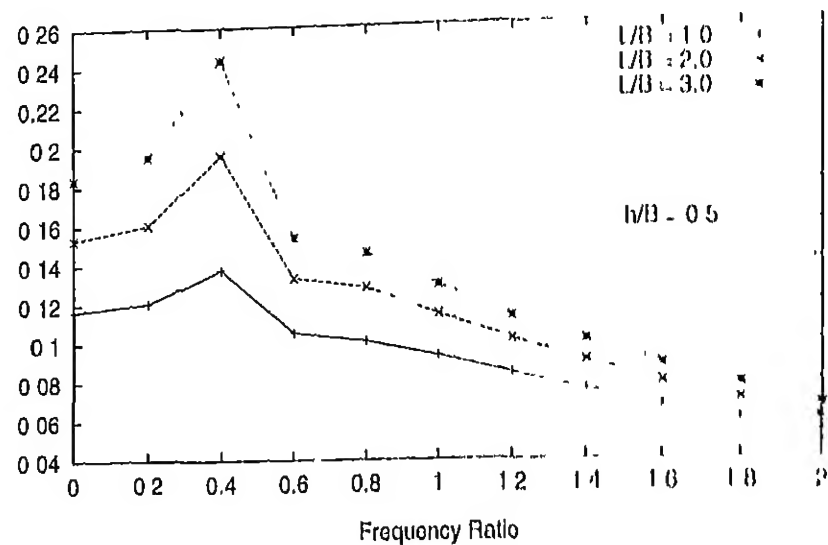


Figure 3.20 Effect of Aspect Ratio on Horizontal Compliance Function for 0.5m embedded Foundation ($h/b = 0.5$)

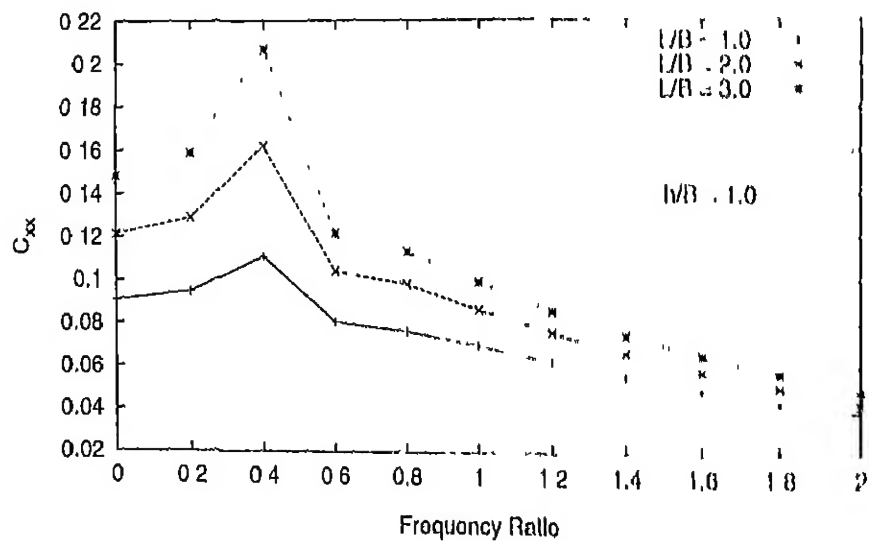


Figure 3.21 Effect of Aspect Ratio on Horizontal Compliance Function for 1.0m embedded Foundation ($h/B = 1.0$)

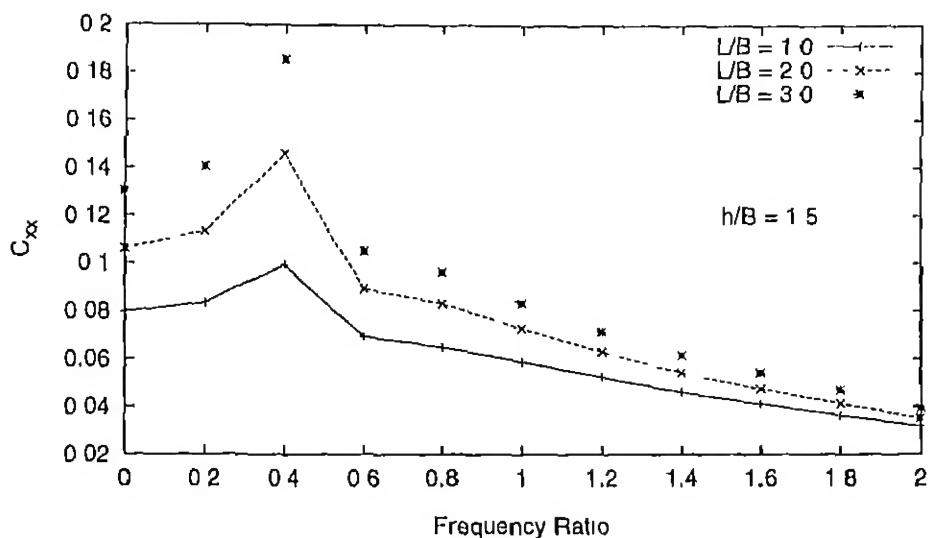


Figure 3.22: Effect of Aspect Ratio on Horizontal Compliance Function for Embedded Foundation ($h/B = 1.5$)

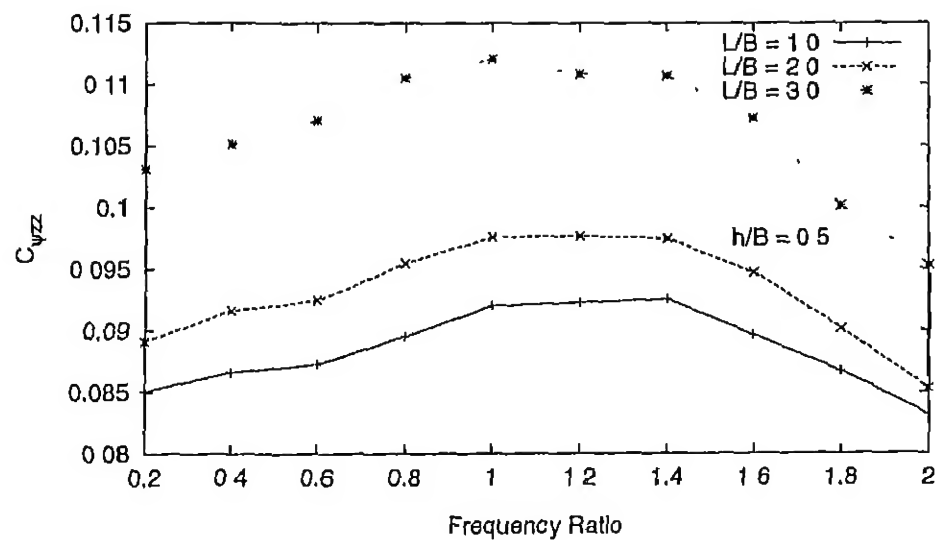


Figure 3.23: Effect of Aspect Ratio on Rotational Compliance Function for Embedded Foundation ($h/B = 0.5$)

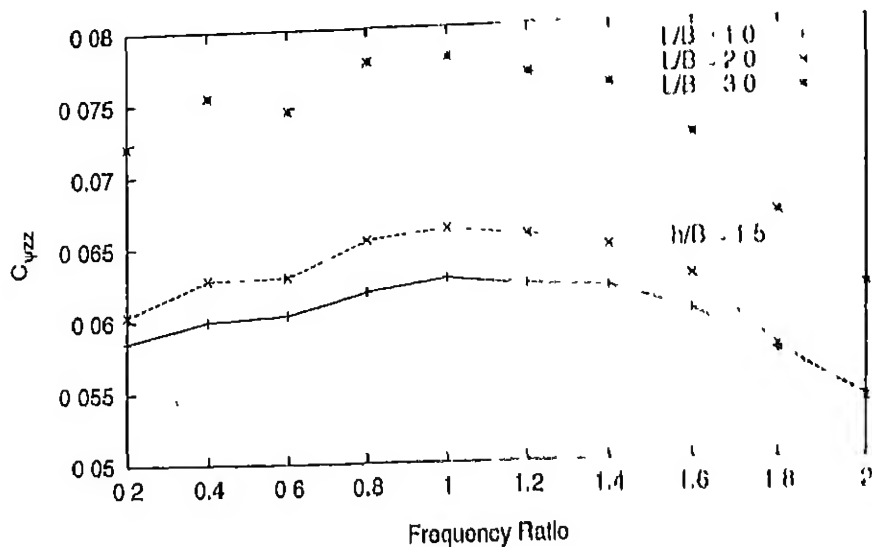


Figure 3.24: Effect of Aspect Ratio on Rotational Compliance Function for $h = B$ bedded Foundation ($h/B = 1.5$)

3.4.4 Effect of Foundation Flexibility

A non dimensional relative flexibility is defined to characterize the foundation flexibility as (Gucunski and Peck (1993)),

$$Fr = \frac{E_s d^3}{E_p B^3} \quad (3.17)$$

where E_p , E_s are Young's modulus of the foundation material and soil respectively.

Displacement amplitudes are computed for square embedded foundation with flexibility ratios Fr of 0.125, 0.0125, and 0.00125. Normalized amplitude is defined as the ratio of the amplitudes at any point on the surface of the foundation to that at the center. A normalized amplitude of 1.0 all along the surface indicates a rigid foundation. The absolute and normalized variation of the amplitudes along the

width of the foundation at different frequency ratios for vertical and horizontal modes of vibration are obtained.

The variation of absolute amplitudes for vertical mode along the normalized width (ratio of distance r of the location of the point from the center to halfwidth of the foundation) is shown in Figure 3.25. Absolute amplitudes rapidly decrease along the width for high flexibility ratio, whereas they do not change much for low flexibility ratios. However, beyond the edge of the foundation flexibility does not have significant effect. Normalized amplitudes at different frequency ratios and flexibility ratios are shown in Figure 3.26. It can be observed that increase in frequency ratio has little effect on the normalized displacements. Normalized displacement variation with different embedment ratios are shown in Figure 3.27. Increase in embedment ratio increases the effective rigidity of the foundation, *i.e.* for the same flexibility ratio increase in the embedment reduces the variation of the normalized displacement.

Variation of absolute and normalized horizontal amplitudes for different flexibility ratios are shown in Figures 3.28 and 3.29. It can be seen that flexibility ratio does not have significant effect in horizontal mode of vibration.

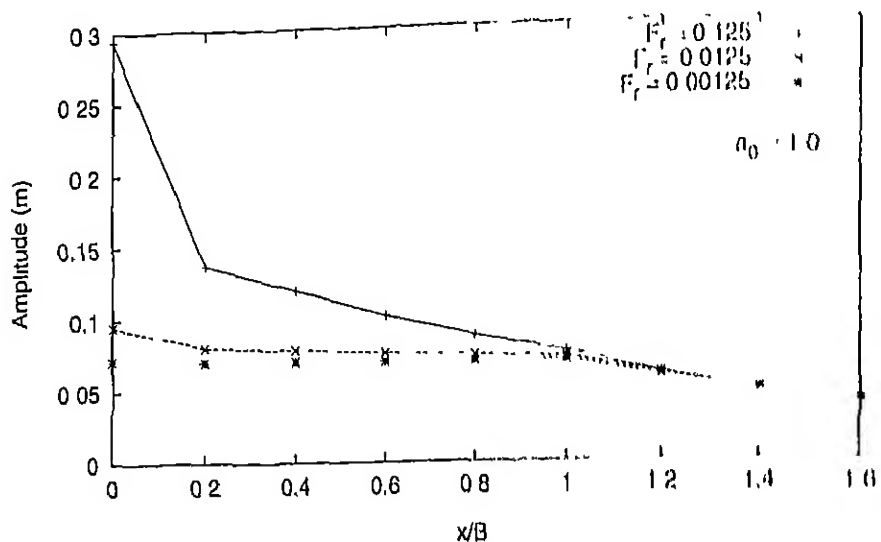


Figure 3.25: Effect of Foundation Flexibility on Absolute Vertical Amplitude

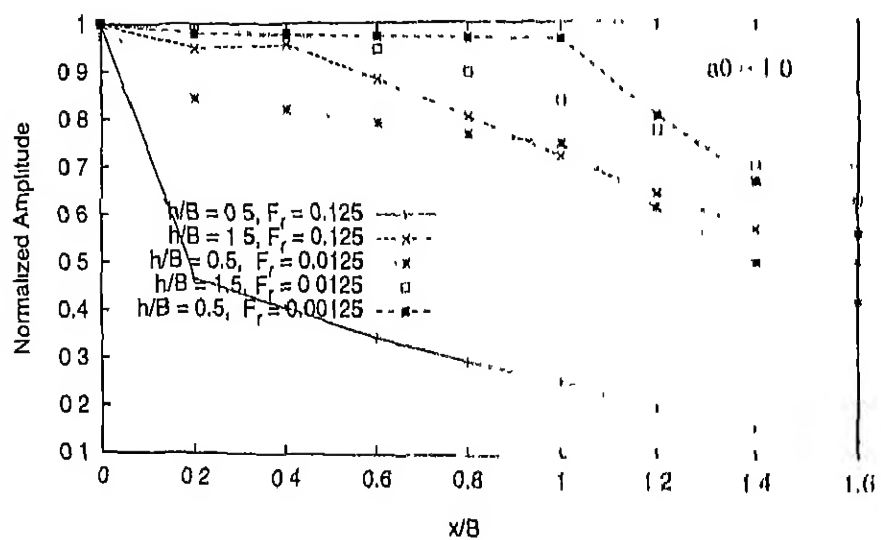


Figure 3.26: Foundation Flexibility vs Normalized Vertical Amplitude

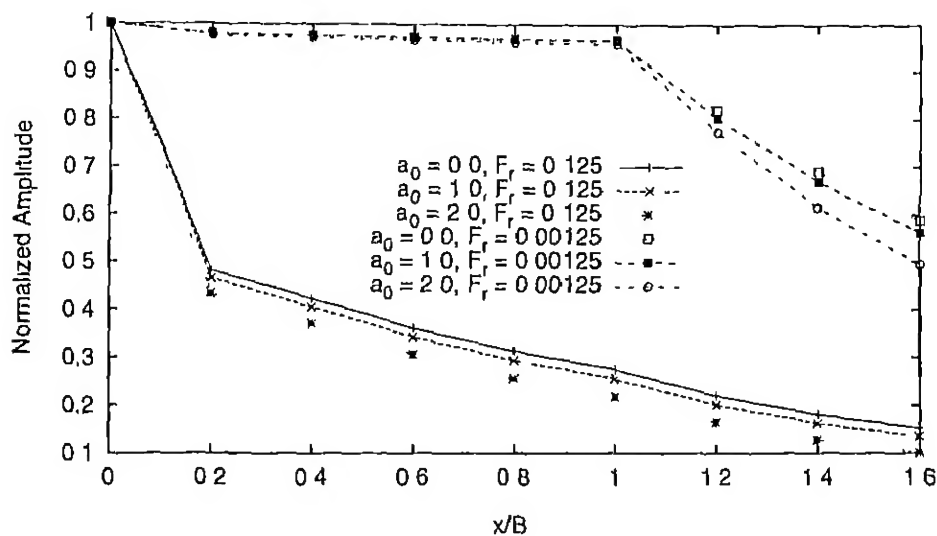


Figure 3.27 Embedment vs Normalized Vertical Amplitude

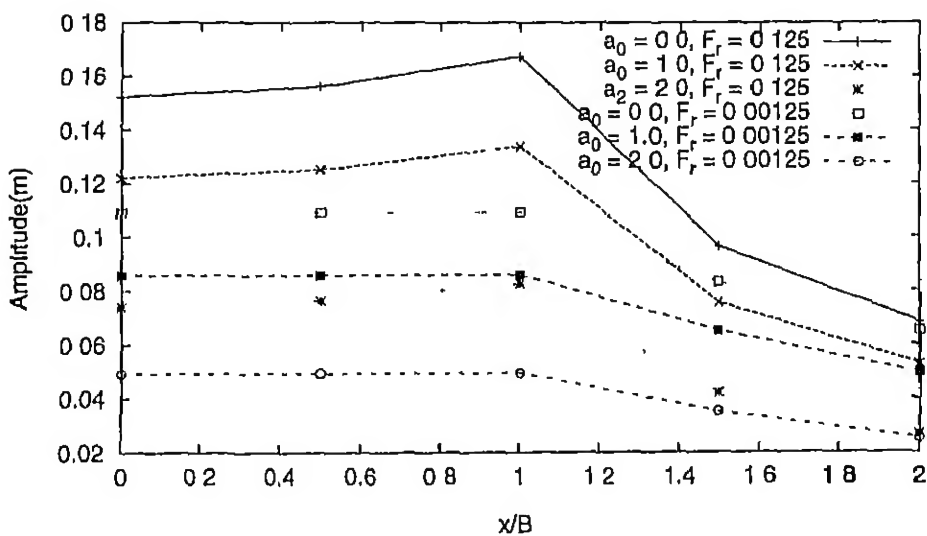


Figure 3.28. Effect of Foundation Flexibility on Absolute Horizontal Amplitude

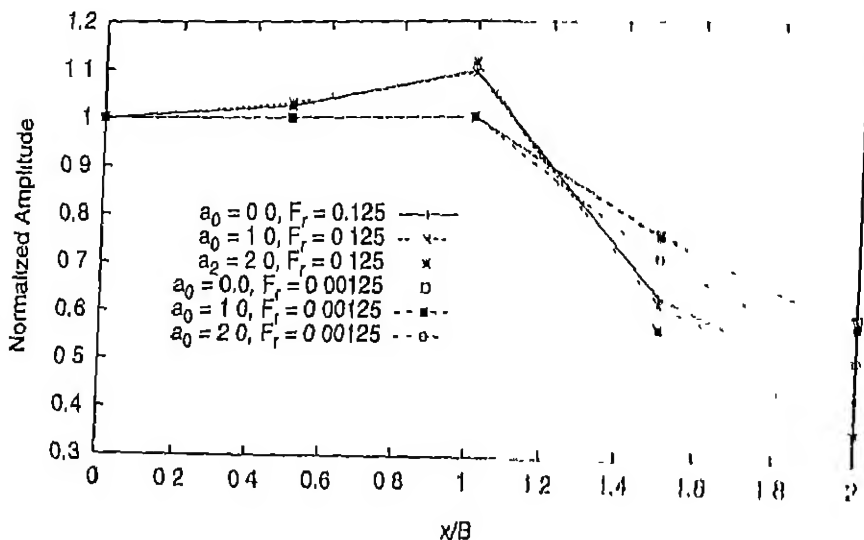


Figure 3.29 Effect of Foundation Flexibility on Normalized Horizontal Amplitude

3.4.5 Effect of Layered Soil

Compliance functions of square embedded foundations resting on two-layered soil system are computed. Effect of top layer thickness and ratio of Young's moduli of the two layers are investigated. Non-dimensional thickness parameter T_r and modular ratio M_r are defined as

$$T_r = \frac{t}{B} \quad (3.18)$$

$$M_r = \frac{E_t}{E_b} \quad (3.19)$$

where t is the thickness of top layer; E_t and E_b are the Young's moduli of top layer and bottom layer respectively.

Compliance functions for vertical mode of vibration for different thickness ratios for a particular modular ratio are shown in Figures 3.30

32. It can be seen that the effect of layering is pronounced (reduction in compliance function for $M_t > 10$ and increase for 1.0) for small values of thickness ratio. It can be said that smallness of the top layer effects the responses considerably. In the mentioned figures the 'half-space' solution represents response homogeneous half-space with modulus equal to E_t . It can be seen that beyond a thickness ratio of 10 layering does not affect response *i.e.* top soil whose thickness equal to 10 times halfwidth of the top layer will only influence the response. The presence of a soft soil ($M_t < 1$) under-lain reduces the resonant frequencies, whereas a hard soil ($M_t > 1$) increase the resonant frequencies. A layered soil system with higher modular ratio with small thickness of the top soil do not exhibit resonant frequencies. Figures 3.34 and 3.33 show the effect of modular ratio at different thickness ratios. It can be observed that effect of modular ratio is strong at low frequencies and low thickness ratios.

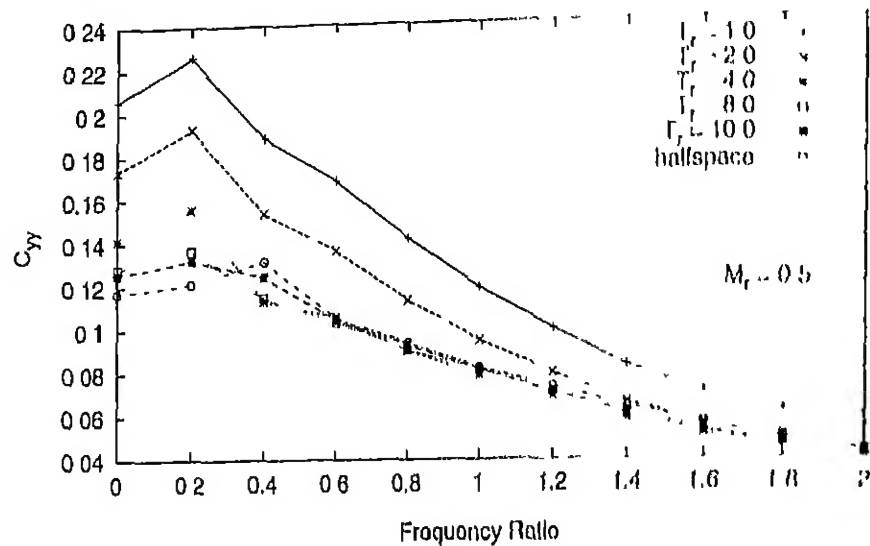


Figure 3.30: Thickness Ratio *vs* Vertical Compliance Function ($M_f = 0.5$)

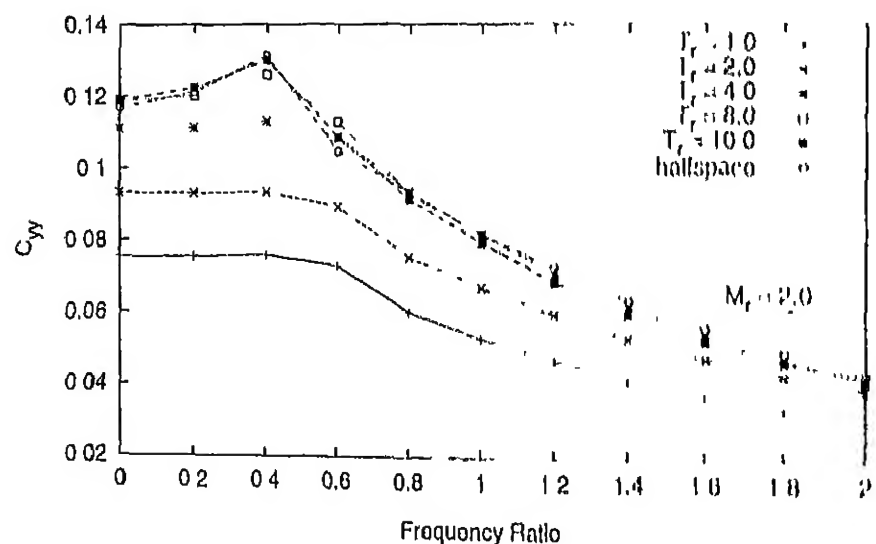
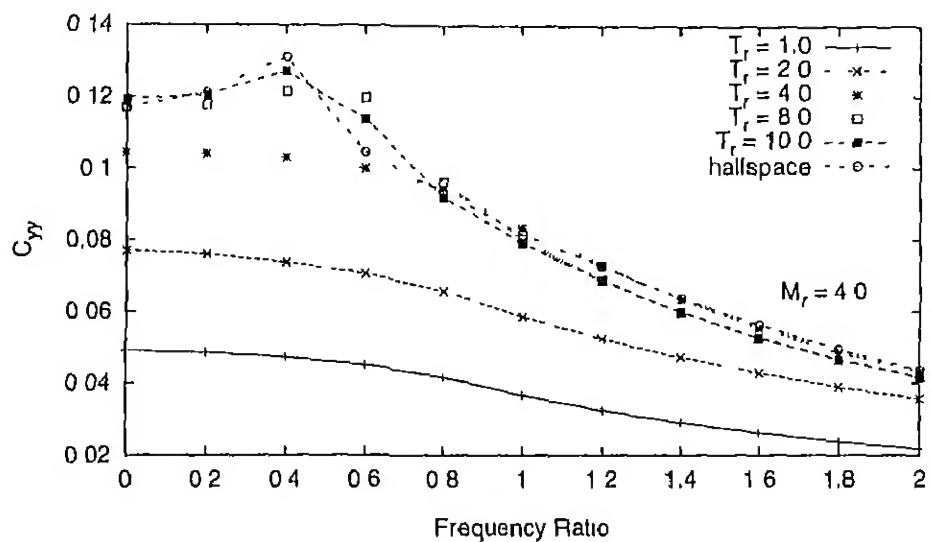
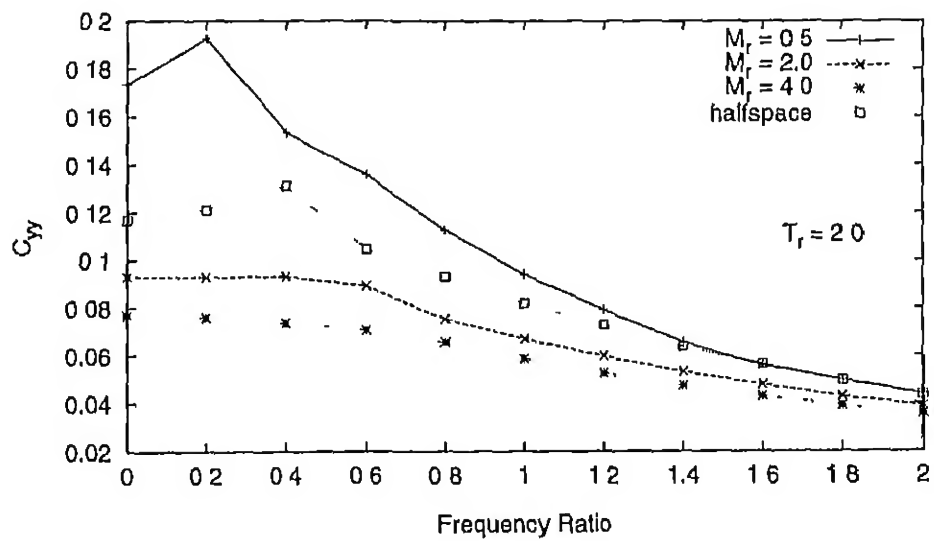


Figure 3.31: Thickness Ratio *vs* Vertical Compliance Function ($M_f = 2.0$)

Figure 3.32 Thickness Ratio *vs* Vertical Compliance Function ($M_r = 4.0$)Figure 3.33 Modular Ratio *vs* Vertical Compliance Function ($T_r = 2.0$)

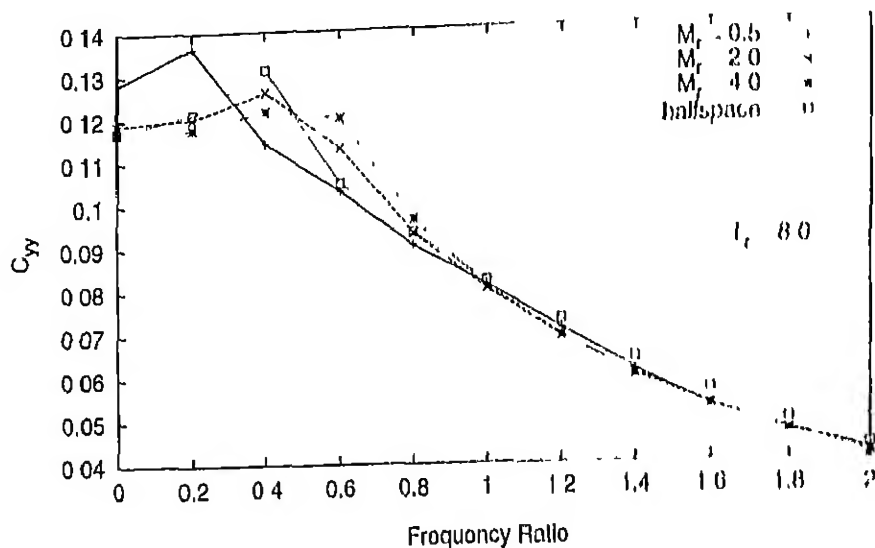


Figure 3.34 Modular Ratio *vs* Vertical Compliance Function ($T_r = 8.0$)

Horizontal compliance functions for different thickness ratios at modular ratios of 0.5, 2.0 and 4.0 are presented in Figures 3.35 to 3.37. In horizontal mode also a small thickness of the top layer effects the responses strongly. For *low* T_r , resonant frequency of the system reduces for $M_r < 1$ and increases for $M_r > 1$. Beyond a thickness of ratio of 8, layering does not have significant effect on the compliance functions. Compliance functions for different modular ratios are shown in Figures 3.38 and 3.39 for thickness ratios of 2 and 8 respectively. It can be seen that unlike vertical mode the modular ratio does not have any significant effect beyond frequency ratios of 0.6 even for low thickness ratios.

Effect of layering on rotational mode of vibration is presented in Figures 3.40 to 3.41. As in the case of horizontal mode, rotational compliance functions are significantly influenced by small thickness of top layer. However the reduction for systems with $M_r > 1$ or increase

for systems with $M_r < 1$, in the compliance functions is small (of the order of 30%)

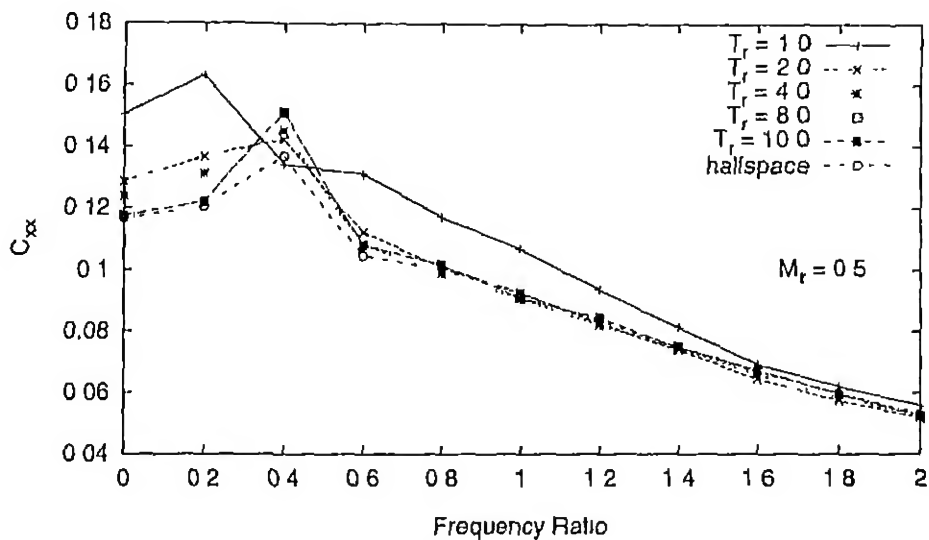


Figure 3.35 Thickness Ratio vs Horizontal Compliance Function ($M_r = 0.5$)

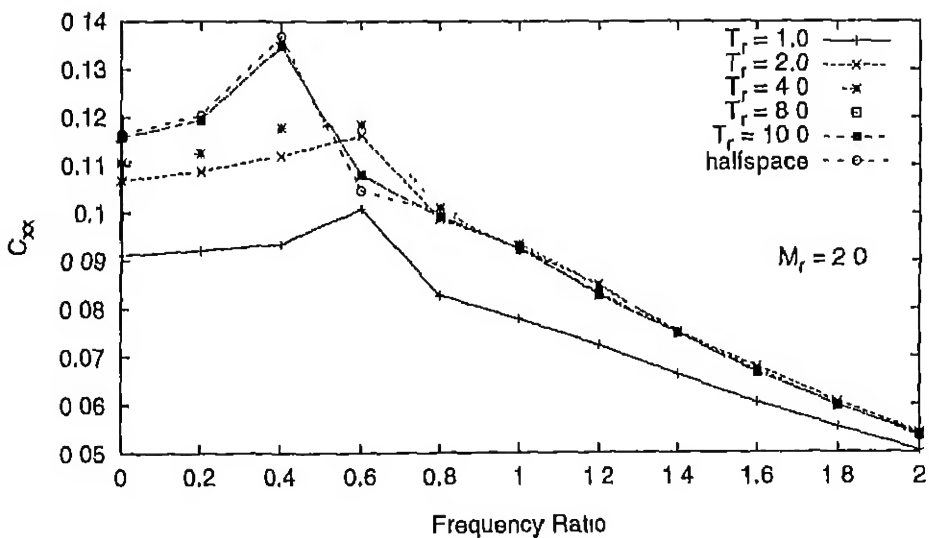
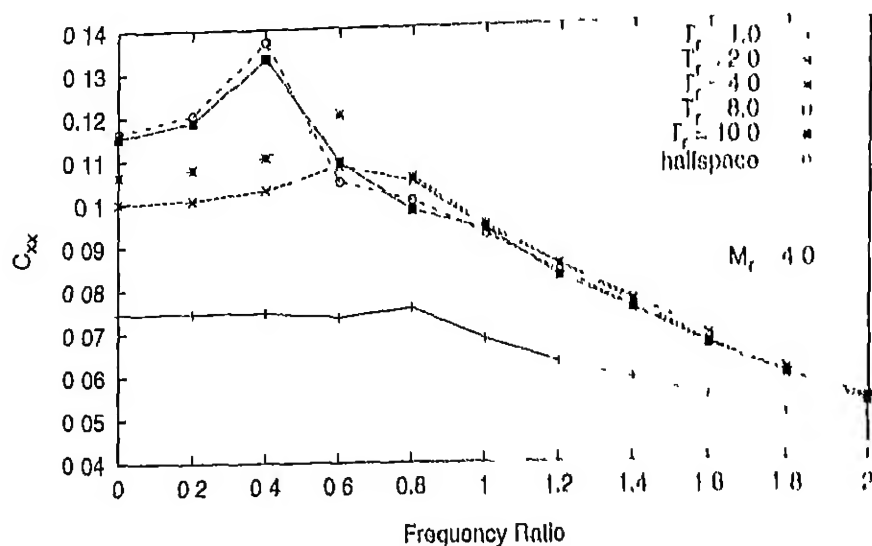
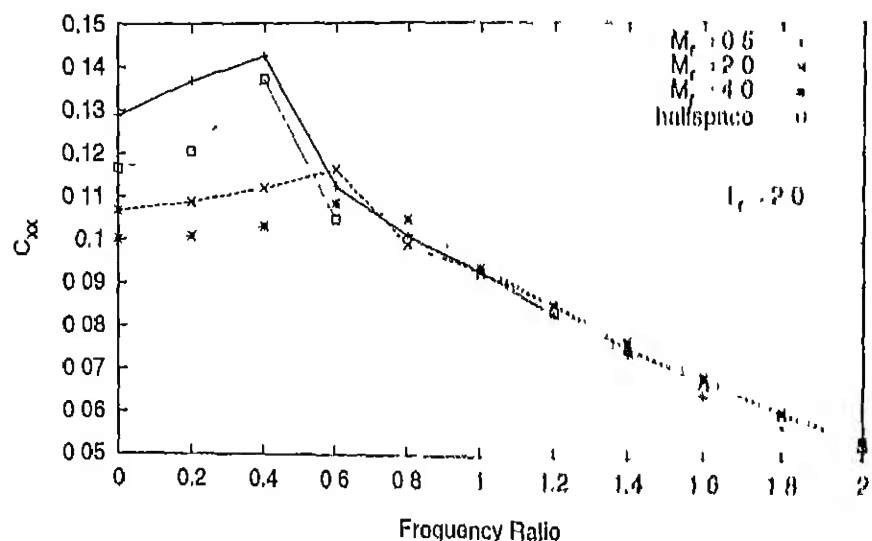


Figure 3.36: Thickness Ratio vs Horizontal Compliance Function ($M_r = 2.0$)

Figure 3.37 Thickness Ratio vs Horizontal Compliance Function ($M_f = 4.0$)Figure 3.38. Modular Ratio vs Horizontal Compliance Function ($T_f = 2.0$)

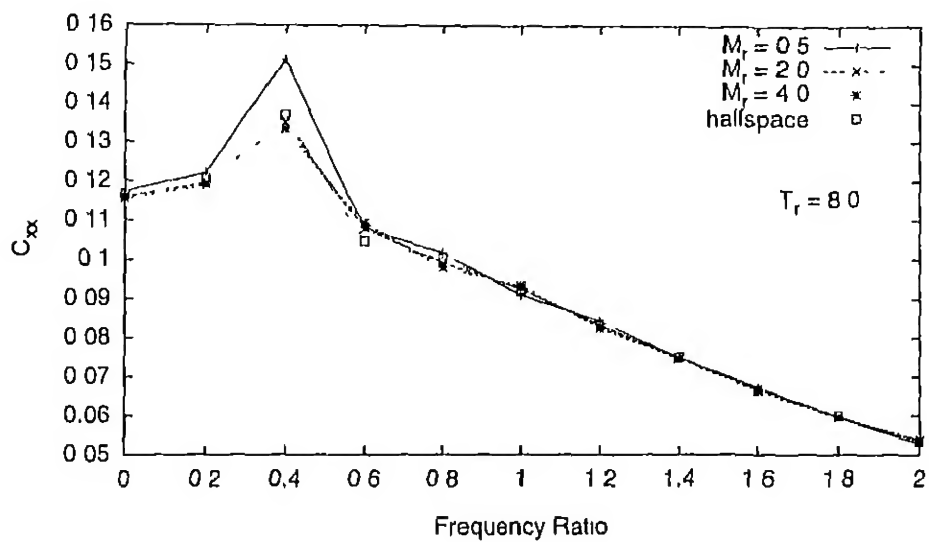


Figure 3.39 Modular Ratio *vs* Horizontal Compliance Function ($T_r = 8.0$)

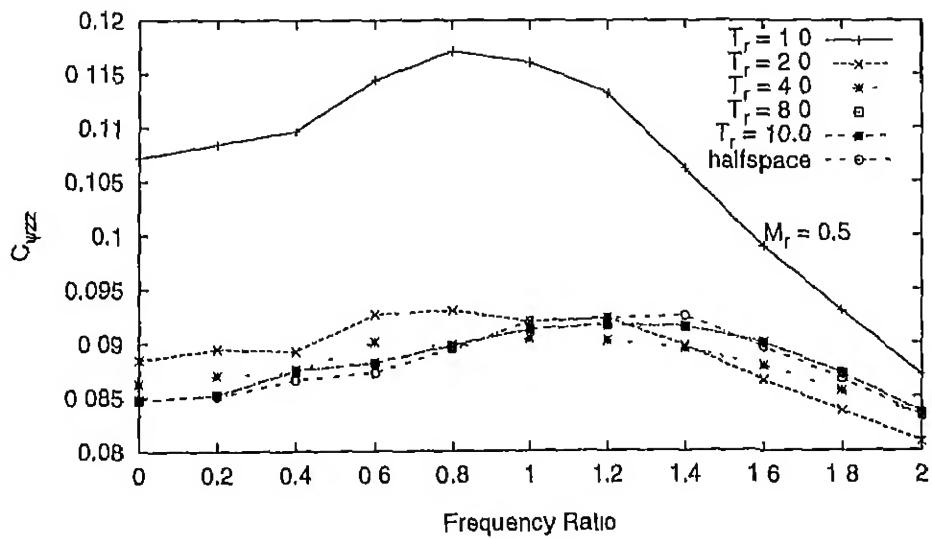


Figure 3.40. Thickness Ratio *vs* Rotational Compliance Function ($M_r = 0.5$)

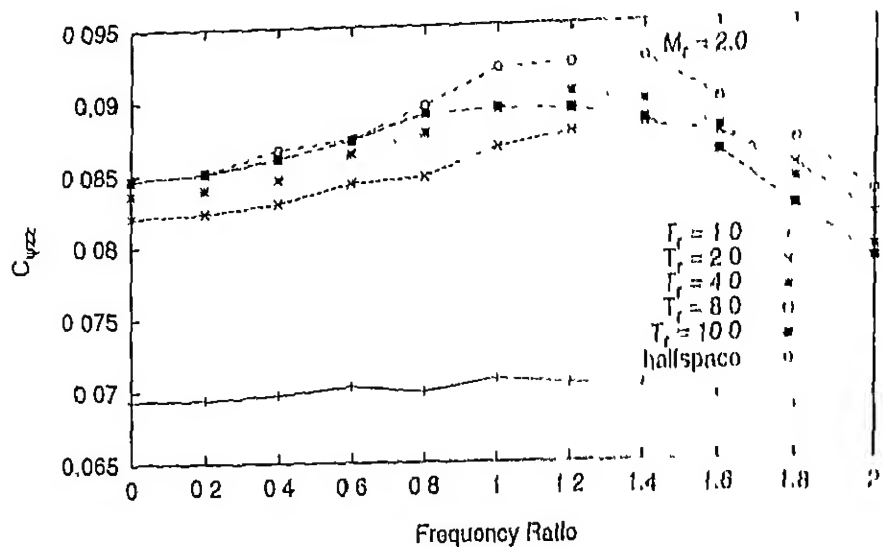


Figure 3.41 Thickness Ratio *vs* Rotational Compliance Function ($M_r = 2.0$)

3.4.6 Effect of Linearly Varying Young's Modulus

Effect of linearly varying Young's modulus on compliance functions of vertical and horizontal modes of vibration is reported in this section. Vertical and Horizontal compliance functions are shown for different values of the parameter a in Figures 3.42 and 3.43. It can be observed that linearly increasing modulus reduces the compliance functions. The reduction is more pronounced in horizontal mode than in vertical mode of vibration. In horizontal mode of vibration an increase in the value a increases the resonant frequency.

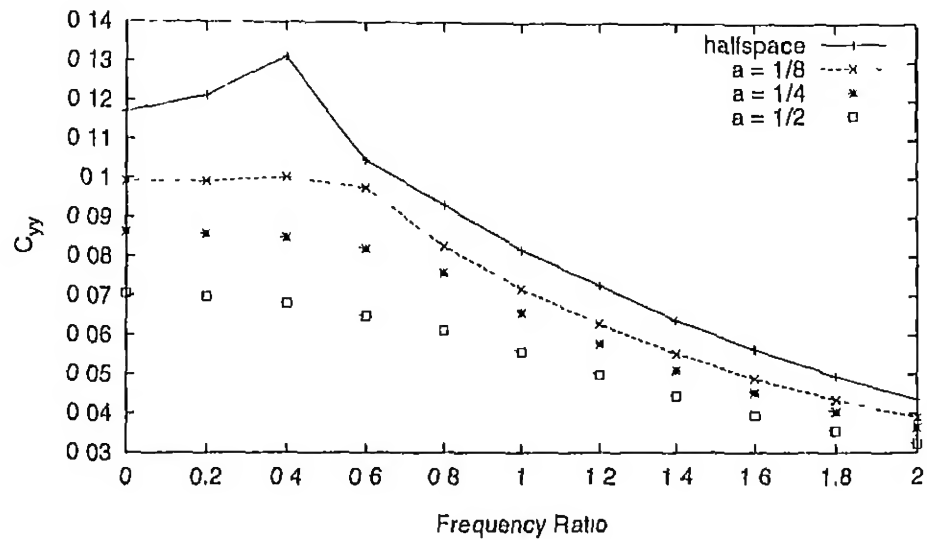


Figure 3.42: Effect of Linearly Varying Modulus on Vertical Compliance Function

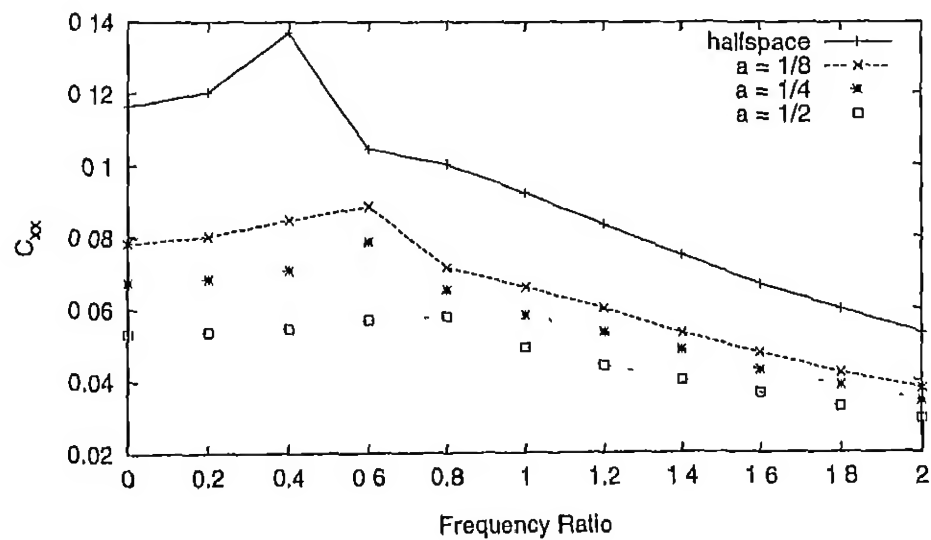


Figure 3.43: Effect of Linearly Varying Modulus on Horizontal Compliance Function

3.4.7 Effect of Rigid Bedrock at Finite Depth

Vertical and Horizontal compliance functions for finite thick (D) compressible layer resting on rigid bedrock are presented in this section. For different values of the ratio D/B , where D is the thickness of the compressible layer, compliance functions for vertical and horizontal modes of vibration are shown in Figures 3.44 and 3.45. It can be observed that vertical responses are strongly influenced, whereas the horizontal responses are less influenced by the presence of hard rock at finite depth.

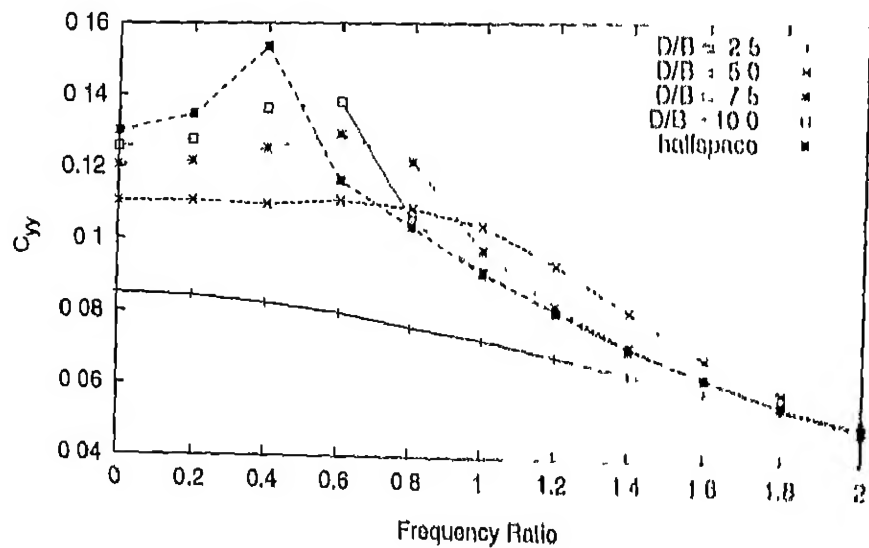


Figure 3.44: Effect of Rigid Bedrock at Finite Depth on Vertical Compliance Function

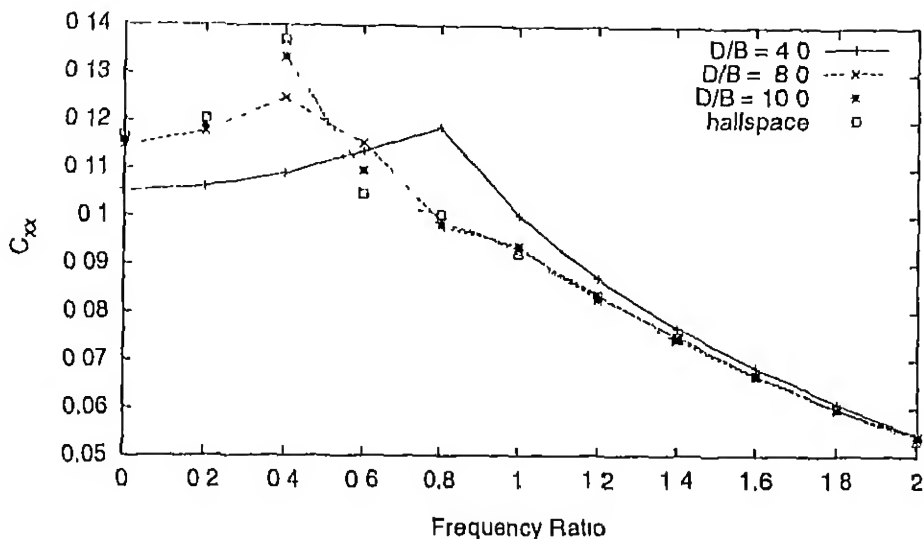


Figure 3.45 Effect of Rigid Bedrock at Finite Depth on Horizontal Compliance Function

3.4.8 Summary

A summary of the conclusions based on the results presented in the earlier sections are presented in this section.

1. The solutions obtained by the present model match well with those obtained by the time domain BEM method.
2. Reduction in compliance functions due embedment is more in horizontal and rotational modes than in vertical mode. Embedment does not significantly alter the resonant frequencies of the system.
3. Increase in aspect ratio (L/B) causes an increase in the compliance functions in all modes. The effect of aspect ratio is small in rotational mode. However at higher frequencies the effect of

aspect ratio is small for all modes of vibration.

4. Foundations behave less rigid (can be quantified in terms of the variation of displacement across) in vertical mode than in horizontal mode for given geometry and material properties (flexibility ratio). Increase in the depth of embedment increases the rigidity of the foundation (in vertical mode) for a given flexibility ratio.
5. Compliance functions are strongly influenced by small thickness of the top layer. Even at low frequencies, soil layer below 10 times the half width of the footing does not influence the behaviour. Due to layering resonant frequencies changes. Soft bottom layers reduce the resonant frequencies whereas the hard bottom layer increase the resonant frequencies of the system.
6. Linearly increasing modulus reduces the compliance functions. The effect is more pronounced for horizontal mode than vertical mode. Linear variation of the modulus increases the resonant frequencies for horizontal mode, whereas vertical mode does not exhibit any resonance.
7. presence of hard rock is strongly felt in vertical mode than horizontal mode of vibration.

Chapter 4

PILE FOUNDATION SOIL SYSTEMS

Pile foundation are usually adopted in situations where – 1. The top soil is highly compressible, 2. It is not strong enough to take the loads through block foundation, 3. It is prone to liquefaction 4. To transfer large magnitudes of lateral loads to the soil. The response of single pile and pile groups subjected to dynamic loads have received a lot of attention over last couple of decades. The development of analytical solutions is accelerated due to growing use of pile foundations in traditional areas such as buildings, machine foundations, nuclear power plants and offshore structures.

4.1 Introduction

The response of piles and their load carrying capacity depends on the pile soil interaction. This interaction modifies the stiffness of the pile and generates damping through energy radiation (geometric damping) due to semi-infinite geometry of the soil and energy dissipation due to material damping. Often the piles are used in a group, which

introduces pile-soil-pile interaction. The combined effect of pile cap and pile group determines the response of the pile foundation system. Due to the complex nature of soil-structure (pile and/or cap) interaction (see Chapter 3) analytical solutions are difficult to obtain.

4.2 Brief Literature Review

Novak (1974) was the first to attempt to analyze the dynamic response of single pile using continuum theory. He modeled the pile as an assembly of beam elements and soil reactions on it were obtained assuming a plane strain condition (infinitely long pile). The same approach was extended by Novak (1977) for the analysis of pile embedded in layered media. Nogami and Novak (1976) and Novak and Nogami (1977) developed closed form solutions, for vertical and horizontal modes of vibration of an end bearing pile, making use of rigorous three dimensional theory. Novak and Howell (1978) obtained the responses of the pile in torsional mode of vibration. Novak and Sheta (1980) have investigated the response of piles including the contact effects using a mass less layer with reduced modulus around the piles. Novak and Sheta (1982) obtained the pile group responses using interaction factors.

Blaney, Kausel and Roesett (1976) studied pile vibration using finite element method with consistent energy absorbing boundary. Kuhlemeyer (1979b), and Kuhlemeyer (1979a) studied vertical and horizontally loaded piles by finite element method. He developed a method for axisymmetrical solids loaded non-axisymmetrically, making use of finite elements and energy absorbing boundary. Dobry, Vincente, *et al.*

(1982) studied the horizontally loaded piles making use of finite element codes available and presented some approximations for stiffness and damping ratios. Wolf and von Arx (1978) extended the finite element analysis to pile groups. Waas and Hartmann (1981) developed a methodology to analyze pile groups in which pile stiffnesses were obtained using a Fourier expansion for axisymmetrical pile groups and finite elements along with consistent energy absorbing boundary for soil. This was extended by Tyson and Kausel (1983) for pile groups with embedded pile raft. Kaynia (1982) developed a three dimensional continuum model for pile groups and obtained dynamic interaction factors and group efficiency ratios.

Sen, Kausel and Banerjee (1985) developed boundary element formulation to obtain the steady state response of piles and pile groups embedded in homogeneous and non-homogeneous soils. Nogami and Kongai (1986) and Nogami and Kongai (1988) developed discrete models for pile soil interaction for vertical and horizontal modes and obtained responses in time domain. Mamoon and Banerjee (1992) developed a direct time-domain and transformed time domain models for dynamic pile soil interaction. They used step-by-step integration scheme using approximate half-space half-space integral formulation to obtain the soil reactions. Cheung, Tham and Lie (1995) used direct boundary element formulation to obtain the response of horizontally loaded pile in time domain.

4.3 Present Model

The procedures for frequency domain analysis of pile foundations are well investigated. Extensive literature is available on dynamic response of single piles. However, usually, piles are used in groups with a cap. As mentioned in the review, the use of dynamic interaction factors to obtain the group response is almost approximate in nature. It is rather prudent to visualize the pile group with cap as a raft foundation supported by piles. Here in this investigation the pile group has been analyzed along with pile cap (or as block foundation supported by group of piles) in an integrated manner, rather than the substructure approach (treating soil and pile separate) adopted by earlier investigators. To appreciate the effect of different parameters on the response of piles a brief study has been presented for single pile response. The computational model used for this investigation is essentially the same utilized for block foundation analysis described in detail in Chapter 3 (Section 3). The piles are modeled using three dimensional 8 noded continuum elements. The time domain solutions obtained by the present model for single pile have been validated with existing solutions.

4.4 Validation of the Model

A typical pile vibrating in vertical and lateral modes due a transient excitation has been chosen for validation. The problem definition is given in Figure 4.1. The excitation is a triangular pulse and is shown in Figure 4.2, where P_{max} is maximum force and duration of the

excitation is Δt . l, d are the length and side of a square pile which is a good approximation for a circular pile. The geometry and material properties of the problems considered in the analysis are as follows

Vertical Mode:

Size of the model	= 100x100x100m
Number of Elements	= 15x15x15 (in x, y, and z directions)
Young's Modulus of Pile Material E_p	= 2.488×10^6 kN/m ³
Poisson's Ratio Pile Material ν_p	= 0.4
Density of Pile Material ρ_p	= 2.7013 kN s ² /m ⁴
Young's Modulus of Soil E_s	= 20×10^3 kN/m ³
Poisson's Ratio Soil ν_s	= 0.4
Density of Soil ρ_s	= 10194 kN s ² /m ⁴
Length of Pile l	= 75m
Diameter of Pile d	= 2m
P_{max}	= 10^6 kN

Horizontal Mode:

Size of the model	= 100x125x50m
Number of Elements	= 30x10x15 (in x, y, and z directions)
Young's Modulus of Pile Material E_p	= 20×10^6 kN/m ³
Poisson's Ratio Pile Material ν_p	= 0.25
Unit weight of Pile Material ρ_p	= 16 kN /m ³
Young's Modulus of Soil E_s	= 20×10^4 kN/m ²

Poisson's Ratio Soil ν_s	= 0.4
Unit weight of Soil ρ_s	= 10 kN /m ³
Length of Pile l	= 75m
Diameter of Pile d	= 2m
P_{max}	= 10^6 kN

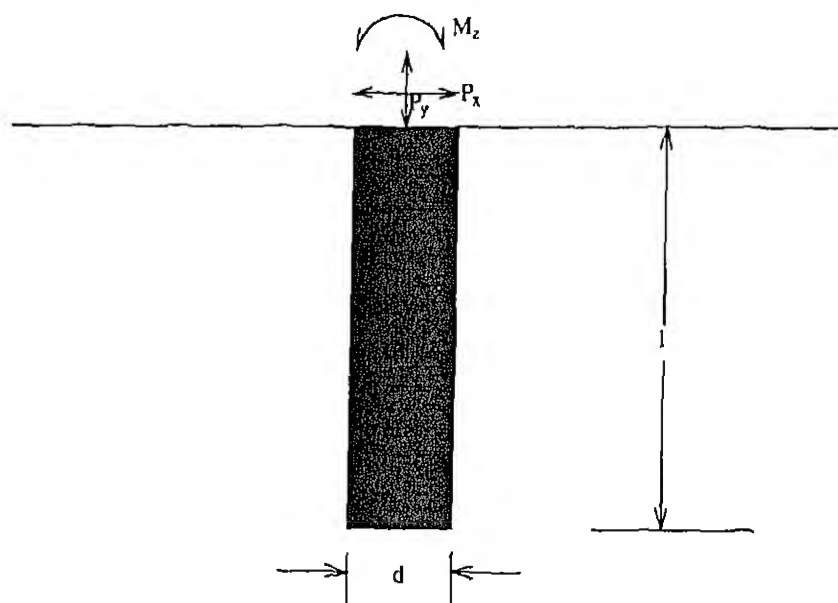


Figure 4.1 Triangular Pulse Excitation

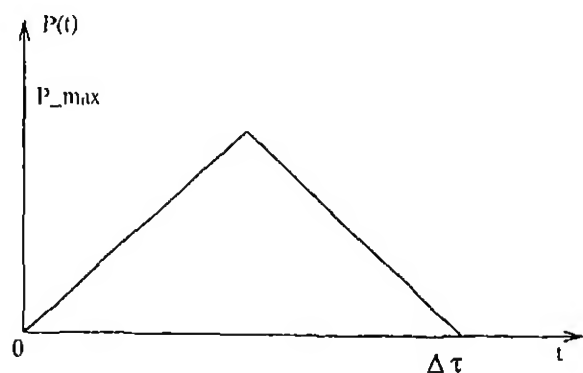


Figure 4.2: Triangular Pulse Excitation

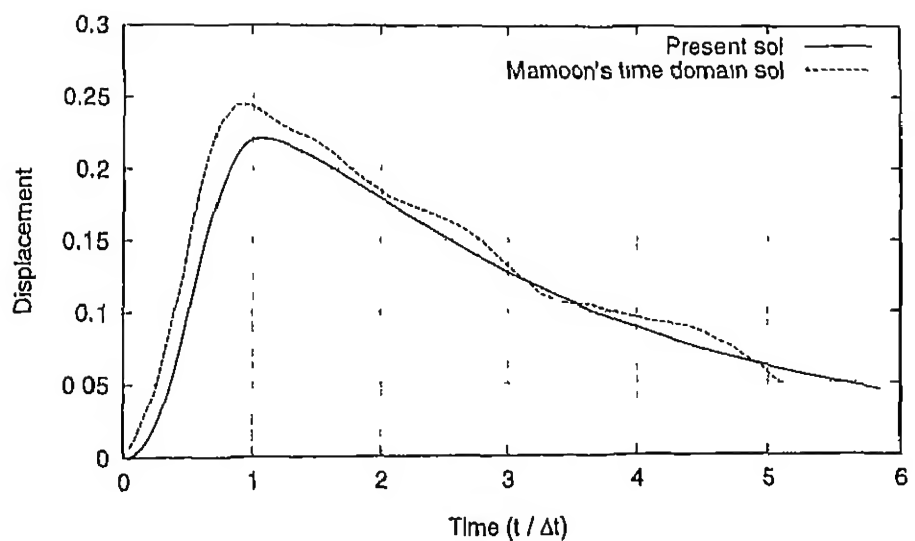


Figure 4.3. Vertical Displacement History of Pile Head Due to Triangular Pulse Load

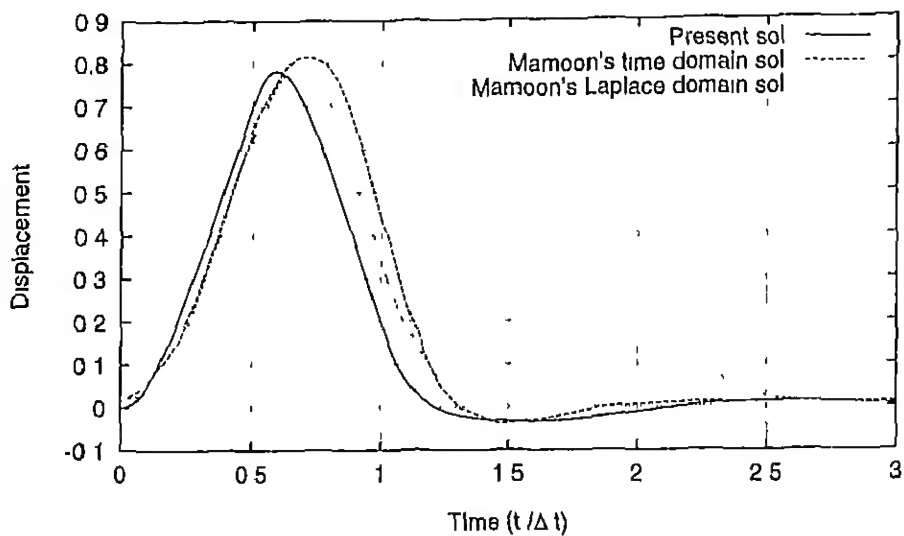


Figure 4.4 Horizontal Displacement History of Pile Head Due to Triangular Pulse Load

The displacement histories obtained with present model along with those of reported by Mamoon and Banerjee (1992) using time-domain BEM are presented in Figures 4.3, 4.4. It can be observed that the results obtained with present model compare well.

4.5 Response of Single Piles

Limited parametric studies have been conducted on the response of single piles. This has been guided by the fact that the similar behaviour of single pile and group of piles with a pile cap can not be expected. The compliance functions defined in Chapter 3 (Section 4) have been utilized for presentation of results by replacing the half-length L and half-width B of foundation block by the half the side d of the pile cross section. Compliance functions reported are computed using the

displacements at the pile head.

4.5.1 Effect of Slenderness Ratio

The slenderness ratio of the pile is defined as ratio of length of pile (l) and side (d) of square pile. For different l/d ratios pile head responses have been obtained in different modes of vibration. Vertical pile head response for different l/d ratios for a given modular ratio E_p/E_s are shown in Figures 4.5 and 4.6. It can be observed that, with increase in l/d ratio, compliance functions reduce, and reduction in compliance functions is more at low frequency ratios.

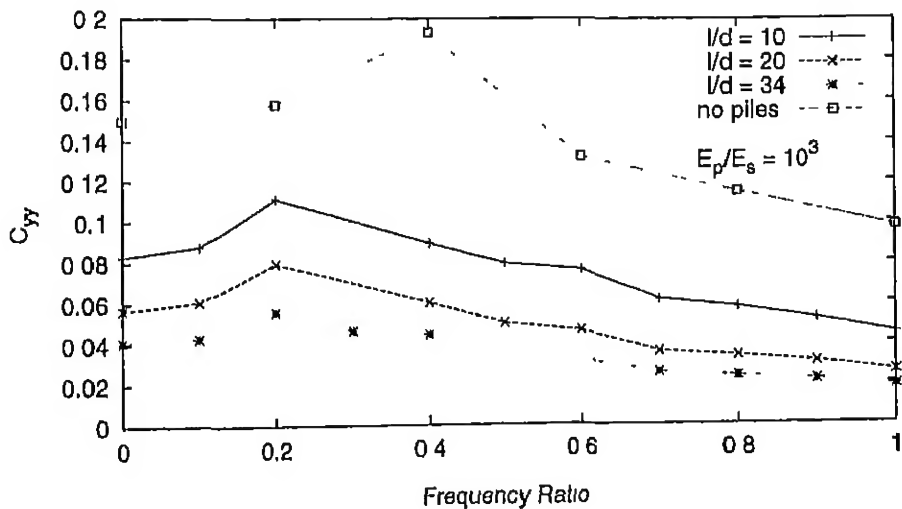


Figure 4.5: Vertical Compliance Function of Pile Head ($E_p/E_s = 10^3$)

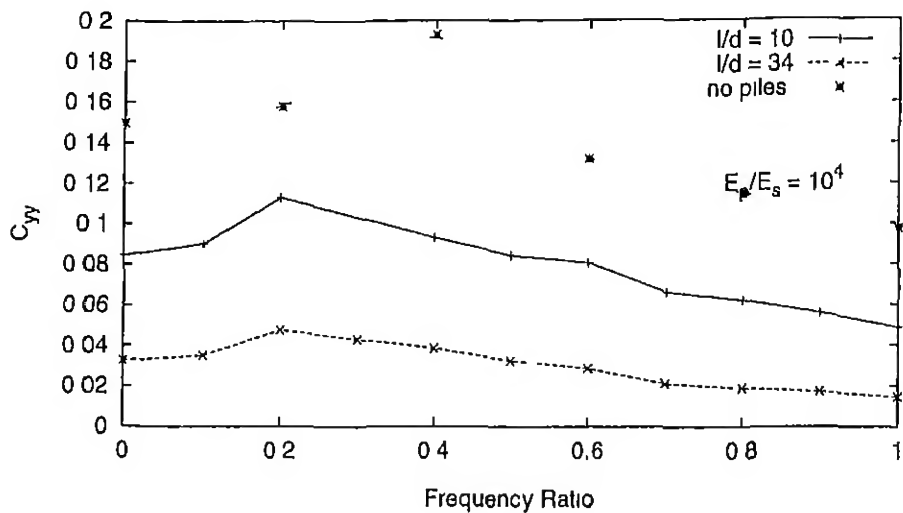


Figure 4.6 Vertical Compliance Function of Pile Head ($E_p/E_s = 10^4$)

For horizontal mode of vibration, the compliance functions are shown in Figures 4.7 and 4.8. It can be seen that for low modular ratio ($E_p/E_s = 10^3$) the l/d ratio does not have significant effect, whereas substantial reduction in compliance function with increase in l/d ratio can be observed for modular ratios of 10^4 .

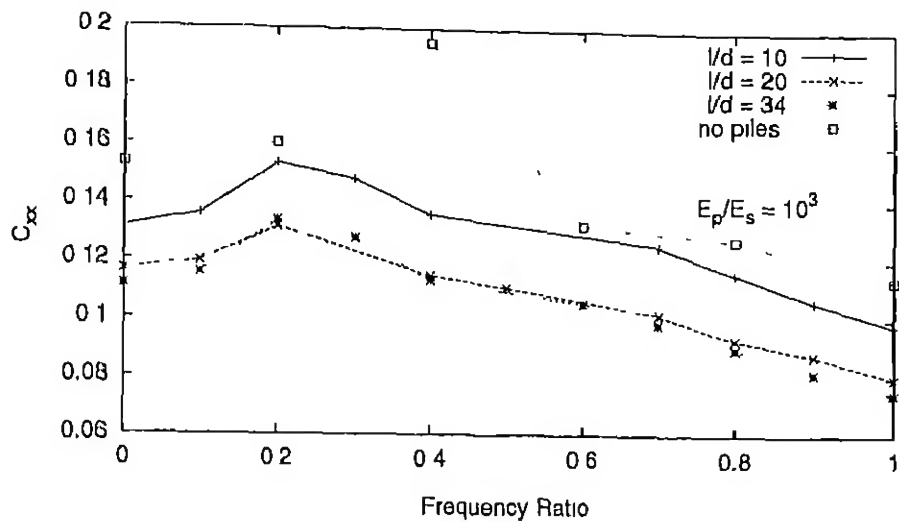


Figure 4.7. Horizontal Compliance Function of Pile Head ($E_p/E_s = 10^3$)

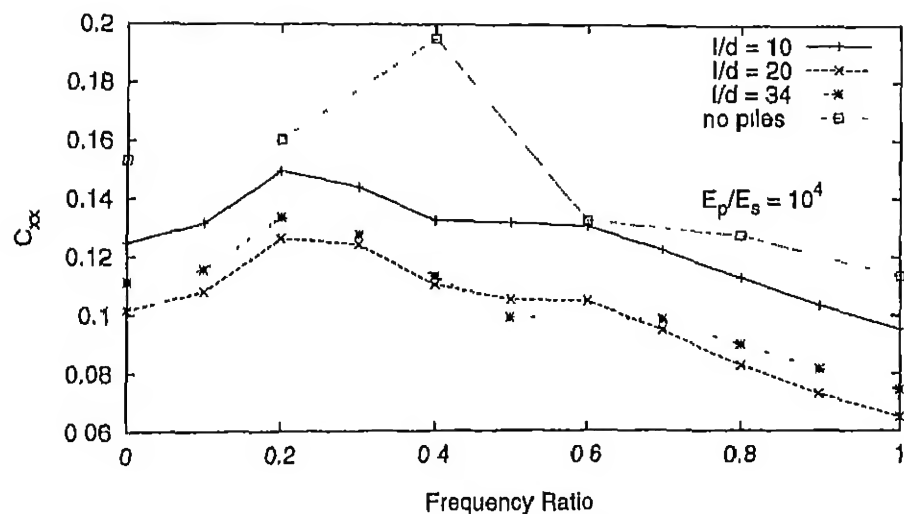


Figure 4.8: Horizontal Compliance Function of Pile Head ($E_p/E_s = 10^4$)

Since the piles are also modeled as continuum elements the rotational moment is simulated using a couple and the rotational displacement

is measured in terms slope of pile head. For rotational mode of vibration, the compliance functions are shown in Figures 4.9 and 4.10. The reduction in compliance functions with increase in slenderness ratio is comparatively small for smaller modular ratio and high at higher modular ratios

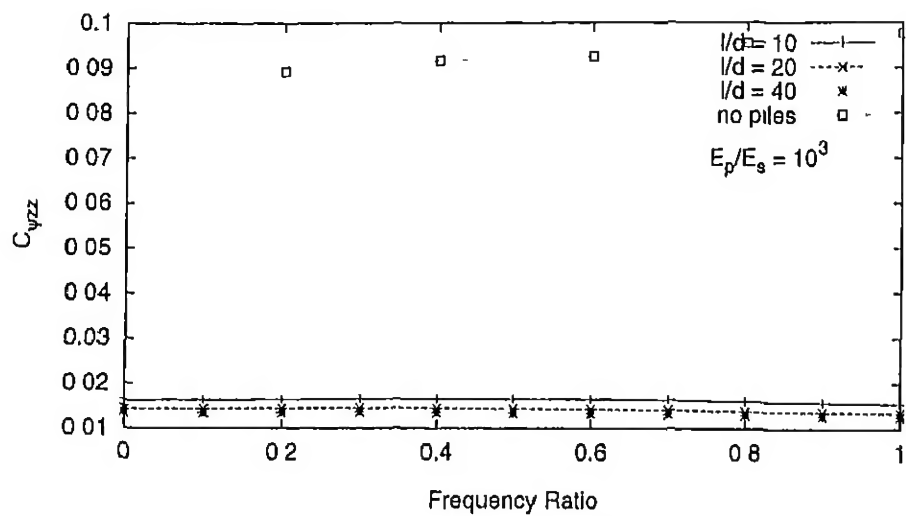


Figure 4.9: Rotational Compliance Function of Pile Head ($E_p/E_s = 10^3$)

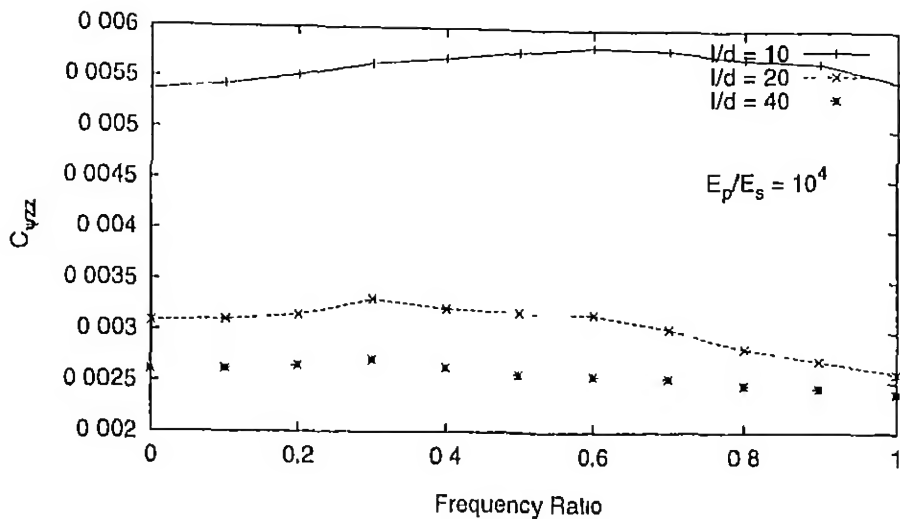


Figure 4.10: Rotational Compliance Function of Pile Head ($E_p/E_s = 10^4$)

4.5.2 Effect of modular ratio

The effect of modular ratio on the compliance functions for vertical, horizontal and rotational modes are shown in Figures 4.11, 4.12 and 4.13. It can be seen that modular ratio has significant effect at higher slenderness ratios. Vertical and rotational modes are strongly influenced by the slenderness ratio and modular ratios.

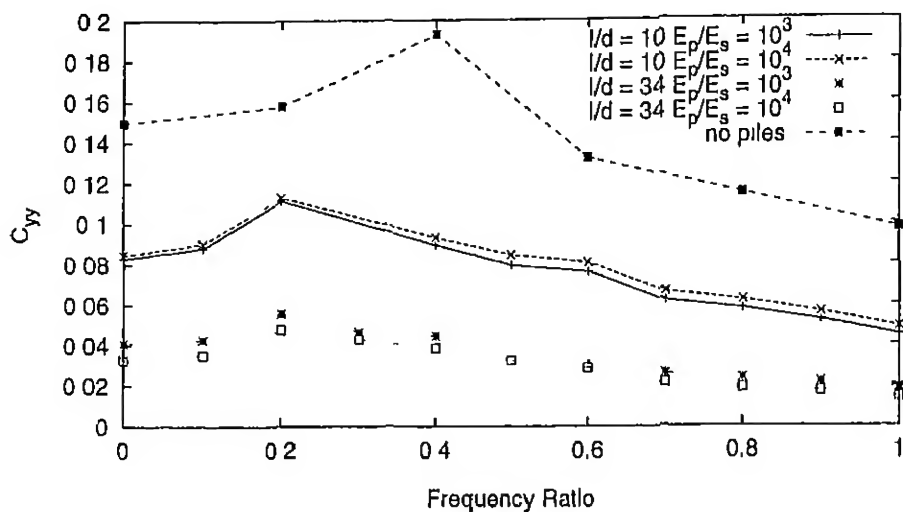


Figure 4.11 Vertical Compliance Functions of Pile Head for Different Modular Ratios

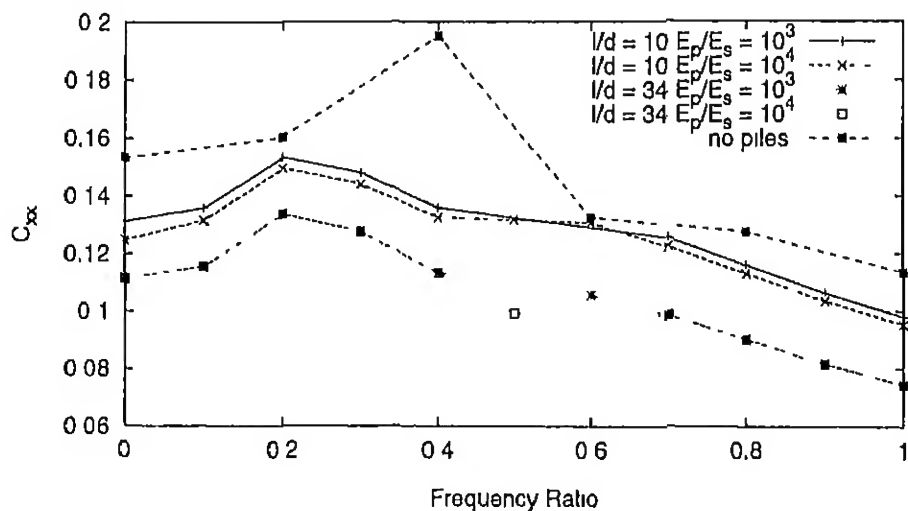


Figure 4.12 Horizontal Compliance Functions of Pile Head for Different Modular Ratios

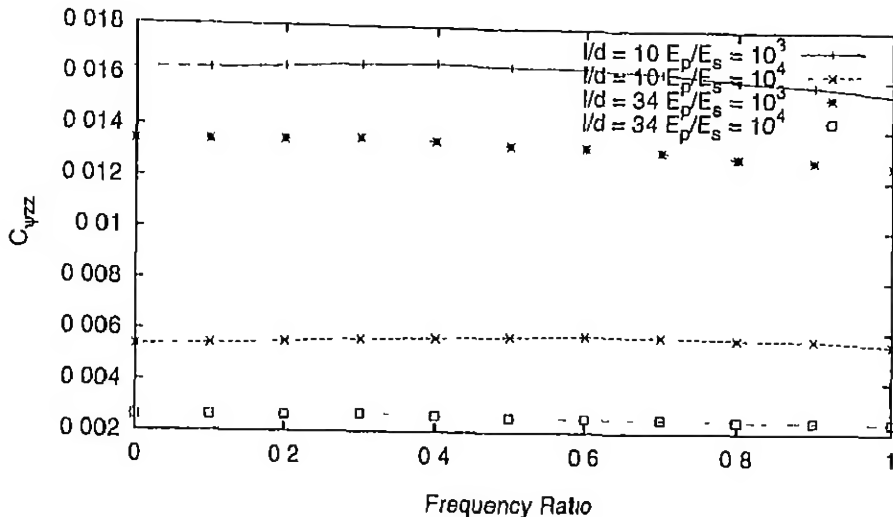


Figure 4.13: Rotational Compliance Functions of Pile Head for Different Modular Ratios

4.6 Response of Pile Foundations

In this section the response of pile foundation soil systems investigated are presented. The parameters that effect the response such as slenderness ratio of piles, number of piles (*i.e.* spacing of piles) modular ratio of pile/pile cap material, soil and effect of layered soils and thickness of pile cap, are considered for the study. The responses for different modes of vibration are presented using the compliance functions defined in Chapter 3 (Section 4). The geometry and the material properties of the system considered for illustration are given below. The pile foundation consists of pile cap of 1.0m thick and four pile at four corners of the cap. The arrangement of piles are shown in Figure 4.14

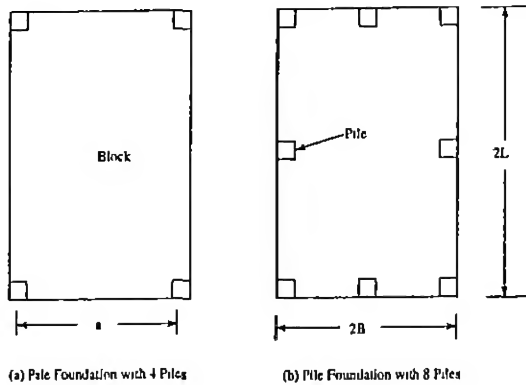


Figure 4.14 Plan Showing the Arrangement of Piles

Size of the model	=	100x50x50m
Number of elements	=	30x10x15(in x, y, and z directions)
Young's modulus of pile material E_p	=	47.03GPa
Poisson's ratio pile material ν_p	=	0.33
Unit weight of pile material ρ_p	=	24.0kN/m ³
Young's modulus of soil E_s	=	47.03MPa
Poisson's ratio soil ν_s	=	0.33
Unit weight of soil ρ_s	=	17.0 kN/m ³
Half-width of cap B	=	2.0m
Half-length of cap L	=	4.0m
Thickness of the cap t	=	1.0m
Depth of embedment of the cap h	=	1.0m
Side of the square pile d	=	1.0m

4.6.1 Effect of Slenderness Ratio

The compliance function of pile foundation with a rigid cap for different modes are obtained with piles of varying slenderness ratios. The vertical compliance of rigid cap with and without piles of different slenderness ratios for a particular modular ratios are shown in Figures 4.15 and 4.16.

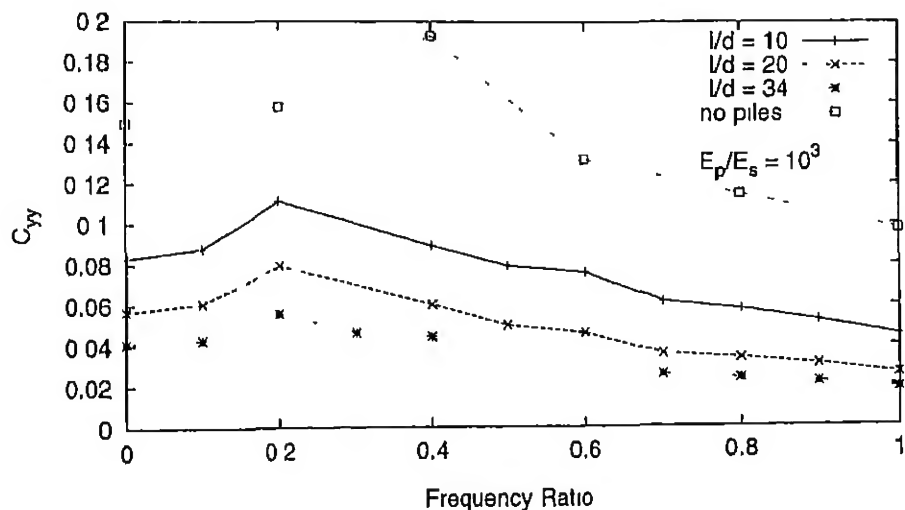


Figure 4.15. Vertical Compliance Functions of Pile Cap ($E_p/E_s = 10^3$)

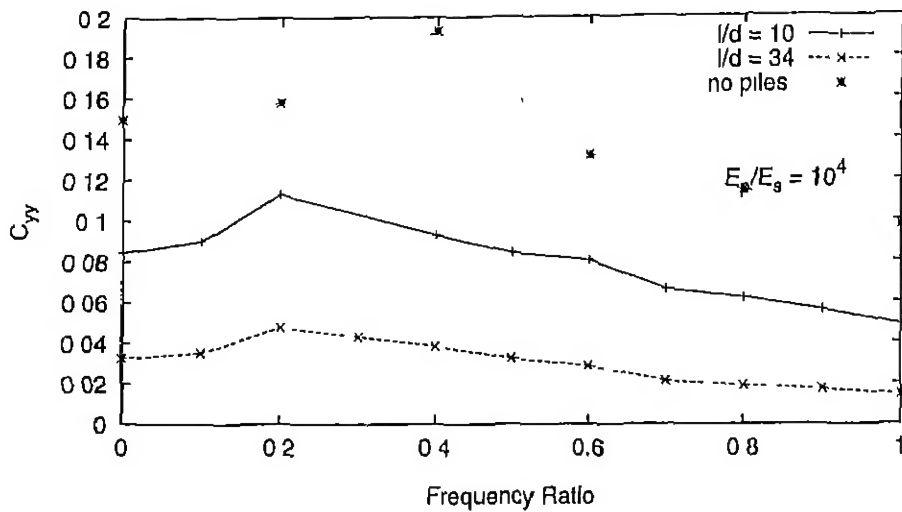
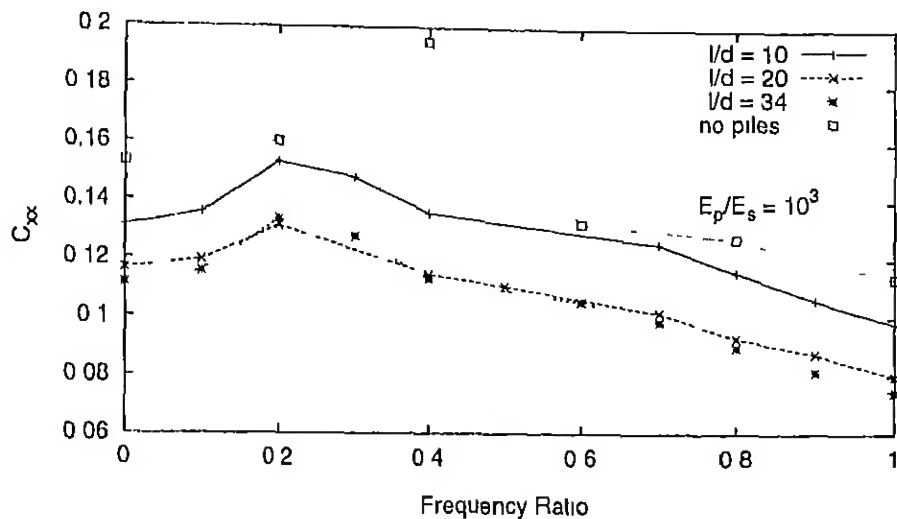
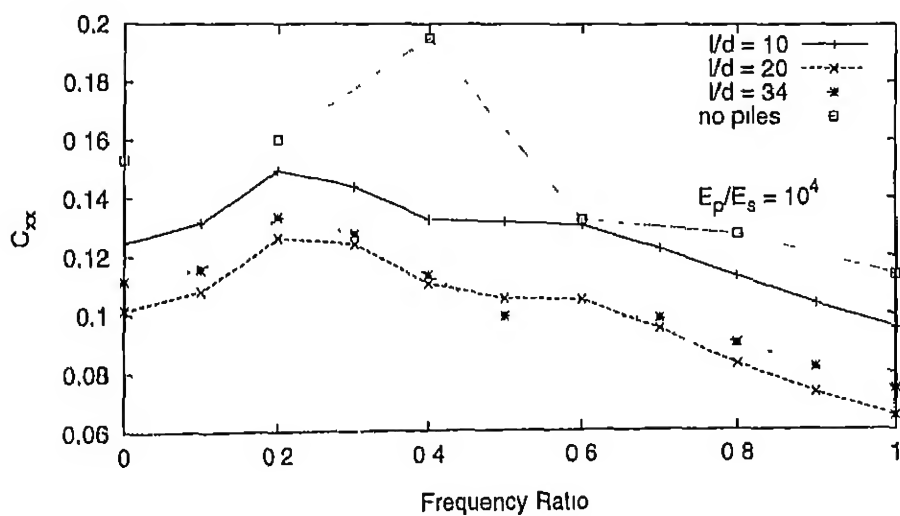


Figure 4.16 Vertical Compliance Functions of Pile Cap ($E_p/E_s = 10^4$)

It can be observed that presence of piles reduce the vertical compliances by a factor of 4 to 5. The resonant frequencies reduce due to presence of piles and so is the sharpness at resonance.

Horizontal compliance functions of the rigid cap of pile group are shown in Figures 4.17 and 4.18. The reduction of compliance functions due to piles is marginal (of the order of 50%). However the resonant frequencies reduce due to presence of piles.

Figure 4.17 Horizontal Compliance Functions of Pile Cap ($E_p/E_s = 10^3$)Figure 4.18. Horizontal Compliance Functions of Pile Cap ($E_p/E_s = 10^4$)

Rotational compliance functions of the pile cap for different l/d ratios are shown in Figures 4.19 and 4.20. It can be observed that the

reduction in rotational compliance function due to the presence of piles is substantial. They reduce almost by a factor of 4 to 20.

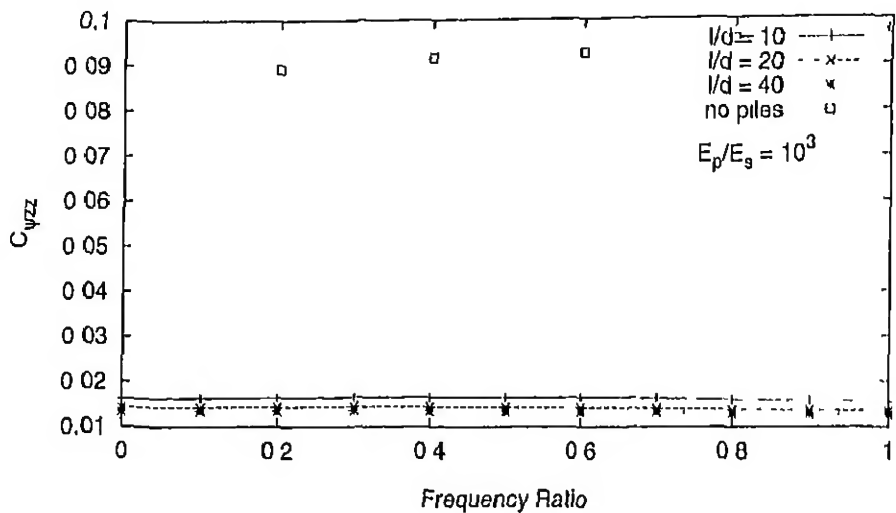


Figure 4.19 Rotational Compliance Functions of Pile Cap ($E_p/E_s = 10^3$)

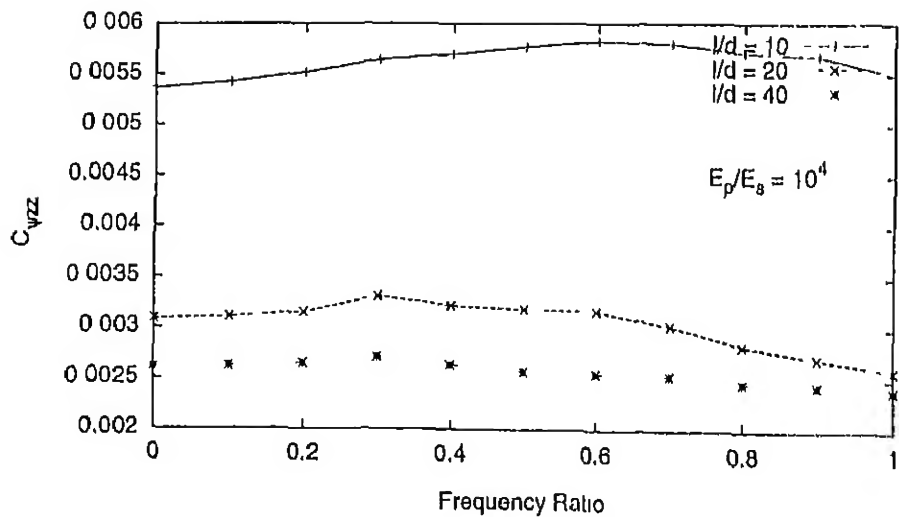


Figure 4.20. Rotational Compliance Functions of Pile Cap ($E_p/E_s = 10^4$)

4.6.2 Effect of Modular Ratio

The effect of modular ratio at different l/d ratios for different modes of vibration are shown in Figures 4.21, 4.22 and 4.23. It can be observed that the increase in modular ratio does not significantly effect the vertical and horizontal compliances, whereas the rotational compliances decrease by a factor of 2 to 5.

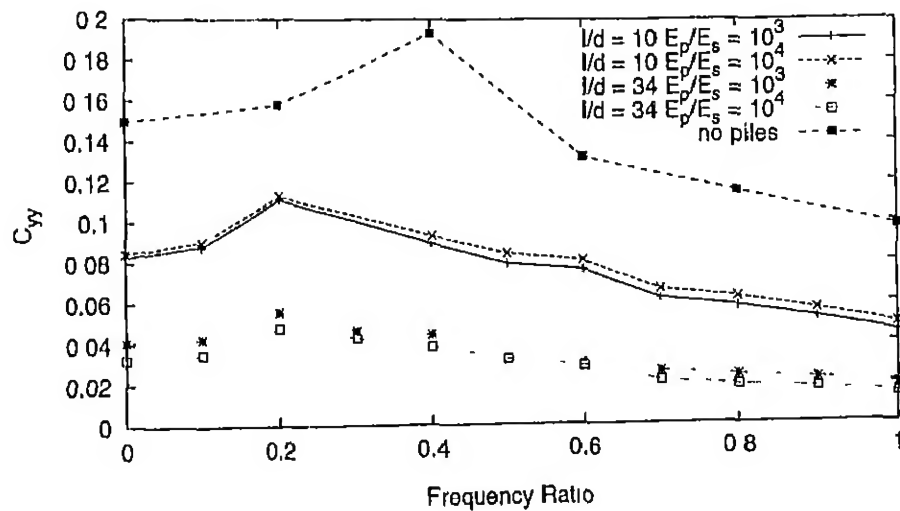


Figure 4.21: Effect of Modular Ratio on Vertical Compliance Functions of Pile Cap

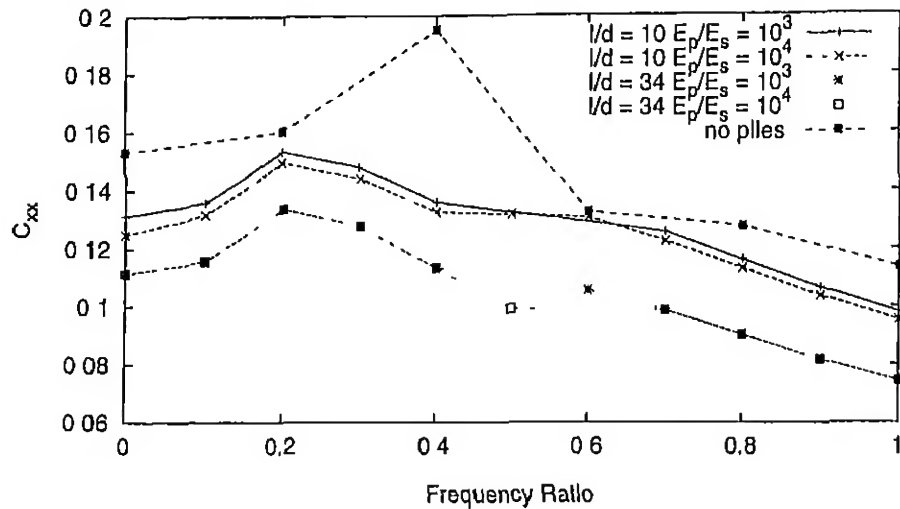


Figure 4.22: Effect of Modular Ratio on Horizontal Compliance Functions of Pile Cap

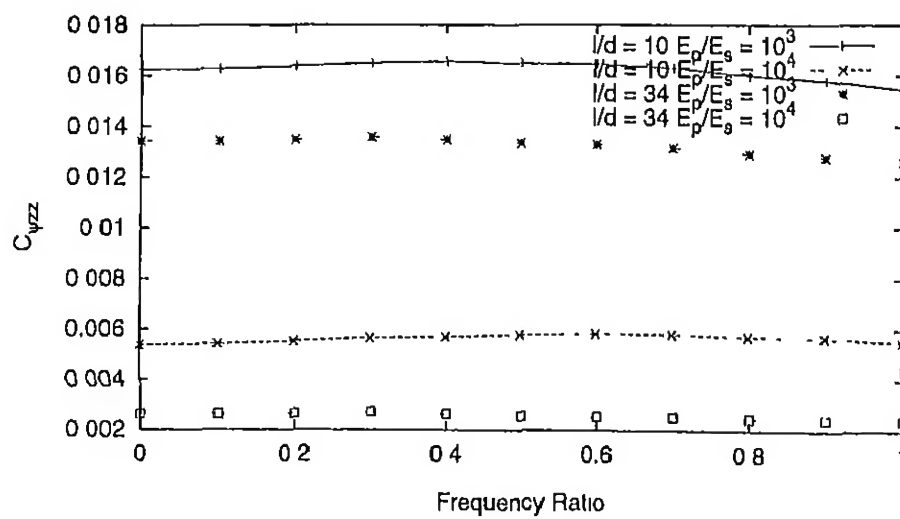


Figure 4.23. Effect of Modular Ratio on Rotational Compliance Functions of Pile Cap

4.6.3 Effect of Layered Soil

Compliance functions of pile foundations in two layered soil system have been investigated. The soil system considered has a top layer with varying thickness and the piles have a slenderness ratio of 20. The modular ratio M_r of the two layers and the thickness ratio T_r , defined in the Chapter 4 (Section 4.5) has been used to present the results. The vertical, horizontal and rotational compliance functions of pile cap are shown for different thickness ratios in Figures 4.24, 4.25 and 4.26. Presence of hard stratum underneath the soil reduces the compliance functions for all modes of vibration and increases the resonant frequencies of the system. The reduction in compliance is highest for vertical and lowest for horizontal mode. Unlike block foundation, the pile foundation responses are influenced by soil of larger thickness.

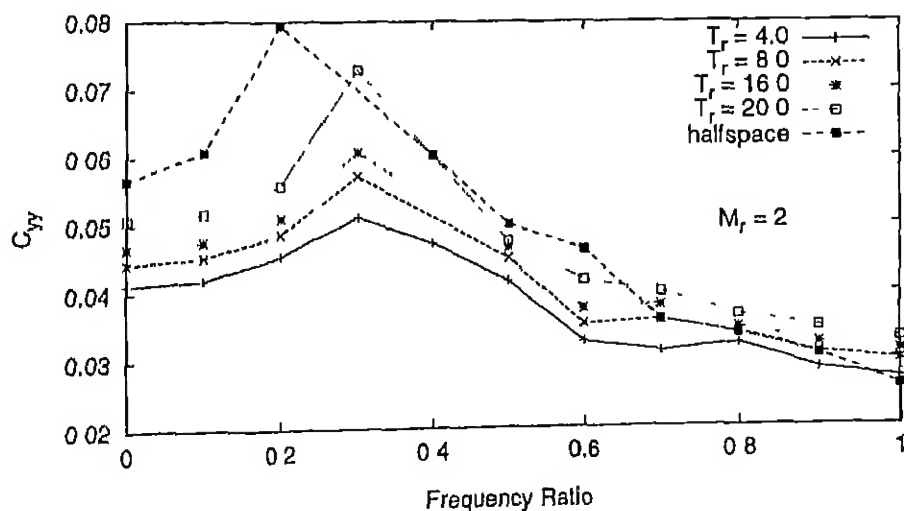


Figure 4.24: Effect of Layer Thickness on Vertical Compliance Functions of Pile Cap

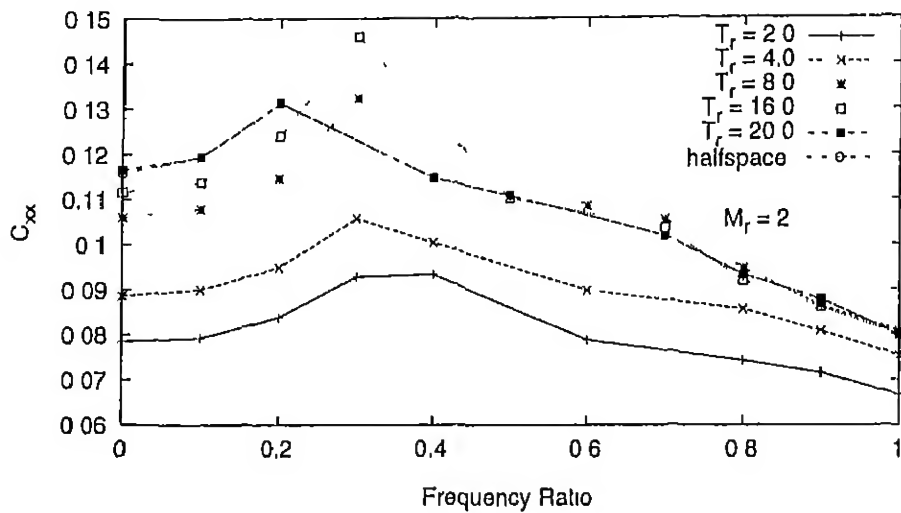


Figure 4.25 Effect of Layer Thickness on Horizontal Compliance Functions of Pile Cap

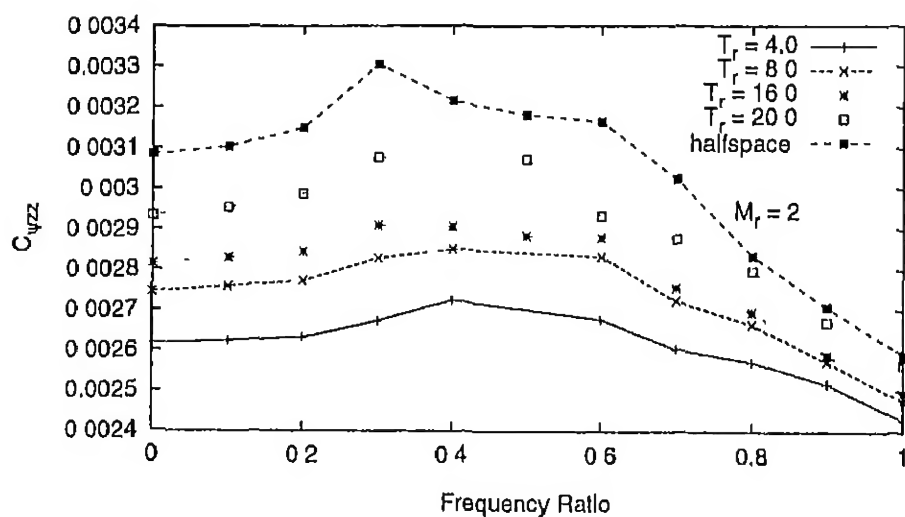


Figure 4.26: Effect of Layer Thickness on Rotational Compliance Functions of Pile Cap

4.6.4 Effect of Number of Piles

To investigate the effect of pile spacing/number of piles on the compliance functions, pile foundation with 8 piles is considered. Here the piles are placed at middle of the sides in addition to the corners as shown in Figure 4.14. Vertical, horizontal and rotational compliance functions with 8 piles are shown in Figures 4.27, 4.28 and 4.29. The reduction in compliance due to reduced spacing is small for vertical and horizontal modes whereas about 50% reduction is observed for rotational modes.

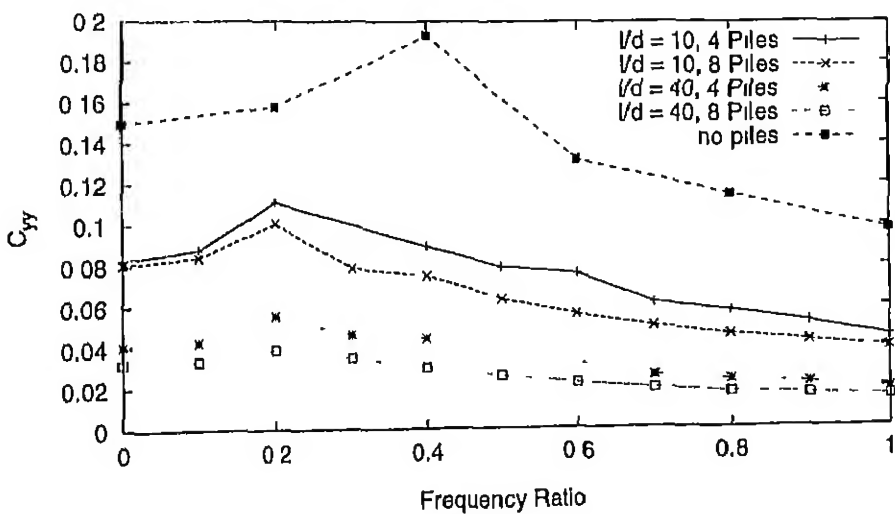


Figure 4.27: Effect of Number of Piles on Vertical Compliance Functions of Pile Cap

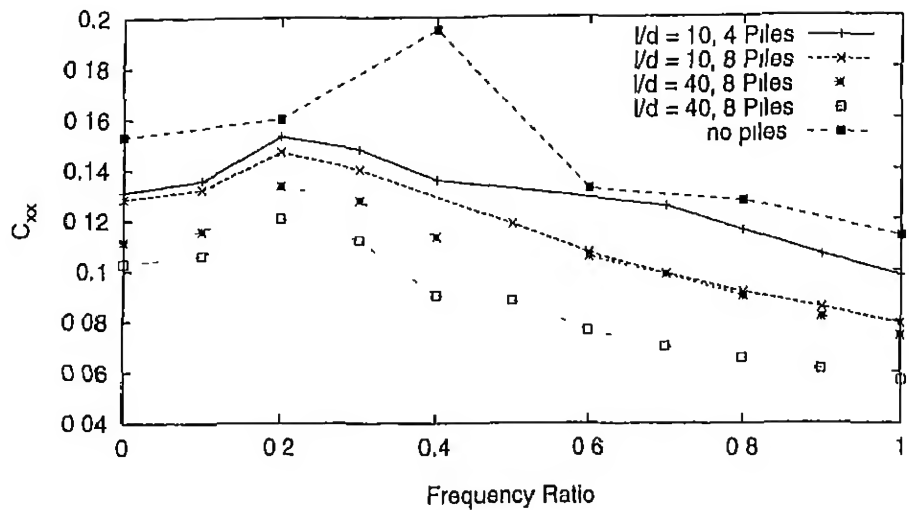


Figure 4.28 Effect of Number of Piles on Horizontal Compliance Functions of Pile Cap

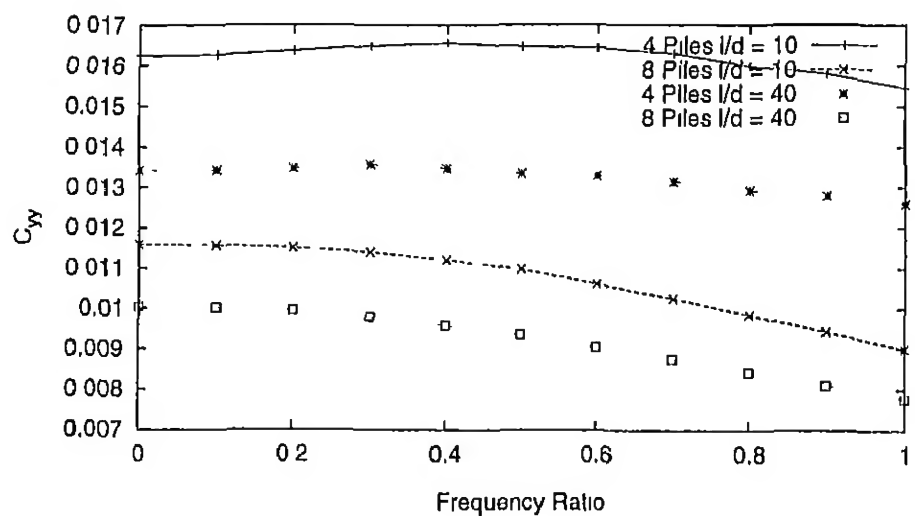


Figure 4.29: Effect of Number of Piles on Rotational Compliance Functions of Pile Cap

4.7 Response of Machine Pile Foundation Systems With and Without Piles

The computational model developed has been utilized to analyze diesel generator foundation. A schematic diagram of the foundation system adopted is shown in Figure 4.32. The machine is transmitting lateral force and rotational and torsional moments which are periodic but not harmonic. The excitations are shown in Figures 4.30 and 4.31. The material properties and the geometry of the foundation system are given below.

Size of the model	= 30x20x30m
Number of elements	= 20x10x15(in x, y, and z directions)
Young's modulus of pile material E_p	= 14.1GPa
Poisson's ratio pile material ν_p	= 0.25
Unit weight of pile material ρ_p	= 24.0kN/m ³
Young's modulus of soil E_s	= 20.0MPa
Poisson's ratio soil ν_s	= 0.25
Unit weight of soil ρ_s	= 16.67 kN/m ³
Width of cap B	= 2.0m
Length of cap L	= 6.0m
Thickness of the cap t	= 0.5m
Depth of embedment of the cap h	= 0.5m
Side of the square pile d	= 0.5m

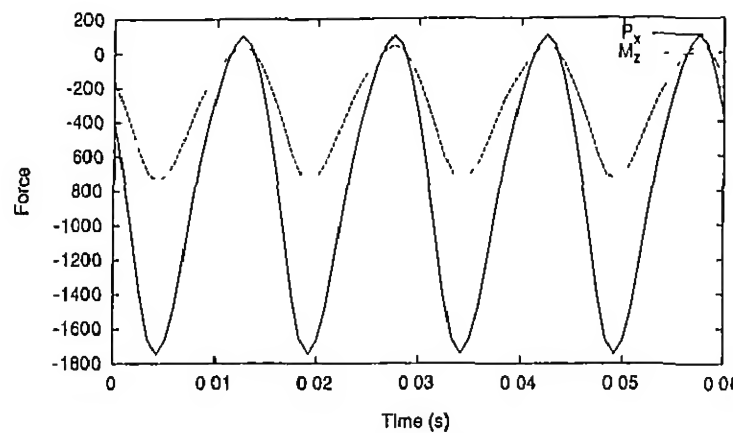


Figure 4.30 Horizontal and Rotational Excitation

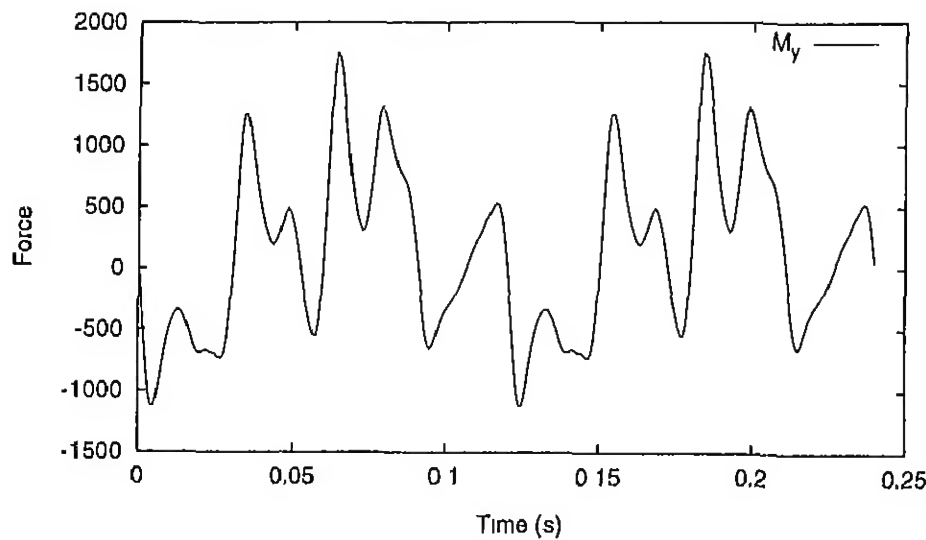


Figure 4.31: Torsional Excitation

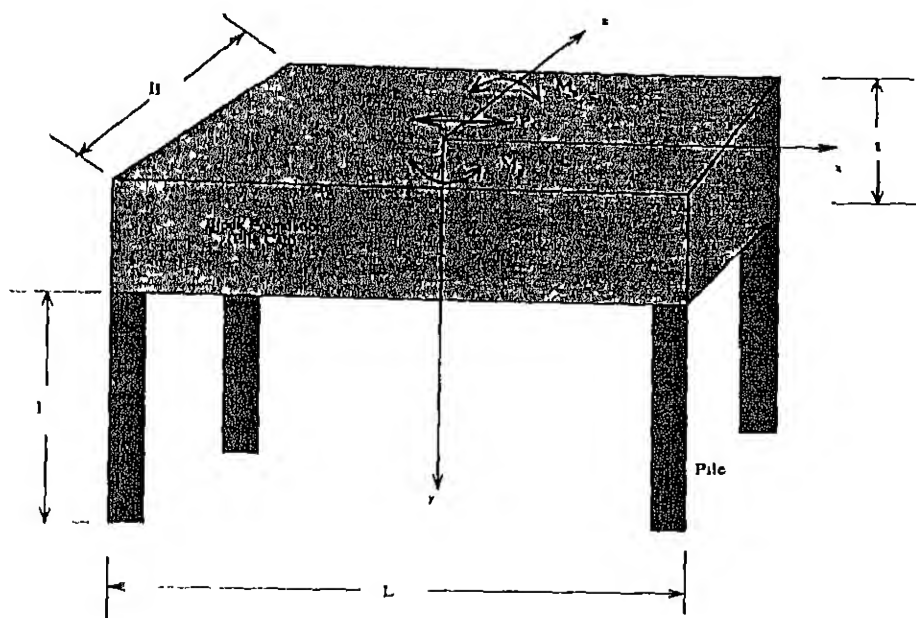


Figure 4.32. Machine Pile Foundation System

Maximum displacements in each of the mode at the center of gravity of the pile cap are used to present the results. The computational model used is essentially the one described in Chapter 3. The numerical integration of the system of differential equations is carried out till the responses reach steady state conditions. The maximum responses (displacements) in steady state region are used to show the effect of pile cap thickness, effect of l/d ratio of the piles and the shear modulus of the soil.

4.7.1 Effect of Shear Modulus

The effect of shear modulus on the maximum displacement of the pile cap/block in horizontal, rotational and torsional modes are shown in Figures 4.33, 4.34 and 4.35. The results shown are for a block

thickness of 0.5m and a slenderness ratio of 20 for the piles. It can be observed that increase in shear modulus beyond $6 MPa$ does not have a significant effect on the responses. The presence of piles have greater effect in rotational and torsional modes than in horizontal mode. Shear modulus of the soil strongly influences the responses of block foundation compared to pile foundation.

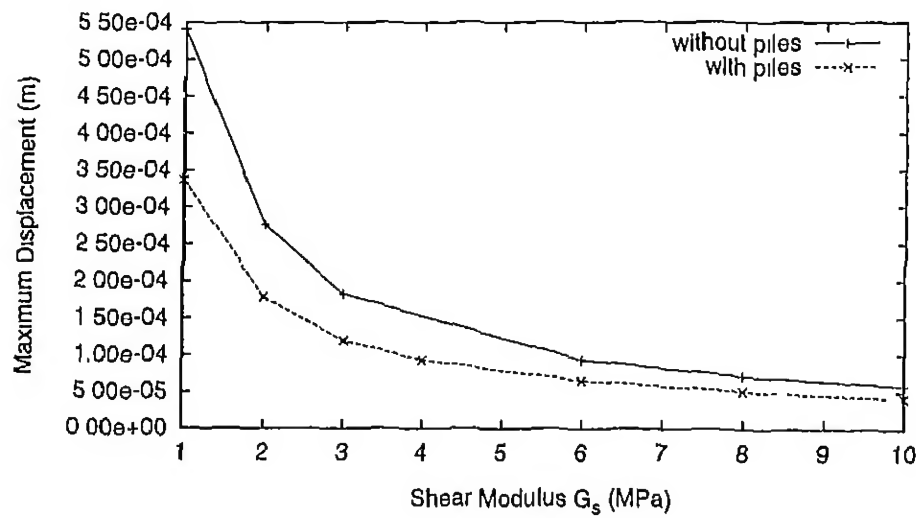


Figure 4.33: Effect of Shear Modulus on Horizontal Response

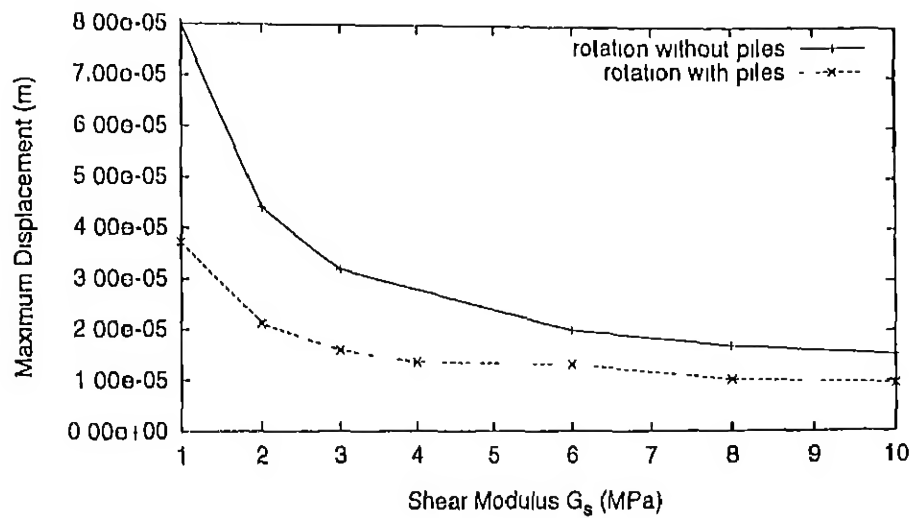


Figure 4.34. Effect of Shear Modulus on Rotational Response

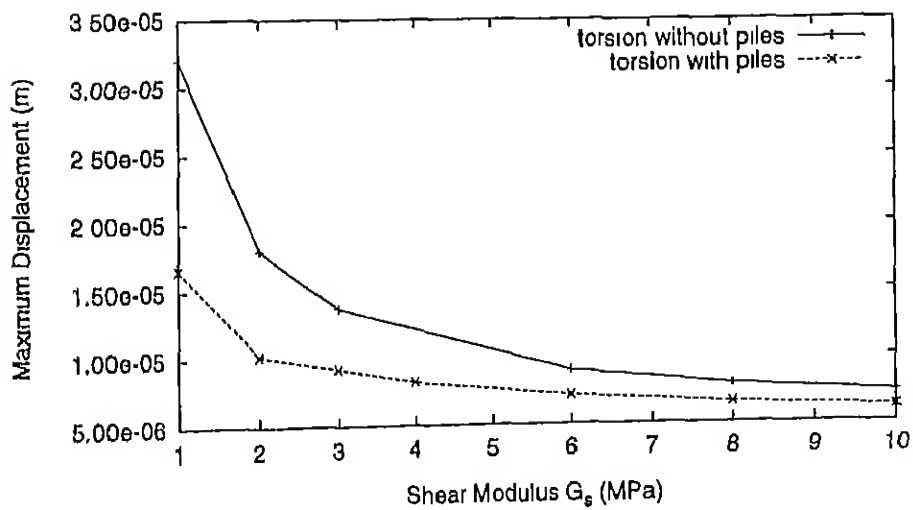


Figure 4.35. Effect of Shear Modulus on Torsional Response

4.7.2 Effect of Block/Pile Cap Thickness

The response of pile foundation system with shear modulus of 10MPa is used to study the effects of slenderness ratio and pile cap/block thickness. The maximum displacements in horizontal, rotational and torsional modes for different values of thickness of pile cap/block, are shown in Figures 4.36, 4.37 and 4.38. Increase in pile cap/block thickness from 0.5m to 1.5m reduce the displacements marginally in horizontal mode where as the reduction is by a factor of 2 in torsional mode. Increase in thickness beyond 1.5m does not reduce the displacements in horizontal and rotational modes significantly. Increase in l/d ratio does not significantly effect the responses.

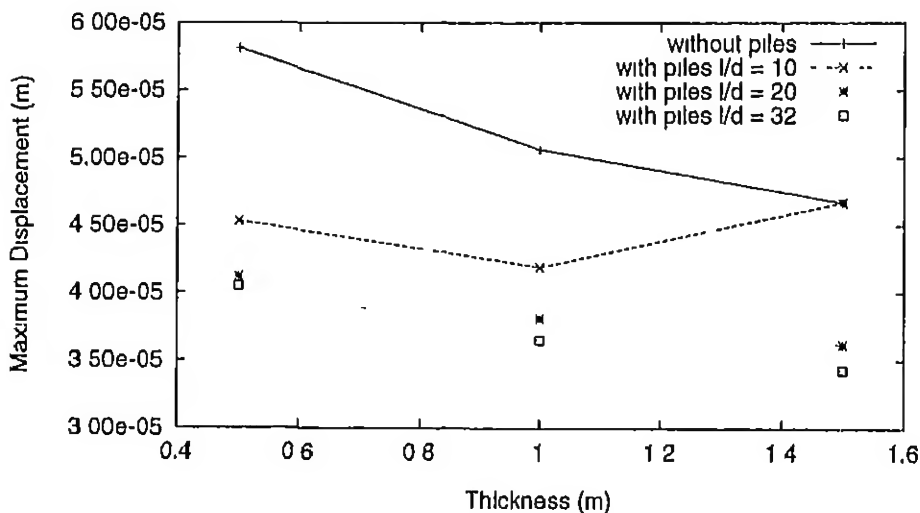


Figure 4.36 Effect of Pile Cap/Block Thickness on Horizontal Response

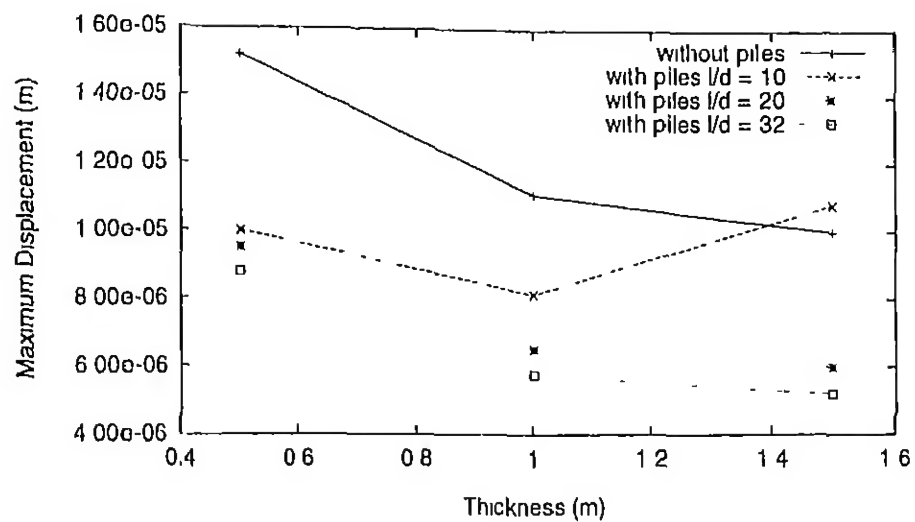


Figure 4.37: Effect of Pile Cap/Block Thickness on Rotational Response

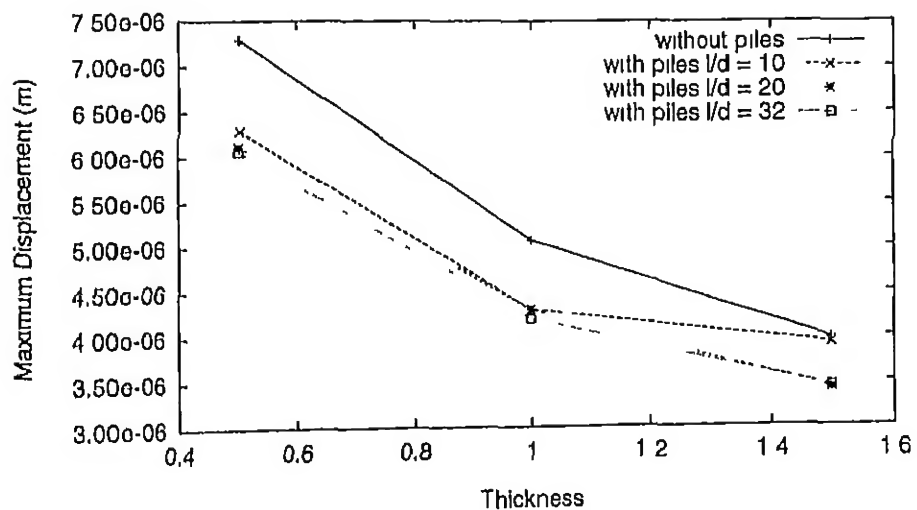


Figure 4.38: Effect of Pile Cap/Block Thickness on Torsional Response

4.8 Summary

A brief summary of the observations made from the studies on the response of pile foundation system are presented in this section.

1. The results obtained with present model agree well with those obtained with time-domain BEM.
2. Slenderness ratio has a very significant effect on the vertical and rotational response of single piles. The reductions in compliances in these modes are by a factor of 4–5 due to increase of l/d ratio from 10 to 40.
3. Modular ratio values beyond 10^4 do not significantly effect the responses of single piles
4. The presence of piles reduce the compliances by a factor of 2 to 4 for vertical mode, and by less than 50% for horizontal mode and by a factor of 10 for rotational mode.
5. Modular ratio does not have significant effect on the pile group response.
6. The presence of piles reduce the resonant frequencies compared to the block foundation for all modes.
7. Stiffer lower layer reduces the compliance functions of the pile group and increase the resonant frequency. Significant thickness of the top layer, effects the responses of the pile foundation in layered soil.

8. Increase in the number of piles reduces the compliances, but the reduction is not proportional to the number of piles. Effect of higher number of piles is felt more at higher frequencies
9. Increase in shear modulus reduces the responses of pile foundation significantly at low moduli
10. The pile cap/block thickness does not significantly effect the lateral and rotational responses, whereas it has significant effect on torsional response.

The capabilities of the present computational model can be summarized as follows:

1. The Present model can simulate semi-infinite half-space.
2. The Present model can describe the dynamic behaviour of a three dimensional discretized model consisting of about 13,000 degrees of freedom by a small fraction of about 30 degrees of freedom.
3. The present model can handle arbitrary excitations and the results obtained will be accurate, since continuous monitoring of local truncation error is carried out.
4. The computational effort is limited, since the computations are done with a few degrees of freedom.
5. The present model can be applied to structures having regular geometry, non-homogeneous domains, non-convex domains
6. An integrated approach wherein soil, structure, foundation can be considered together without any need for substructuring is presented in this model.

Chapter 5

ANALYSIS OF VIBRATION ISOLATION PROBLEMS

5.1 Introduction

Vibrations caused by machine foundations, traffic, blasting propagate through ground motion causing disturbances to adjacent structures and may affect the operation of sensitive equipment. Most of the energy affecting the adjacent structures is transmitted by Rayleigh waves which travel close to the surface of the ground (F. E. Richart, Hall and Woods, 1970). Placing a wave barrier in the ground before the structure (receiver) to reduce the disturbances is called passive isolation. On the other hand placing a barrier near the source of vibration is called active isolation (F. E. Richart, Hall and Woods, 1970). The effectiveness of the wave barriers depend upon the absorption or screening of the Rayleigh wave energy introduced by them. Generally open trenches, in-filled trenches, sheet pile walls, or rows of piles are provided to achieve vibration isolation.

In recent times vibration isolation is being studied using numerical and experimental research. Analytical or closed form solutions are extremely difficult, if not impossible, owing to the geometry and non homogeneity of the material involved. An efficient numerical technique can provide an insight in to the vibration isolation phenomenon.

Woods (1967) performed a series of field experiments on active isolation, where the trenches are put near the source, and passive isolation, where the trenches are placed at far field. Based on his experimental results, he presented a some guidelines for the dimensions of the open trench to achieve an amplitude reduction of 75% or more. In past couple of decades, number of researchers used various numerical techniques to study the vibration-screening problems. Aboudi (1973) used finite difference method (FDM) with special treatment of external boundaries to evaluate ground response of elastic half-space with thin barrier embedded. He concluded that better screening is observed in the case of shallow screen, by using low velocity and low density barriers. Haupt (1977) studied the vibration isolation of concrete walls. He used finite element method with an influence matrix boundary condition. He concluded that only cross section area influences the isolation effect but not the geometrical shape of the barrier. Segol, Lee and Abel (1978) developed a method in which vertical boundary forces were obtained in terms of modal matrix of eigen vectors and eigen values. They used finite element method for near field. They concluded that ratio of trench depth to shear wave length is an influencing factor of vibration isolation. Fuyuki and Matsumoto (1980) have investigated the Rayleigh wave scattering by rectangular trenches using finite difference method with improved absorbing boundary

conditions. They found that width of shallow open trenches could have significant effect on vibration isolation. May and Bolt (1982) have studied the effectiveness of open trenches on vibration screening to horizontally propagating P, SV and SH waves in a two-layered soil system.

Recently, boundary element methods have emerged as an alternative numerical scheme for solving wave propagation problems involving semi-infinite domains. Emad and Manolis (1985) have studied vibration isolation by open trenches in frequency domain. Beskos, Dasgupta and Vardoulakis (1986) have studied vibration isolation of open and concrete trenches due to transient wave source in Laplace domain. Leung, Beskos and Vardoulakis (1990) used thin layer Green's function developed by Kausel and Peek (1982) and Hull and Kausel (1984) to study the vibration isolation in layered soils. Dasgupta, Beskos and Vardoulakis (1988) and Banerjee, Ahmad and Chen (1988) applied 3D-BEM to vibration isolation by open trenches. Beskos and Vardoulakis (1990) have presented results of earlier work on vibration screening of open and filled trenches. They used a frequency domain boundary element method for 3-D and plane strain idealization of waves generated by rigid vibrating foundations. They used full-space Green's functions for homogeneous soil and those developed by Kausel and Peek (1982) for layered soil. They showed that in-filled trench performed better than open trench when 3-D analysis is adopted. Chouw, Le and Schmid (1990) have studied vibration isolation of open trenches due to harmonically excited strip footings using boundary element method. They have conducted a detailed parametric study on the effectiveness of the open trenches for vibration isolation due

to strip footing vibrating in different modes. Ahmad and Al-Hussaini (1991) have studied the vibration isolation by open and filled trenches using 2-Dimensional BEM using higher order elements in frequency domain. They carried out parametric studies and developed some simplified models and suggested design guidelines. Al-Hussaini and Ahmad (1991) have studied vibration isolation by open trenches due to horizontal vibrating source.

5.2 Present Model

Most of the existing procedures for analysis of filled and open trenches use two dimensional modeling. Few of the three dimensional time domain BEMs use constant/linear elements. It has been pointed out (Von Estorff, Pais and Kausel, 1990) that the results obtained using time-domain methods do not obey the causality condition for non-convex domains like the present vertical trenches. As already pointed out the time-domain BEMs require huge computational resources. Most of the studies ignore the effect of trench width possibly due to the presumed fact that the 2/3 of energy is transmitted by the surface waves. Recently Meek and Wolf (1993) have shown that the partition of the energy between the body waves and surface waves change with frequency ratio, and at higher frequency ratios body waves carry higher energies. Another anomaly observed by Beskos, Dasgupta and Vardoulakis (1986) is that 2D modeling and 3D modeling resulted in opposite conclusions about the efficiency of open and filled trenches. There exist a need for systematic study of open and filled trenches using 3D models in time-domain. The effect of layering, the location,

width and depth of open and filled trench are some of the parameters that need detailed investigation in three dimensions. The present study makes use of the model described in Chapter 2 to study these problems. The modeling consists of – 1. discretizing a *large* domain using the 3D 8 noded elements and generating mass stiffness and damping matrices and load vector which describe equations of motion, 2. Generating load dependent Lanczos vectors and transforming the equations of motion to Lanczos space, and 3. Solving the transformed equations of motion in time domain by adaptive time stepping scheme and obtaining the responses in original space

5.3 Presentation of The Results

The problem definition of an active vibration isolation system in three dimensional idealization using an open and filled (barrier) trenches are shown in Figure 5.1. The geometry of the system (cross section across the footing) is shown in Figure 5.2. The dimensions of the trench/barrier – Location l , depth d , width w and width of foundation w_f of the trench/barrier are expressed in non-dimensional quantities as,

$$L = L_r l$$

$$D = L_r d$$

$$W = L_r w$$

$$W_f = L_r w_f \quad (5.1)$$

Since most of the energy transmission takes place through Rayleigh

waves, and consequent screening of it results in vibration isolation, the depth, width and location of the trench/barrier are normalized with respect to Rayleigh wave length. The efficiency of the trench is usually measured in terms of amplitude reduction behind the trench/barrier. A non-dimensional parameter A_r (Amplitude reduction ratio) at any point, expressed as the ratio of amplitude of the ground surface with trench to that of without trench/barrier is used to express the vibration isolation efficiency. Contours of amplitude reduction ratio A_r are used to present the results. The properties of the footing are used for material of the barrier also.

$$A_r = \frac{v_t}{v_{t0}} \quad (5.2)$$

where v_t and v_{t0} are the amplitudes with and without trench respectively.

5.3.1 Comparison of The Model

A machine foundation system surrounded by an open trench at short distance acting as an active isolation system studied by Dasgupta and Vardoulakis (1986) has been used for comparison. The geometry and the problem definition is shown in Figure 5.1. The material and geometric parameters of the system are given below.

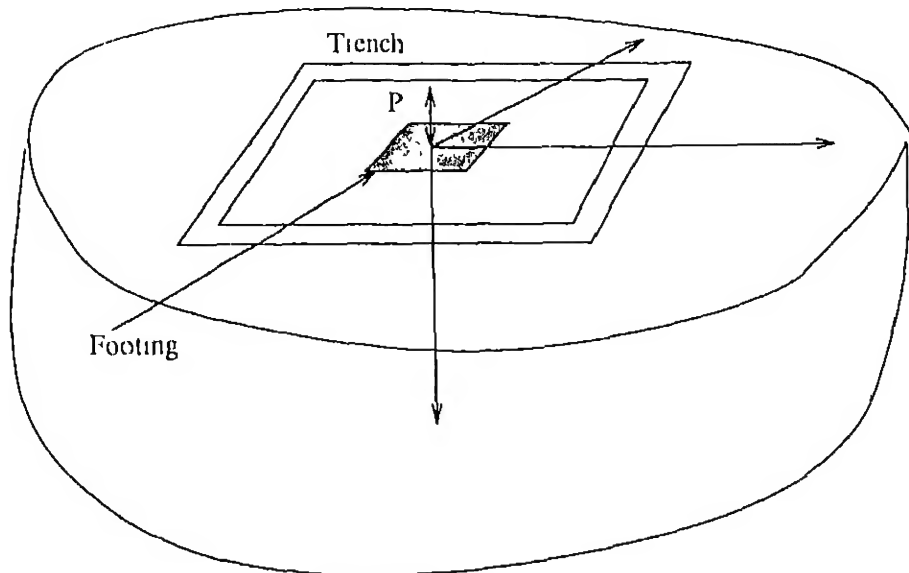


Figure 5.1 Open Trench Surrounding Machine Foundation

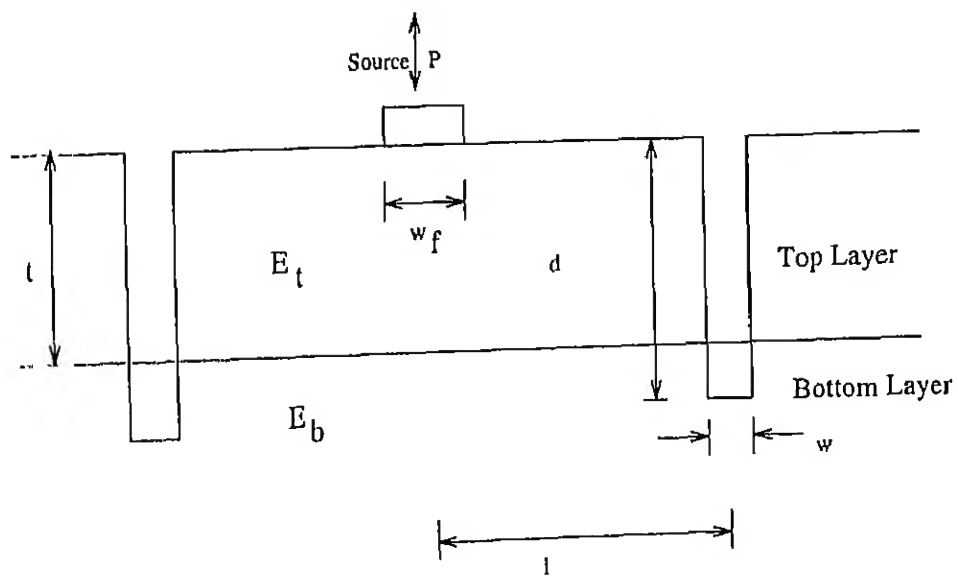


Figure 5.2: Cross section of Vibration Isolation System

Size of the model	= 12x12x12m
Number of Elements	= 18x10x18
Young's Modulus of Footing Material E_p	= 11315 MPa
Poisson's Ratio Footing Material ν_p	= 0.25
Unit Weight of Footing Material ρ_p	= 24.0 kN/m ³
Young's Modulus of Soil E_s	= 330 MPa
Poisson's Ratio Soil ν_s	= 0.25
Unit Weight of Soil ρ_s	= 17.0 kN/m ³
Width of the Trench w	= 0.3m
Depth of the Trench d	= 2.5m
Location of the Trench l	= 2.0m

The contours of amplitude reduction ratio of the surface for the trench obtained with present model and the that of Dasgupta and Vardoulakis (1986) using linear elements and of Banerjee, Ahmad and Chen (1988) using higher order elements are shown in Figure 5.3. It can be seen that the difference between the two results is small behind the trench.

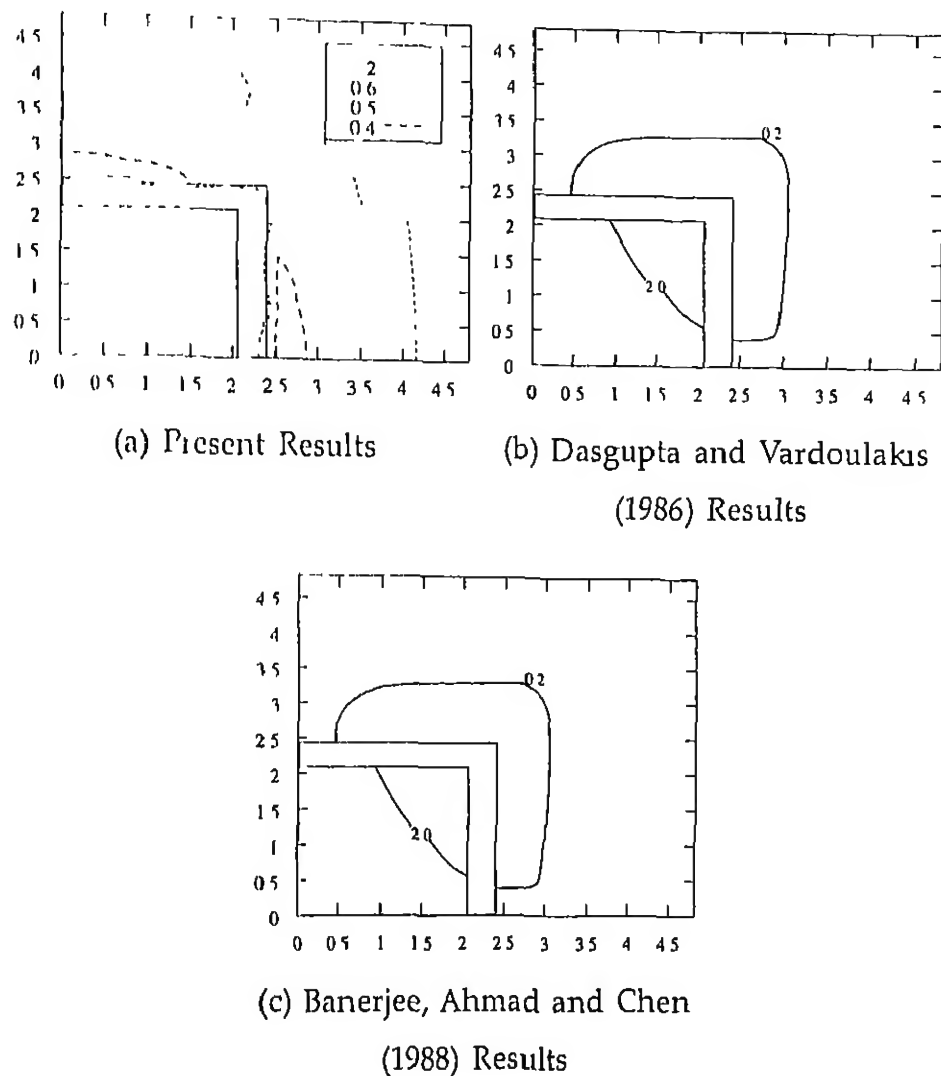


Figure 5.3: Comparison of Amplitude Reduction Ratio Contours

5.3.2 Effect of Trench/Barrier Depth

Since effective screening of the wave energy leads to proper vibration isolation and Rayleigh waves carry most of it, the length of the path before the waves reach the target (area which is to be screened) determines the efficiency. An easy way to achieve such an objective

is to have trench with sufficient depth near the target. The non dimensional trench/barrier depth D defined in (5.1) is used to study the effect. The *contours of amplitude reduction ratio of the surface* for different values of D are shown in Figure 5.4. Successful vibration isolation is defined by F. E. Richart, Hall and Woods (1970) as the one which yield an amplitude reduction ratio of 0.25. It can be seen that the trench with a normalized depth of 0.27 does not screen effectively, yielding a reduction ratio of 0.7, whereas the trench with $D = 0.82$ gives an amplitude reduction ratio of 0.2 over a large area. The open trench causes an amplification of the displacements in front of the trench to as high as 2.

The screening effect of barrier has also been studied with different depths of barrier. The amplitude reduction is shown in Figures 5.5 for different values of nondimensional depth parameter D . The amplitude reduction ratio achieved with a barrier is on the higher side compared to that of an open trench. The maximum reduction ratio achieved is of the order of 0.4 only with a barrier of depth $D = 0.82$. However there is no amplification of the displacements in front of the barrier as in the case of the trench.

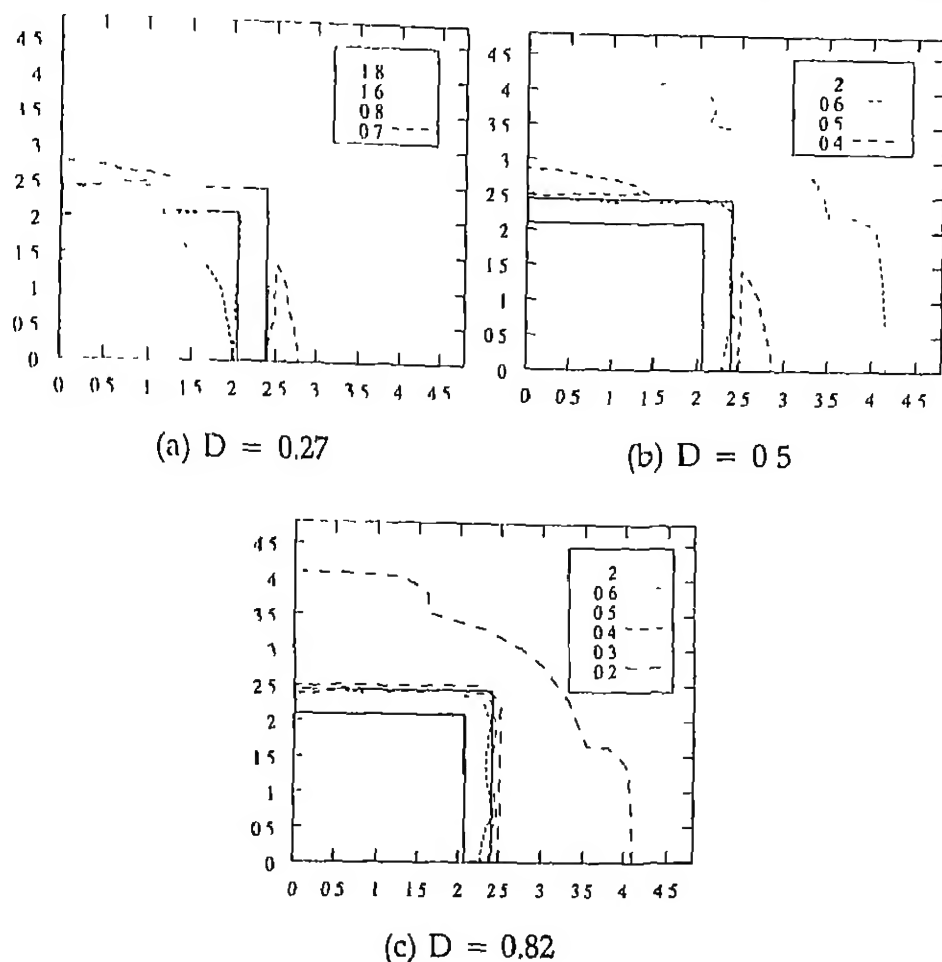


Figure 5.4. Effect of Trench Depth on Amplitude Reduction Ratio

The screening effect of barrier has also been studied with different depths of barrier. The amplitude reduction is shown in Figures 5.5 for different values of nondimensional depth parameter D . The amplitude reduction ratio achieved with a barrier is on the higher side compared to that of an open trench. The maximum reduction ratio achieved is of the order of 0.4 only with a barrier of depth $D = 0.82$, however there is no amplification of the displacements in front of the barrier as in the case of the trench.

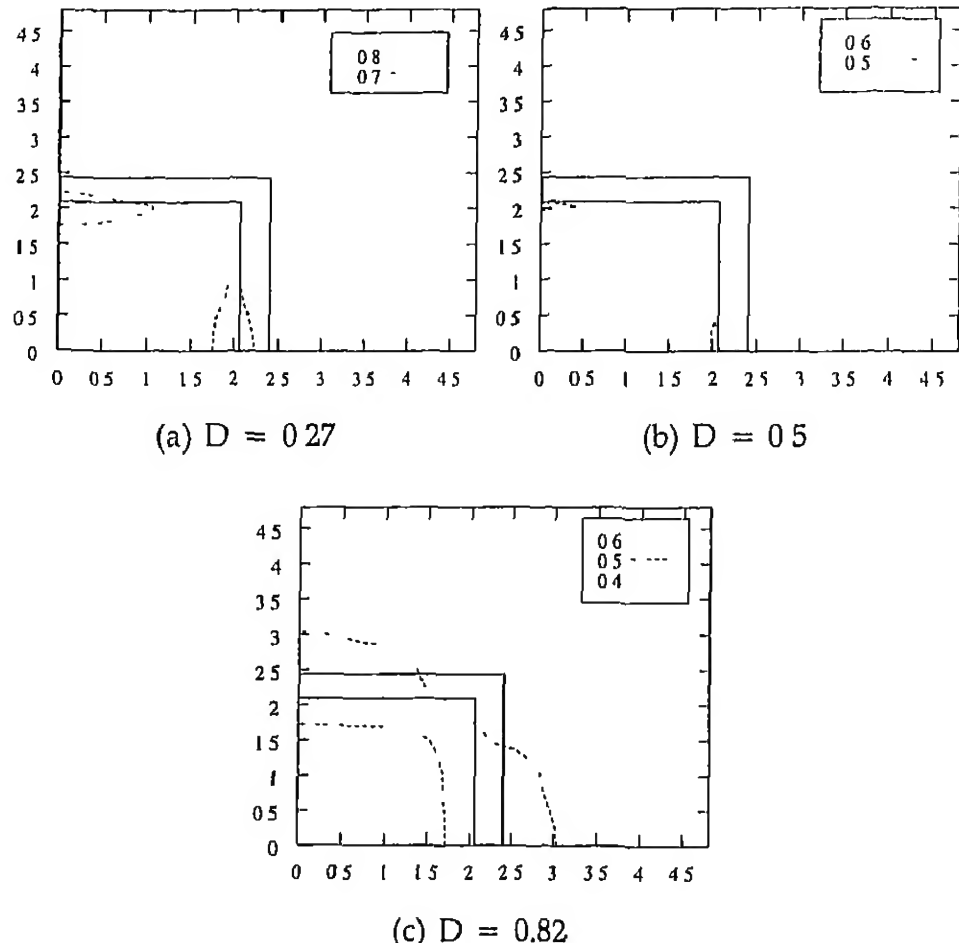


Figure 5.5 Effect of Barrier Depth on Amplitude Reduction Ratio

5.3.3 Effect of Trench/Barrier Width

The effect of trench/barrier width on vibration isolation has been investigated. The amplitude reduction ratio contours for different nondimensional widths W for a depth ratio D of 0.5 is shown in Figures 5.6 and 5.7. It can be seen that the amplitude reduction ratio is not significantly influenced by the width of the open trench. A trench width of $W = 0.6$ gave higher amplitude reduction. In

case of concrete barrier (Figure 5.7) the width of the barrier does not have significant effect on amplitude reduction ratio. The amplitude reduction (screening) extends to a small area behind the barrier

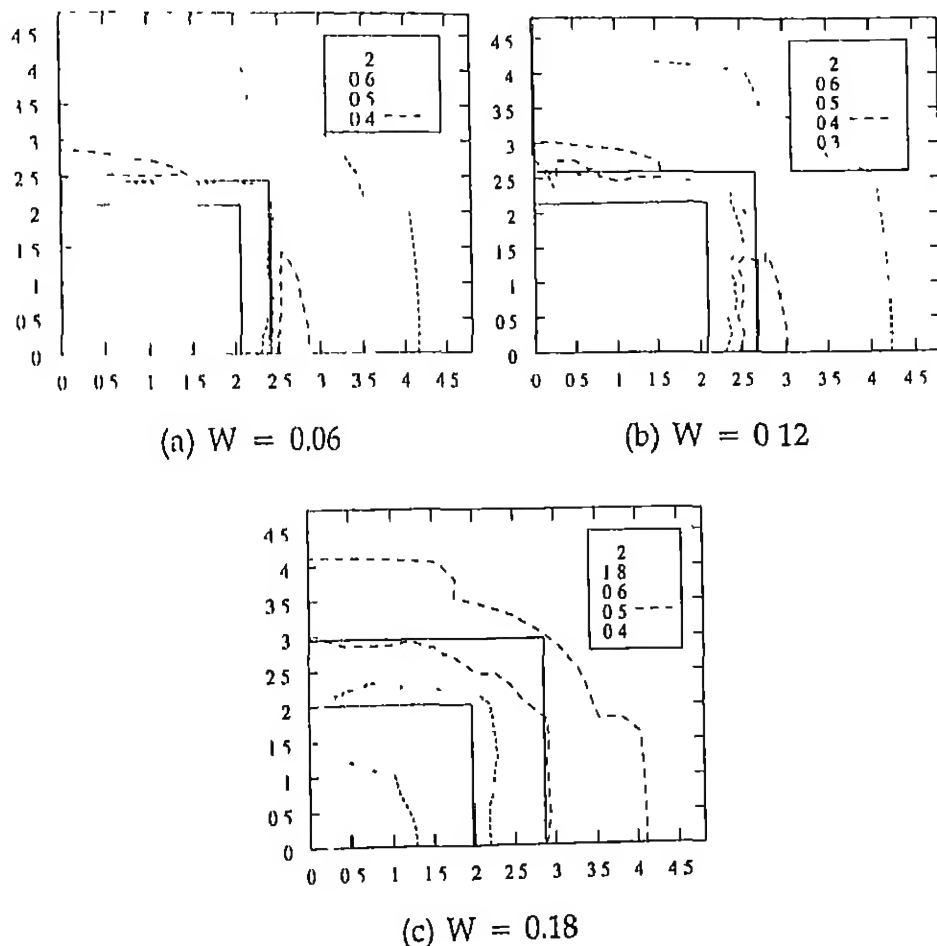


Figure 5.6: Effect of Trench Width on Amplitude Reduction Ratio

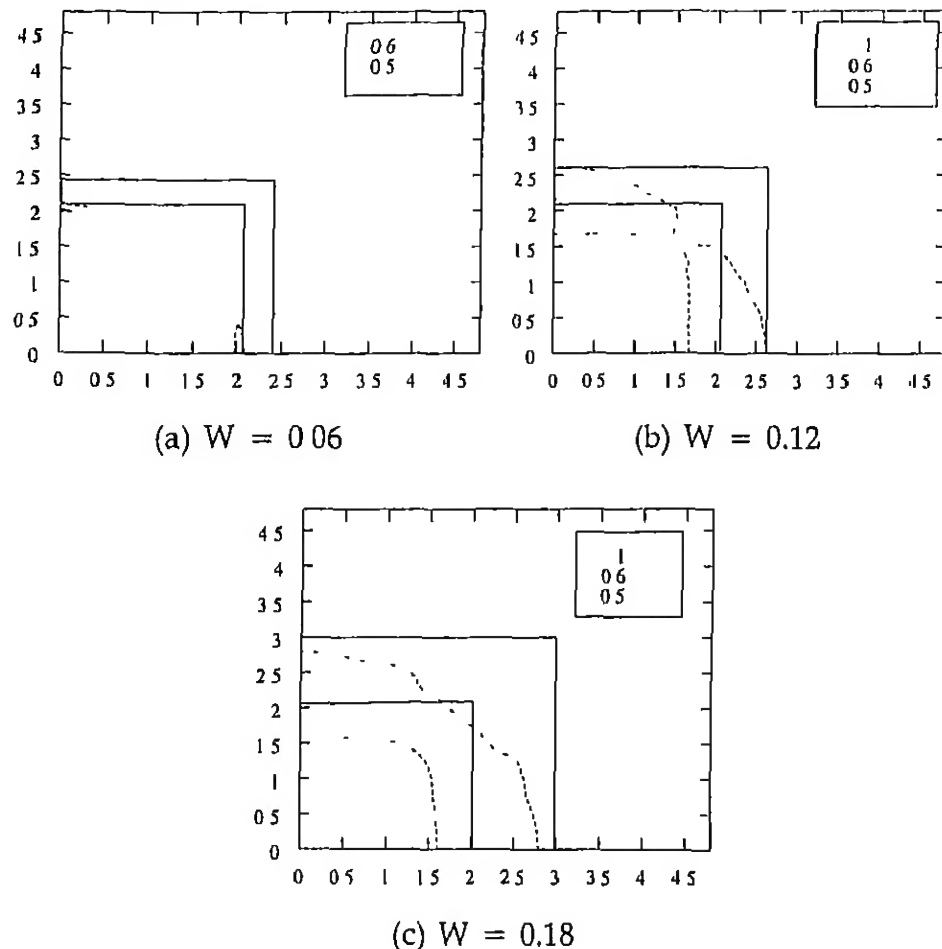


Figure 5.7 Effect of Barrier Width on Amplitude Reduction Ratio

5.3.4 Effect of Layered Soils

Vibration isolation efficiency of an open trench in a two layered soil system has been investigated. The system considered in this study consists of a finite thick top layer on half-space. The thickness of the top layer and the moduli ratio of top and bottom soils have been used to present the results. A non-dimensional top thickness T_r and modular ratio M_r are defined as

$$T_r = t/L_r$$

$$M_r = E_b/E_r \quad (5.3)$$

where t is the thickness of top soil layer, E_b E_r are young moduli of bottom and top soils respectively (Figure 5.2)

The amplitude reduction ratio contours of the surface for layered soils with different top layer thickness values as well as for half-space with trench depth $D = 0.5$ are shown along with the results for homogeneous half-space in Figures 5.8 and 5.9

It can be seen that softer layer beneath stiff top layer, *i.e.* $M_r < 1.0$, (Figure 5.8) reduces the vibration isolation efficiency of the trench. Increasing the top layer thickness increases the efficiency. Whereas a stiff layer beneath a soft soil, *i.e.* $M_r > 1.0$, improves the vibration isolation efficiency of the trench (Figure 5.9)

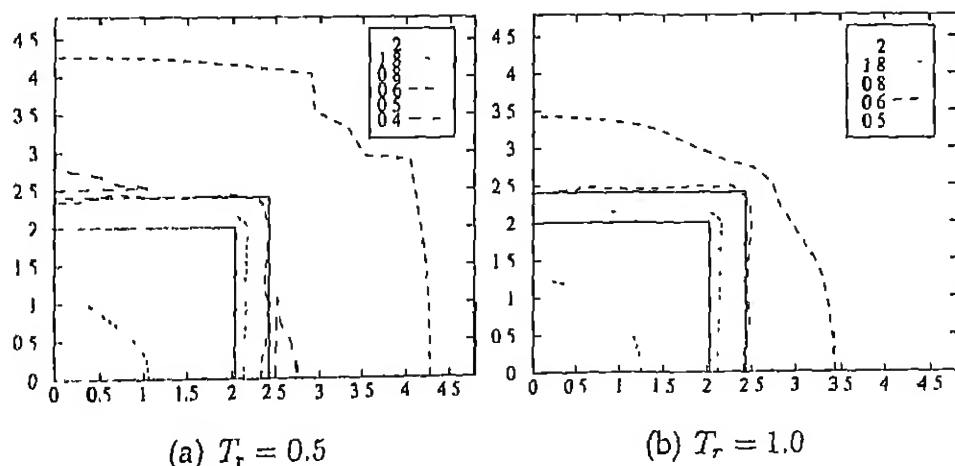


Figure 5.8 Effect of Top Layer Thickness on Amplitude Reduction Ratio for $M_r = 0.5$

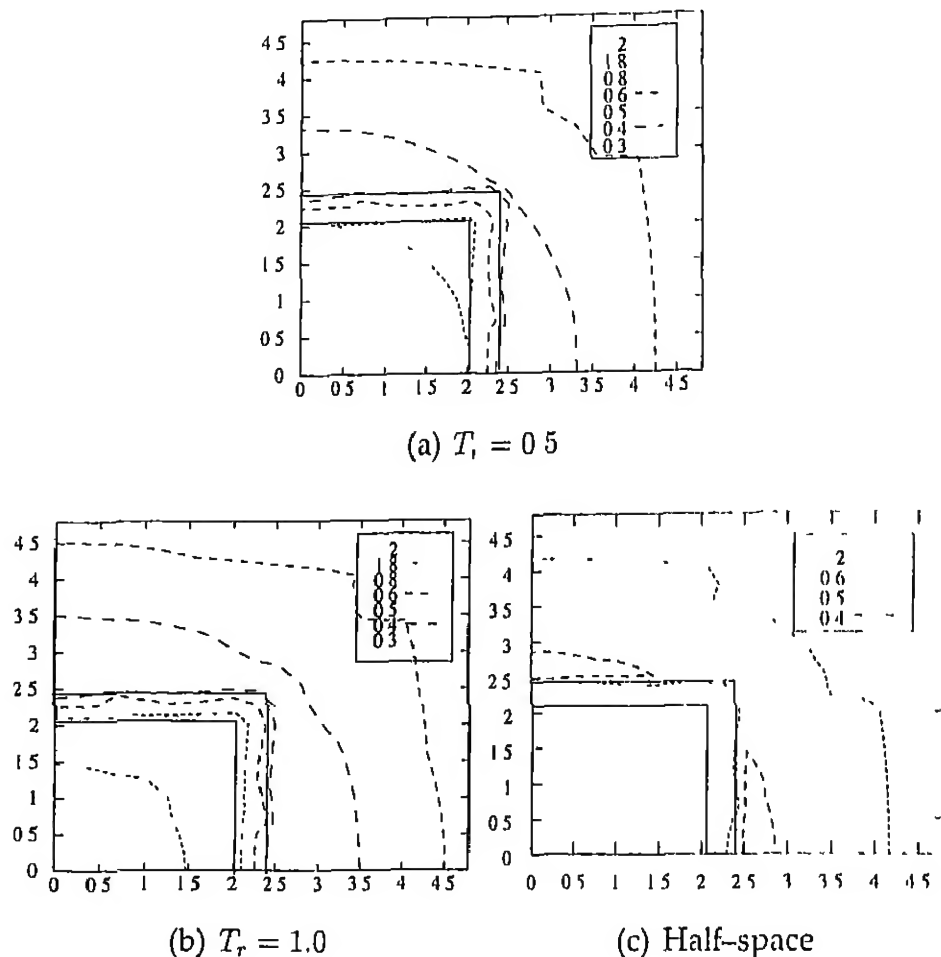


Figure 5.9 Effect of Top Layer Thickness on Amplitude Reduction Ratio of an Open Trench with $M_r = 2.0$

The amplitude reduction contours for concrete trench in two layered system is shown in Figure 5.10. It can be observed that stiffer bottom layer improves the screening efficiency of the barrier. As the thickness of top layer reduces the efficiency improves.

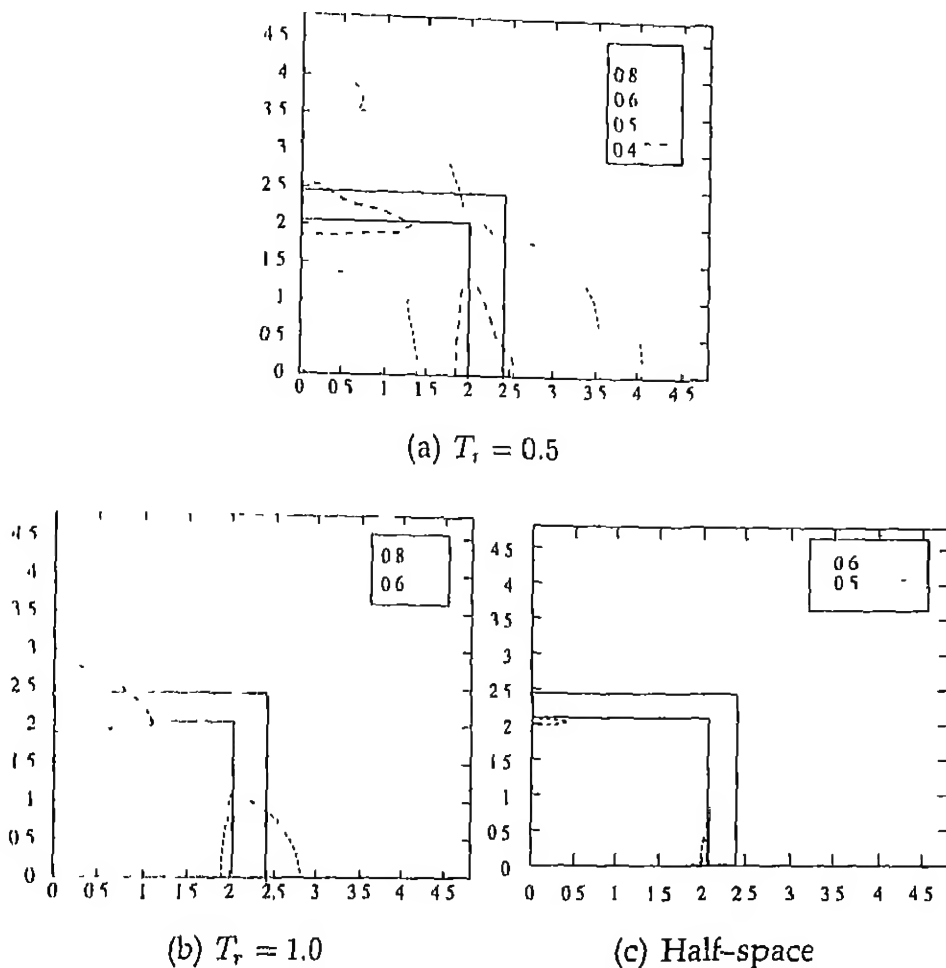


Figure 5.10: Effect of Top Layer Thickness on Amplitude Reduction Ratio of Barrier with $M_r = 2.0$

5.3.5 Effect of Frequency Ratio

As mentioned in the previous section the ratio of energy transmitted by the Rayleigh wave reduces with increasing frequency ratio, the effect of frequency ratio on the efficiency of the open trenches is investigated. Frequency ratio is changed by changing the dimensions of the foundation, keeping the excitation frequency same. The effect of frequency ratio for given frequency for different widths of the trench

is investigated. Amplitude reduction ratio contours are shown for different frequency ratios in Figure 5.11. It can be observed that, for wider trenches (*i.e.* $W = 0.18$), there is small improvement in efficiency at higher frequency ratio. For practical range of frequency ratios this effect is not significant.

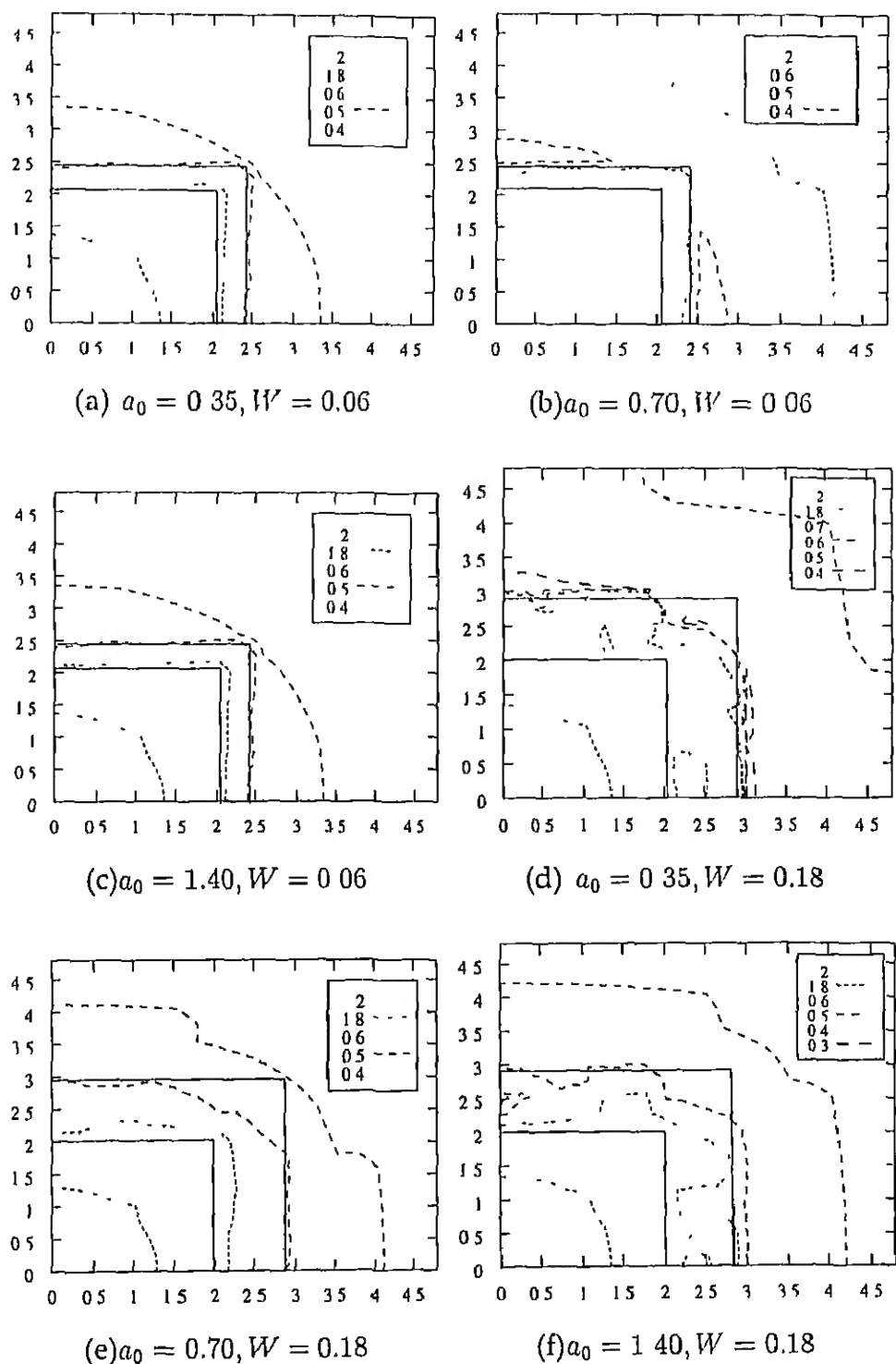


Figure 5.11 Effect of Frequency Ratio on Amplitude Reduction Ratio of an Open Trench

5.4 Summary

Based on the limited parametric studies carried out, the following observations can be made.

1. The present computational scheme predicts a higher amplitude reduction ratios compared to those obtained with BEMs.
2. In general open trenches produce better screening than concrete barriers. However no amplification of the displacements occurs in front of the trench due barriers.
3. Trench/Barrier depths have significant effect on the vibration isolation efficiency. An open trench with a depth $D = 0.82$ produces successful screening.
4. Trench/Barrier width does not significantly effect the vibration isolation. Similar observations was made by Woods (1967).
5. Layering has stronger influence on concrete barriers than open trenches.
6. Frequency ratio does not significantly effect the vibration isolation.

Chapter 6

CONCLUSIONS AND SCOPE FOR FUTURE STUDY

6.1 Introduction

The results obtained in the present investigation for different class of problems have already been discussed at the end of the respective chapters. The advantages of the computational scheme and observations made from the results obtained for various class of problems and performance of the scheme are summarized in the following section. Possible extensions of the study and scope are indicated in Section 6.3.

6.2 Conclusions

The computational scheme developed in this investigation is capable of analyzing wide class of time domain soil-structure interaction problems accurately. The advantages of the method, as brought out from the study, are summarized below.

1. A large mesh coupled with Lanczos transformation scheme could represent semi-infinite soil mass, with out any need for artificial boundaries, for computational purposes.
2. The present scheme can handle transient as well as periodic excitations containing arbitrary amplitudes and different frequencies.
3. An adaptive strategy is incorporated for error control due to temporal discretization and coordinate transformation, thus avoiding problems of stability, convergence *etc.* .
4. The error due to transformation decreases exponentially with increase in number of Lanczos vectors. The incremental computational cost per vector remains almost constant, and hence desired level of accuracy can be obtained.
5. Even though the transformation matrices are load dependent, the same can be used in similar loading conditions.
6. A few degrees of freedom (about 20-40) could simulate the behaviour of a physical model represented by few thousands degrees of freedom.
7. The present model can effectively analyze both convex as well as non-convex domains. The solutions obey causality conditions.
8. The computational scheme is local both in space and time.
9. The present scheme demands moderate computational resources in terms of storage, but requires small amount of processor time.

- 10 In the present scheme a unified analytical framework is available for soil-structure interaction problems considering the soil, structure and foundation as an integrated model.

Compliance functions of embedded foundations are obtained, using three dimensional modeling, for different modes of vibration. Effect of embedment, aspect ratio, flexibility of the footing and layering of soil, linearly varying modulus and finite thickness of the strata on compliance of the footing have been presented. The present investigation presented a methodology to study the realistic response of the foundation in both time and frequency domain. Based on the numerical simulations carried out the following observations can be made:

1. Reduction in compliance functions due to embedment is more in horizontal and rotational modes than in vertical mode. Embedment does not alter the resonant frequency of the system in any significant manner.
2. Increase in aspect ratio increases the compliance functions in all modes. However the effect is small in rotational modes. The effect of aspect ratio is small at higher frequencies.
3. Compliance functions are strongly influenced by a small thickness of soil at the surface.
4. The foundation flexibility effects vertical compliances strongly.
5. Linearly increasing modulus increases the resonant frequencies and reduces the sharpness of the peaks at resonance.

6. Presence of bedrock at finite depth influences vertical compliances strongly compared to those of other modes

Response of single piles and group of piles with cap have been investigated. The parameters that effect the response such as slenderness ratio of pile, modular ratio of pile material, thickness of pile cap, number of piles and layering of soil have been investigated. The results in terms of compliance functions have been presented and observations made from the results obtained are summarized. The present model has been applied to investigate a real life problem of foundation for machine generating periodic but non harmonic excitation. A brief parametric study of the machine foundation is carried out to bring out the parameters which effect the response. Some of the important observations made from the study are summarized below:

- 1 Slenderness ratio has significant effect on vertical compliances of the pile. The decrease can be seen to be of the order of 1/4 to 1/5 due to increase in l/d ratio from 10 to 40.
- 2 Modular ratio values beyond 10^4 do not effect the response of single piles.
3. The presence of piles reduce the compliances of the block/cap by a factor of 2 to 4 for vertical mode, and by less than 50% in horizontal mode and by a factor of 10 for rotational mode.
4. The presence of piles reduce the resonant frequencies.
5. The pile cap/block thickness does not significantly effect the lateral and rotational responses, whereas torsional responses reduce with increase in thickness.

6. The reduction in the response of the machine foundation to the presence of piles is more at lower shear modulus

A brief study is carried out on vibration isolation performance of open trenches and concrete barriers. A machine foundation surrounded by a trench/barrier has been used to investigate the efficiency of the isolation system. The effect of depth, width of the trench/barrier, the frequency ratio of the system, layering of soil on the efficiency of the vibration isolation system have been investigated. The results in terms of amplitude reduction ratio contours have been presented. A summary of the observations made from the parametric study conducted are presented below.

1. Open trenches provide better screening than concrete barriers. The open trenches amplify the displacements in front of the trench
2. Open trench with depth ratio $D = 0.82$ provide successful vibration isolation.
3. Efficiency of the isolation system increases with depth of trench/barrier.
4. Width of trench/barrier does not significantly influence the efficiency.
5. Frequency ratio does not significantly effect the vibration isolation efficiency over wide range of trench widths.
6. Layering has stronger influence on concrete barriers than open trenches.

6.3 Scope for Future Study

A wide class of *linear* time-domain soil structure interaction problems have been analyzed in the present investigation. The objective of the study is to provide a comprehensive affordable computational framework to analyze problems in time domain. A logical extensions of the present study could be in the following directions.

1. Incorporation of non-linear material models.
2. Separate material model/elements to account for soil-structure interface.
3. Effect of partial uplift due to impact, strong ground motion *etc* .
4. Kinematic interaction of adjacent structures.
5. More detailed investigation of active and passive isolation problems.
6. Efficiency of isolation systems against earthquakes (transient excitation).

REFERENCES

Abascal, R. and Dominguez, J. (1986). Vibrations of footings on zoned viscoelastic soil. *ASCE Journal of Engineering Mechanics Division*, Vol 112:433–447.

Aboudi, J. (1973). Elastic half-space with thin barrier. *ASCE Journal of Engineering Mechanics Division*, Vol 99:69–73.

Ahmad, S. and Al-Hussaini, T. M. (1991). Simplified design for vibration screening by open and in-filled trenches. *ASCE Journal of Geotechnical Engineering Division*, Vol 117:67–88.

Ahmad, S. and Banerjee, P. K. (1988). Time-domain transient elasto dynamic analysis of 3-d solids by bem. *International Journal for Numerical Methods in Engineering*, Vol 26:1709–1728.

Al-Hussaini, T. M. and Ahmad, S. (1991). Design of wave barriers for reduction of horizontal ground vibration. *ASCE Journal of Geotechnical Engineering Division*, Vol 117:616–636.

Arnold, R. N., Bycroft, G. N. and Warburton, G. B. (1955). Forced vibrations of a body on a infinite elastic solid. *Journal of Applied Mechanics*, Vol 248:391–400.

Banerjee, P. K., Ahmad, S. and Chen, K (1988). Advanced applications of bem to wave barriers in multilayered three dimensional soil media *Earthquake Engineering and Structural Dynamics*, Vol 16 1041–1060.

Barkan, D. D. (1969). *Dynamics of Bases and Foundations*. McGraw–Hill Book Co., Inc , New York.

Barros, F. C. P. De and Luco, J. E. (1990). Discrete models for vertical vibration of surface and embedded foundations. *Earthquake Engineering and Structural Dynamics*, Vol 19 289–303.

Bayo, E. P. and Wilson, E. L. (1984). Use of ritz vectors in wave propagation and foundation response. *Earthquake Engineering and Structural Dynamics*, Vol 11:499–505.

Beskos, D. E. and Vardoulakis, I. G. (1990). Vibration isolation by trenches in homogeneous and layered soils, in *Structural Dynamics* (Kratzig, editors), pages 693–700. Balkema, Rotterdam.

Beskos, D. E., Dasgupta, G. and Vardoulakis, I. G. (1986). Vibration isolation using open or filled trenches, part 1: 2–D homogeneous soil. *Computational Mechanics*, Vol 1:43–63.

Blaney, G. W., Kausel, E. and Roesett, J. M. (1976). Dynamic stiffness of piles, in *Second International Conference on Numerical Methods in Geomechanics*, pages 1001–1012.

Bycroft, G. N. (1956). Forced vibrations of rigid circular plate on a semi-infinite elastic space and on elastic stratum. *Philosophical Transactions of Royal Society*, Vol 248:327–368.

Cheung, Y. K., Tham, L. G. and Lie, Z. X. (1995). Transient response of single pile under horizontal excitation. *Earthquake Engineering and Structural Dynamics*, Vol 24 1017-38.

Chouw, Nawawi, Le, Rong and Schmid, Günther (1990) Vibration transmitting behaviour of the soil, in *Structural Dynamics* (Krätsig, editors), pages 701-708. Balkema, Rotterdam

Cohen, M. and Jennings, P. C. (1984). *Computational Methods for Transient Analysis*, chapter 7. Silent Boundary Methods for Transient Analysis. North-Holland, Amsterdam.

Cook, R. D. (1974). *Concepts and Applications of Finite Element Analysis*. John Wiley & Sons Inc., New York.

Coutinho, Alvaro L. G. A, Landau, Luiz, et al. (1987). The application of the lanczos mode superposition method in dynamic analysis of offshore structures. *Computers & Structures*, Vol 25:615-625.

Cullum, J. K. and Willoughby, R. A. (1985). *Lanczos Algorithms for Large Symmetric Eigenvalue Computations*, volume 1 and 2. Birkhauser Boston Inc., U. S. A.

Dahlquist, G (1963). A special stability problem for linear multistep methods. *BIT*, Vol 3:27-43.

Dasgupta, B. and Vardoulakis, I. G. (1986). *Innovative Numerical Methods in Engineering*, chapter 3-D Vibration Isolation Using Open Trenches, pages 385-392. Springer-Verlag, Berlin.

Dasgupta, G., Beskos, D. E. and Vardoulakis, I. G. (1988) 3-D analysis of vibration isolation of machine foundations, in *Proc 10th Boundary*

Elements Conference (Brebbia, C. A., editors), volume 4, pages 59-73. Springer-Verlag

Dasgupta, S. P. and Kameswara Rao, N. S. V. (1978). Dynamics of rectangular footings by finite elements *ASCE Journal of Geotechnical Engineering Division*, Vol 104:621-637

Desai, C. S. and Abel, J. F. (1972) *Introduction to the Finite Element Method* Von Nostrand Reinhold Co., New York.

Dobry, R., Vincente, E., et al. (1982) Horizontal stiffness and damping of single piles. *ASCE Journal of Geotechnical Engineering Division*, Vol 108:439-459.

Dominguez, J. (1978). Dynamic stiffness of rectangular foundations. Technical Report R78-20, Dept of Civil Engineering, MIT, Cambridge, Mass.

Emad, K. and Manolis, G. D. (1985). Shallow trenches and propagation of surface waves. *ASCE Journal of Engineering Mechanics Division*, Vol 111:279-282.

F. E. Richart, Jr. (1960). Foundation vibrations. *Journal of the Soil Mechanics and Foundations Division, Proc. ASCE*, Vol 86:1-34.

F. E. Richart, Jr., Hall, J. R. and Woods, R.D. (1970) *Vibrations of Soils and Foundations*. Prentice-Hall Inc., Englewood Cliffs, N J.

Fuyuki, M. and Matsumoto, Y. (1980). Finite difference analysis of Rayleigh wave scattering at a trench. *Bull. Seismol Soc. America*, Vol 70:2051-2069.

Gaitanaros, A. P. and Karabalis, D. L. (1988) Dynamic analysis of 3d flexible embedded foundations by frequency domain bem-fem *Earthquake Engineering and Structural Dynamics*, Vol 16:653-674

Gazetas, G. and Tassoulas, J. L. (1987a). Horizontal damping of arbitrary shaped embedded foundations. *ASCE Journal of Geotechnical Engineering Division*, Vol 113:458-475.

Gazetas, G. and Tassoulas, J. L. (1987b) Horizontal stiffness of arbitrary shaped embedded foundations *ASCE Journal of Geotechnical Engineering Division*, Vol 113:440-457

Givoli, Dan (1992). *Numerical Methods for Problems in Infinite Domains*. Studies in Applied Mechanics 33. Elsevier Science Publishers B.V, Amsterdam.

Gucunski, N. and Peek, R. (1993). Parametric study of vertical vibrations of circular flexible foundations on layered media *Earthquake Engineering and Structural Dynamics*, Vol 22:685-694

Haupt, W. A. (1977). Isolation of vibration by concrete core walls, in *Proc, 9th Int. Conf. Soil Mech and Found. Engg.*, volume 2, pages 251-256. Japanese Society of Soil Mech. Found. Engg

Higdon, R. L. (1992). Absorbing boundary conditions for acoustic and elastic waves in stratified media. *Journal of Computational Physics*, Vol 101:386-415.

Hilber, H. M., Hughes, T. J. R. and Taylor, R. L. (1977). Improved numerical dissipation for time integration algorithms in structural dynamics. *Earthquake Engineering and Structural Dynamics*, Vol 5:283-292.

Hoff, C. and Pahl, P. J. (1988). Development of an implicit method with numerical dissipation from a generalized single step algorithm for structural dynamics. *Computer Methods in Applied Mechanics and Engineering*, Vol 67:367-385

Hughes, T. J. R. (1984). *Computational Methods for Transient Analysis*, chapter 2. Silent Boundary Methods for Transient Analysis. North-Holland, Amsterdam.

Hughes, T. J. R. (1987). *The Finite Element Method*. Prentice-Hall, Inc, N.J.

Hull, S. W. and Kausel, E. (1984). Dynamic loads in layered half-space, in *Engineering Mechanics in Civil Engineering* (Boris, A. P. and Chong, K. P., editors), pages 201-204. ASCE, New York.

Ibrahimbegovic, A., Harn, C. Chen, et al. (1990). Ritz method for dynamic analysis of large discrete linear systems with non-proportional damping. *Earthquake Engineering and Structural Dynamics*, Vol 19:877-889.

Iguchi, M. and Luco, J. E. (1981). Dynamic response of flexible rectangular foundations. *Earthquake Engineering and Structural Dynamics*, Vol 9:239-249.

Karabalis, D. L. and Beskos, D. E. (1984). Dynamic response of 3-d rigid surface foundations by time domain boundary element method. *Earthquake Engineering and Structural Dynamics*, Vol 12:73-93.

Karabalis, D. L. and Beskos, D. E. (1985). Dynmaic response of 3-d flexible foundations by the time-domain bem-fem. *Soil Dynamics and Earthquake Engineering*, Vol 4:91-101.

Karabalis, D. L. and Beskos, D. E. (1986) Dynamic response of 3d embedded foundations by the boundary element method *Computer Methods in Applied Mechanics and Engineering*, Vol 56 91-119

Kausel, E. (1974) Forced vibrations of circular foundations on layered media. Technical Report Research Report R74-11, Dept of Civil Engineering, MIT, Cambridge, Mass

Kausel, E. and Peek, R. (1982). Dynamic loads in the interior of a layered stratum: an explicit solution. *Bull. of the Seism. Society of America*, Vol 72:1459-1481.

Kausel, E. and Roesett, J. M. (1975). Dynamic stiffness of circular foundations. *ASCE Journal of Engineering Mechanics Division*, Vol 101:771-785.

Kaynia, A. M. (1982). Dyanmic stiffness and seismic response of pile groups. Technical Report R82-03, Departmenet of Civil Engineering, MIT, Cambridge, Mass.

Kobori, T. (1962). Dynamical response of rectangular foundations on an elastic half-space, in *Proc Japanese National Symposium on Earthquake Engineering*, pages 81-86

Kuhlemeyer, R. L. (1979a). Static and dynamic laterally loaded floating piles. *ASCE Journal of Geotechnical Engineering Division*, Vol 105:289-304.

Kuhlemeyer, R. L. (1979b). Vertical vibration of piles. *ASCE Journal of Geotechnical Engineering Division*, Vol 105.273-287.

Lamb, H. (1904). On the propagation of tremors over the surface of an elastic solid. *Philosophical Transactions of the Royal Society*, Vol 203:1-42.

Leung, K. L., Beskos, D. E. and Vardoulakis, I. G. (1990) Vibration isolation using open or filled trenches part 3: 2-D non-homogeneous soil. *Computational Mechanics*, Vol 1:43-63.

Luco, J. E. (1976). Vibrations of a rigid disc on a layered viscoelastic medium. *Nuclear Engineering Design*, Vol 36:325-340.

Luco, J. E. and Westmann, R. A. (1971). Dynamic response of circular footings. *ASCE Journal of Engineering Mechanics Divison*, Vol 97:1381-1395.

Lysmer, J. and Kuhlemeyer, R. L. (1969). Finite dynamic model for infinite media. *ASCE Journal of Engineering Mechanics Divison*, Vol 95:859-877.

Lysmer, J. and Waas, G. (1972). Shear waves in plane infinite structures. *ASCE Journal of Engineering Mechanics Divison*, pages 85-105.

Mamoon, S. M. and Banerjee, P. K (1992). Time-domain analysis of dynamically loaded single piles *ASCE Journal of Engineering Mechanics Divison*, Vol 118.140-160.

May, T. W. and Bolt, B. A. (1982). The effectiveness of trenches in reducing seismic motion. *Earthquake Engineering and Structural Dynamics*, Vol 10.195-210

Meek, J. W. and Wolf, J. P. (1993). Cone models for nearly incompressible soil. *Earthquake Engineering and Structural Dynamics*, Vol 22:649-664.

Mita, A. and Luco, J. E. (1989). Impedance functions and input motions for embedded square foundation *ASCE Journal of Geotechnical Engineering Divison*, Vol 115:491-503.

Nogami, T. and Kongai, K. (1986). Time domain axial response of dynamically loaded single piles. *ASCE Journal of Engineering Mechanics Division*, Vol 112:1241-1252.

Nogami, T. and Kongai, K. (1988) Time domain flexural response of dynamically loaded piles. *ASCE Journal of Engineering Mechanics Division*, Vol 114:1512-1525.

Nogami, T. and Novak, M. (1976) Soil-pile interaction in vertical vibration. *Earthquake Engineering and Structural Dynamics*, Vol 4:277-93

Nour-Omid, B. and Clough, R. W. (1984) Dynamic analysis of structures using lanczos co-ordinates. *Earthquake Engineering and Structural Dynamics*, Vol 11:565-577.

Novak, M. (1974). Dynamic stiffness and damping of piles. *Canadian Geotechnical Journal*, Vol 11:574-598.

Novak, M. (1977). Vertical vibration of floating piles. *ASCE Journal of Engineering Mechanics Division*, Vol 103:153-68.

Novak, M. and Howell, J. F. (1978). Dynamic response of pile foundations in torsion. *ASCE Journal of Geotechnical Engineering Division*, Vol 104:535-552.

Novak, M. and Nogami, T. (1977). Resistance of soil to a horizontally vibrating pile. *ASCE Journal of Engineering Mechanics Division*, Vol 5:249-261.

Novak, M. and Sheta, M (1980). Approximate approach to contact problems of piles, in *Proc. Geotech Eng. Div of ASCE, National Convention Dynamic Response of Pile Foundations: Analytical Aspects*, pages 53-79

Novak, M. and Sheta, M (1982) Dynamic response of piles and pile groups, in *Proc 2nd Int. Conf. Num. Methods Offshore Piling*, pages 489–507.

Paige, C. (1976) Error analysis of the lanczos algorithm for triadiagonalizing a symmetric matrix. *J. Inst. Math. Appl.*, Vol 18:341–349.

Paige, C. (1980). Accuracy and effectiveness of the lanczos algorithm for symmetric eigenproblem. *Linear Algebra Applications*, Vol 34:235–258.

Parlett, B. N. and Nour-Omid, B. (1985). The use of a refined error bound when updating eigenvalues of tridiagonals. *Linear Algebra and Its Applications*, Vol 68:179–219.

Parlett, B. N. and Scott, D. S. (1979). The lanczos algorithm with selective orthogonalization. *Mathematics of Computation*, Vol 33:217–238.

Quinlan, P. M. (1953). The elastic theory od soil dynamics, in *Symp on Dynamic Testing of Soils, ASTM-STP No.156*, pages 3–34

Reddy, J. N. (1984). *An Introduction to the Finite Element Method*. McGraw–Hill Book Comapny, New York.

Reddy, J. N. (1986). *Applied Functional Analysis and Variational Methods in Engineering*. McGraw–Hill Book Company, New York.

Reissner, E. (1936). Stationäre, axialsymmetrische durch eine schittelnde masserregte schwingungen eines homogenen elastischen halbraums. *Ingenieur-Archiv*, Vol 7:381–396.

Schwarz, H. R. (1988). *Finite Element Methods (English Translation)*. Academic Press, London.

Segol, G., Lee, P. C. Y. and Abel, J. F. (1978). Amplitude reduction of surface waves by trenches. *ASCE Journal of Geotechnical Engineering Division*, Vol 104:621-641.

Sen, R., Kausel, E. and Banerjee, P. K. (1985). Dynamic behavior of axially and laterally loaded piles and pile groups embedded in in-homogeneous soil. *International Journal for Numerical and Analytical Methods in Geomechanics*, Vol 9.507-524

Simon, H. D. (1984). The lanczos algorithm with partial reorthogonalization. *Mathematics of Computation*, Vol 42.115-142.

Stoer, J. and Bulrsch, R. (1980). *Introduction to Numerical Analysis*. Springer-Verlag, New York.

Sung, T. Y. (1953). Vibrations in semi-infinite solids due to periodic surface loadings, in *Symp on Dynamic Testing of Soils, ASTM-STP No.156*, pages 35-64.

Thomson, W. T. and Kobori, T. (1962). Dynamic compliance of rectangular foundations on an infinite half-space. Technical Report Report No. 62.9, University of California, Los Angeles.

Tyson, T. R. and Kausel, E. (1983). Dyanmic analysis of axisymmetric pile groups. Technical Report R83-07, Departmenet of Civil Engineering, MIT, Cambridge, Mass.

Underwood, P. G. and Geers, T. L. (1978). Doubly asymptotic boundary element analysis of dynamic soil-structure interaction. Technical Report DNA Report 4512T, Defense Nuclear Agency, Washington.

Venugopala Rao, R. and Kameswara Rao, N. S. V. (1994). Dynamic analysis of foundations using infinite elements, in *8th International Conference of the IACMAG, West Virginia, USA*

Von Estorff, O., Pais, A. L. and Kausel, E. (1990) Some observations on time domain and frequency domain boundary elements. *International Journal for Numerical Methods in Engineering*, Vol 29:785–800.

Waas, G. and Hartmann, H. G. (1981). Pile foundations subjected to dynamic horizontal loads, in *6th International Conference on Structural Mechanics in Reactor Technology*, pages 85–105.

Wilson, E. L., Yuan, M. and Dickens, J. M. (1979). Dynamic analysis by direct superposition of ritz vectors. *Earthquake Engineering and Structural Dynamics*, Vol 7.405–411.

Wolf, J. P. (1988). *Soil-Structure Interaction Analysis in Time Domain*. Prentice-Hall, Englewood Cliffs, NJ 07632

Wolf, J. P. and von Arx, G. A. (1978). Impedance functions of a group of vertical piles, in *ASCE Specialty Conference on Earthquake Engineering and Soil Dynamics*, pages 1024–1041.

Woods, R. D. (1967) *Screening of Elastic Surface Waves by Trenches*. PhD thesis, University of Michigan.

Zeng, L. F. Wiberg, N. E., et al. (1992). A posteriori local error estimation and adaptive time-stepping for newmark integration in dynamic analysis. *Earthquake Engineering and Structural Dynamics*, Vol 21:555–571.

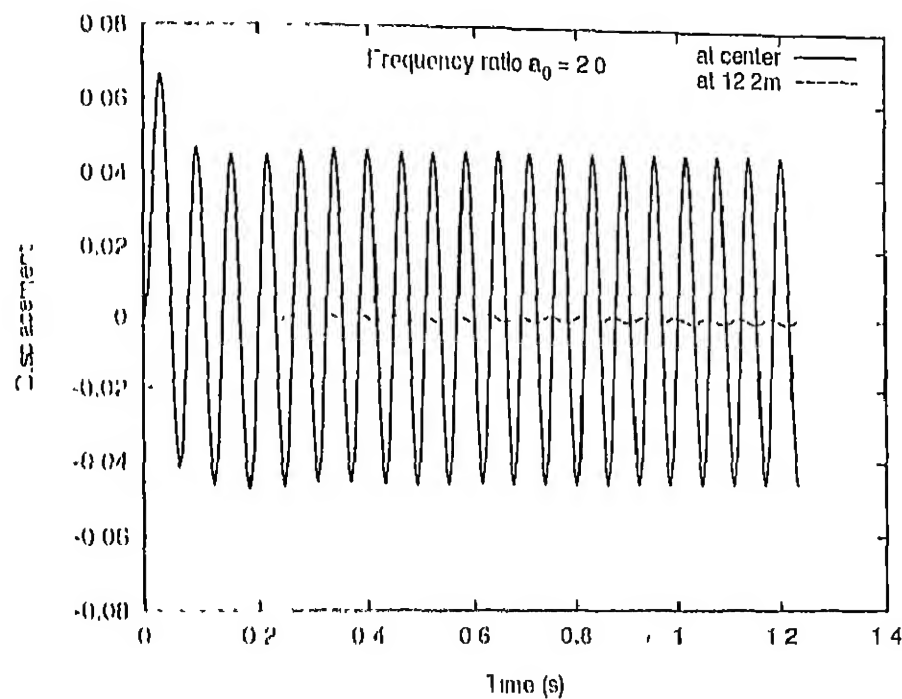
Zhang, Chuhan and Zhao, Chongbin (1987a). Coupled method of finite and infinite elements for strip foundation wave problems. *Earthquake Engineering and Structural Dynamics*, Vol 15:839-857.

Zhang, Chuhan and Zhao, Chongbin (1987b). Vertical vibration of three-dimensional rigid foundations on layered media. *Earthquake Engineering and Structural Dynamics*, Vol 15:585-594.

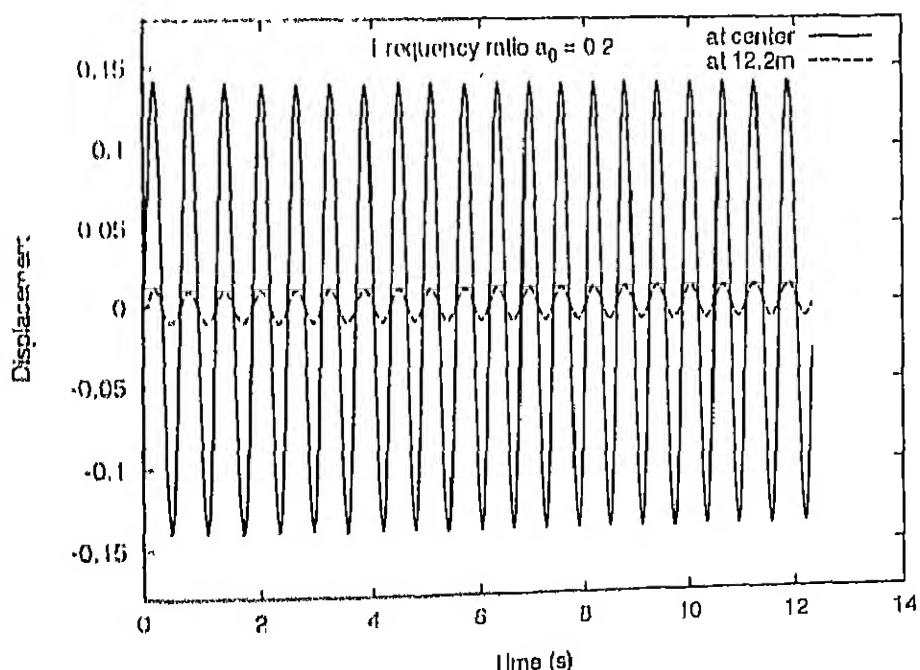
Zienkiewicz, O. C., Wood, W. L., et al. (1984). A unified set of single step algorithms, part 1: General formulation and applications. *International Journal for Numerical Methods in Engineering*, Vol 20:1529-1552.

APPENDIX

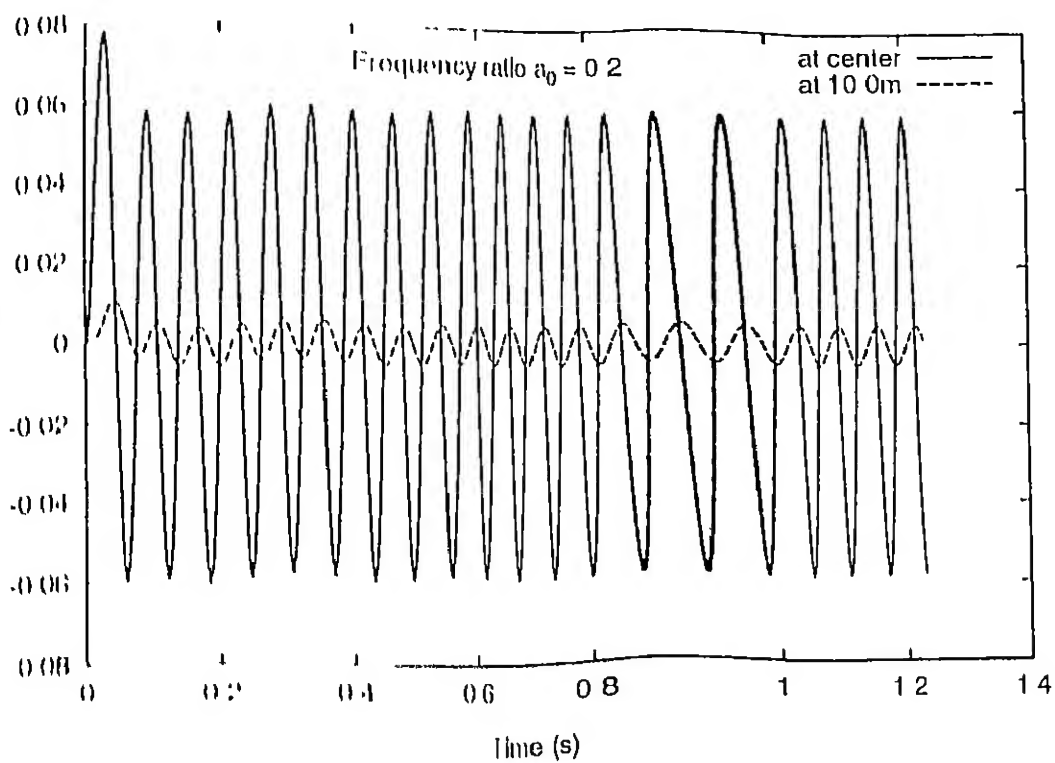
placement histories for horizontal and vertical loading for frequency ratios of 0.2 and 2.0 are shown in the following figures. This is to show that the amplitudes do not vary as the time progresses indicating stability.



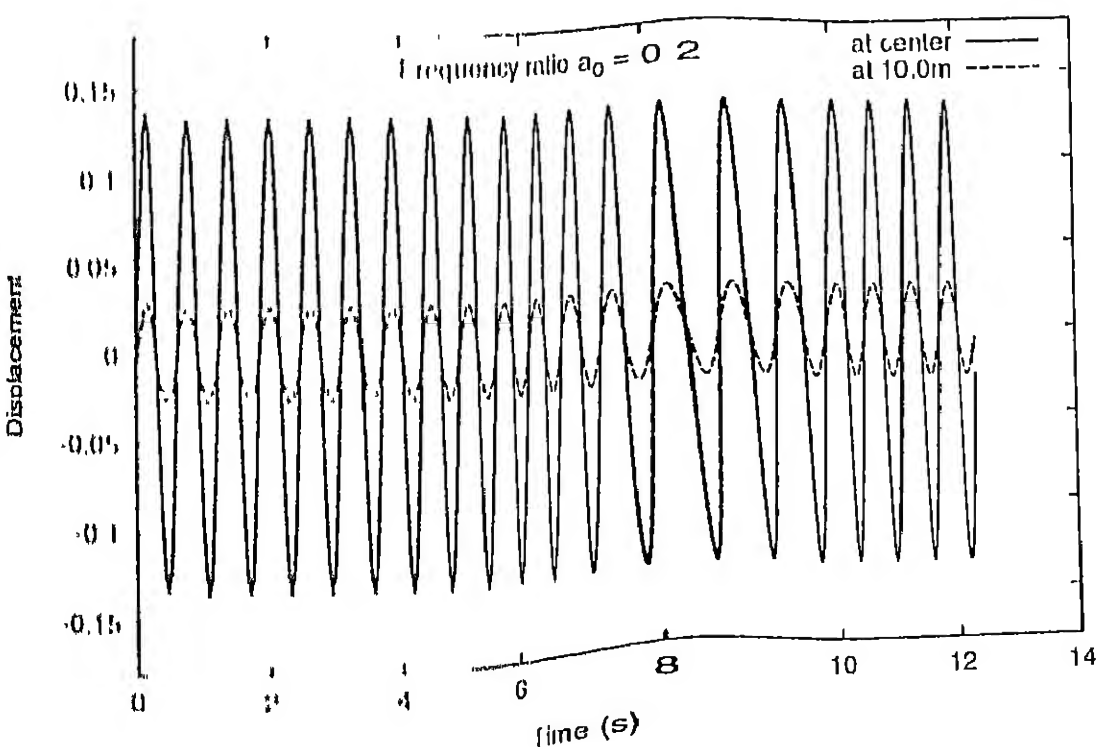
Vertical Displacement History for Frequency Ratio of 2.0



Vertical Displacement History for Frequency Ratio of 0.2



Horizontal Displacement History for Frequency Ratio of 0.2



Horizontal Displacement History for Frequency Ratio of 0.2

A 125692

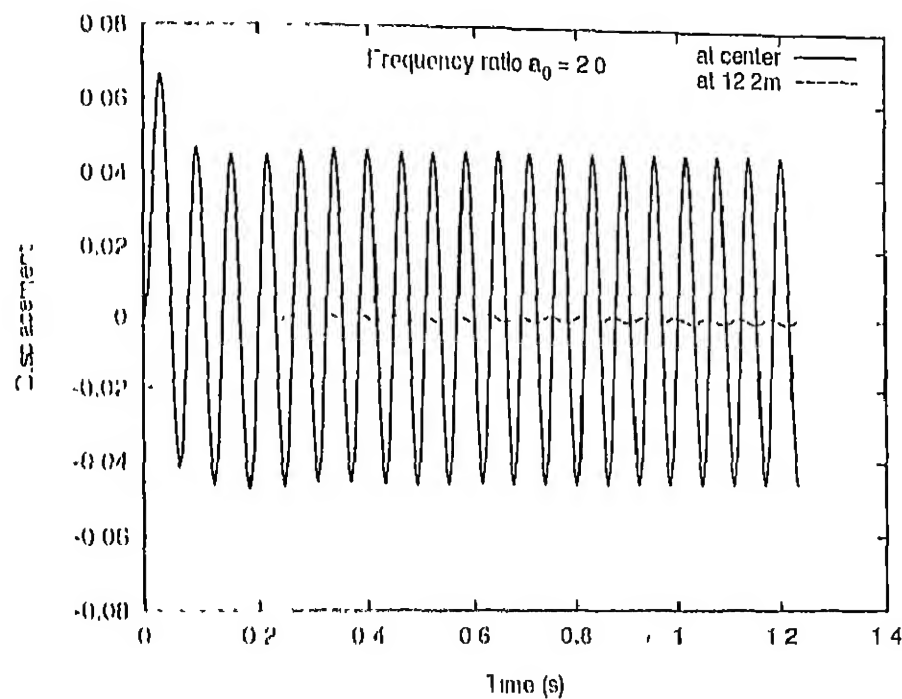
CE-1995-D-RAO-TIM



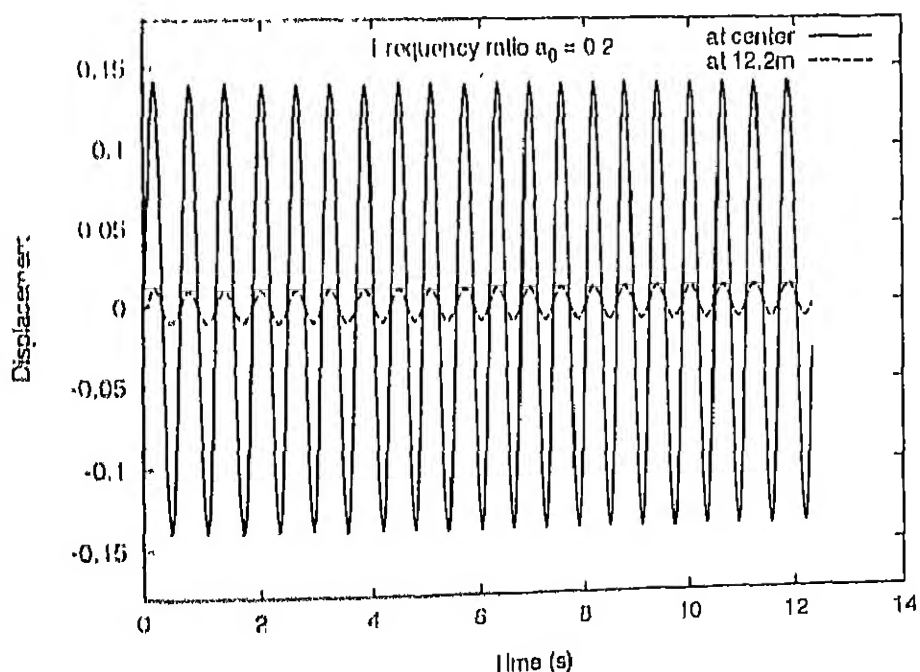
A125692

APPENDIX

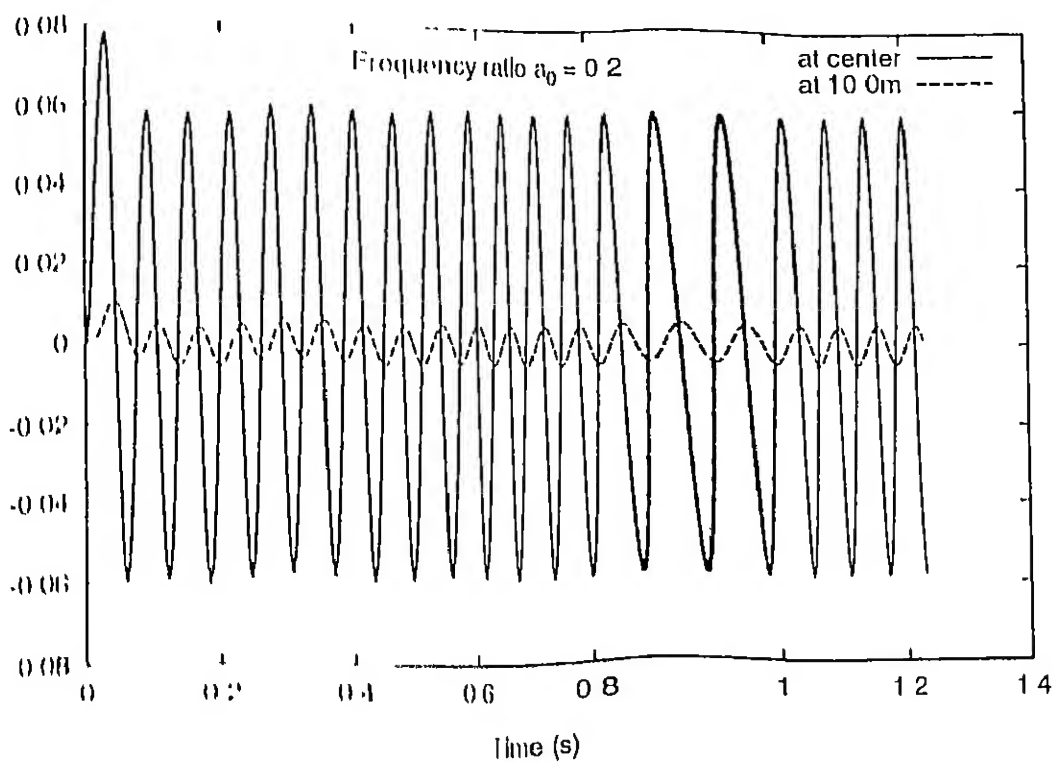
placement histories for horizontal and vertical loading for frequency ratios of 0.2 and 2.0 are shown in the following figures. This is to show that the amplitudes do not vary as the time progresses indicating stability.



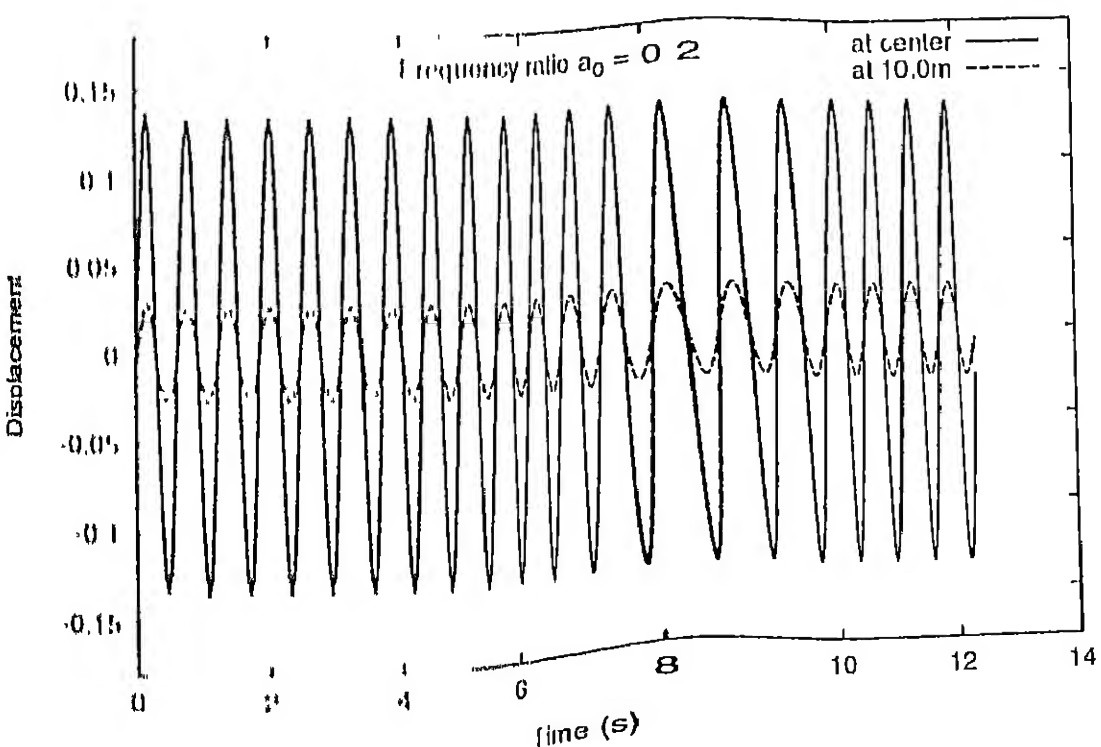
Vertical Displacement History for Frequency Ratio of 2.0



Vertical Displacement History for Frequency Ratio of 0.2



Horizontal Displacement History for Frequency Ratio of 0.2



Horizontal Displacement History for Frequency Ratio of 0.2

A

125692

CE-1995-D-RAO-TIM



A125692